

GO METALS
MONSTER PROJECT
GRAVITY INVERSION PROJECT

JANUARY 2020

SGC3626



SOUTHERN GEOSCIENCE
CONSULTANTS

Client: Go Metals	Project(s): Monster Project (Yukon Territory)
Report Number: SGC3626	Date: January, 2020
Compiled By: Robert Hearst, Chief Geophysicist - Americas, robert.hearst@sgc.com.au	
Author(s): Robert Hearst	
Peer Reviewed By: Bill Peters, Chairman	

Key words: Gravity, Magnetic, magnetic susceptibility, inversion

Commodity: Gold, copper

Province / State, Country:

Yukon Territory, Canada

1:20,000 map sheet(s):

1:50,000 map sheet(s):

1:10,000 map sheet(s)

CONTENTS

CONTENTS.....	ii
LIST OF FIGURES	iii
LIST OF TABLES	vii
LIST OF APPENDICES	vii
ABBREVIATIONS	viii
SUMMARY	ix
1 INTRODUCTION	1
1.1 Background.....	1
1.2 Previous Work.....	1
1.3 Scope.....	3
1.4 Objectives	3
2 GEOLOGICAL SETTING	3
3 STUDY DATA SET DETAILS	4
3.1 Aeromagnetic and Radiometric Data	4
3.2 Gravity Data	4
3.3 DC Resistivity and Induced Polarisation Data (DCIP)	6
3.4 Rock Physical Property Data	6
4 GRAVITY DATA INVERSION.....	7
5 RESULTS AND INTERPRETATION	8
5.1 Property Coverage.....	8
5.2 West Area Of Interest	17
5.3 Central Area Of Interest.....	30
5.4 East Area Of Interest.....	45
6 CONCLUSIONS AND RECOMMENDATIONS.....	58
7 REFERENCES	60

LIST OF FIGURES

Figure 1: Location of belts of Wernecke Breccia (red), original Monster Project properties (grey outline) and area of known Cu mineralization within the Coal Creek Inlier of the Ogilvie Mountains (after Setterfield and Tykajlo, 2003).	2
Figure 2: Survey and Study Area Location Map – Location of the various datasets used in the study are illustrated. Airborne survey flight (black), gravity sites (grey dots), DCIP lines (purple), GMM Areas Of Interest (AOI) (white), gravity detail study areas (red) on a drone DEM (masl) with a Bing satellite imagery background.....	5
Figure 3: Complete Bouguer Gravity Anomaly (CBA) for Bouguer Density 2.67g/cm^3 . Gravity sites are indicated by red dots. Contour interval is 0.04, 0.2 and 1.0 g/cm^3 . On a Bing satellite image base.	8
Figure 4: CBA 2.67g/cm^3 contours (0.04, 0.2 and 1.0 g/cm^3) overlain on drone DEM image.	9
Figure 5: 1VD of the CBA 2.67 g/cm^3 overlain with drone DEM contours (50/250/1000 m) ON a Bing satellite image base.....	11
Figure 6: Analytic Signal of the CBA 2.67 g/cm^3 overlain with drone DEM contours (50/250/1000 m) ON a Bing satellite image base.....	12
Figure 7: Tilt Derivative of the CBA 2.67 g/cm^3 overlain with drone DEM contours (50/250/1000 m) on a Bing satellite image base.....	12
Figure 8: Reduced to the Pole (RTP) total magnetic intensity (TMI) from the airborne survey with contour overlay of the CBA 2.67g/cm^3 on a Bing satellite image base.....	13
Figure 9: Airborne radiometric ternary plot with contour overlay of the CBA 2.67g/cm^3 on a Bing satellite image base.....	13
Figure 10: Airborne radiometric Potassium (K) with contour overlay of the CBA 2.67g/cm^3 on a Bing satellite image base.....	14
Figure 11: Airborne radiometric Thorium (Th) with contour overlay of the CBA 2.67g/cm^3 on a Bing satellite image base.....	14
Figure 12: Airborne radiometric Uranium (U) with contour overlay of the CBA 2.67g/cm^3 on a Bing satellite image base.....	15
Figure 13: 3D Voxi inversion of the CBA 2.67g/cm^3 data. View is looking north. The iso-surface/shell for a density contrast of 0.05 g/cm^3 (corresponding to a density of 2.72 g/cm^3) shown. Topographic surface (drone DEM) is plotted in addition to surface mapped faults (green lines), gravity measurement sites (purple dots) and GMM defined AOI (white polygons).....	15
Figure 14: 3D Voxi inversion of the CBA 2.67g/cm^3 data. View is looking north. The iso-surface/shell for a density contrast of 0.15 g/cm^3 (corresponding to a density of 2.82 g/cm^3) shown. Topographic surface (drone DEM) is plotted in addition to surface mapped faults (green lines), gravity measurement sites (purple dots) and GMM defined AOI (white polygons).....	16

- Figure 15: 3D Voxi inversion of the CBA 2.67g/cm^3 data. View is looking north. The iso-surface/shell for a density contrast of 0.05 g/cm^3 (corresponding to a density of 2.72 g/cm^3) shown. Magnetic susceptibility iso-surface (0.0028 SI ; grey surfaces) and 2D modelling results (dark blue) are plotted. Topographic surface (drone DEM) is plotted in addition to surface mapped faults (green lines), gravity measurement sites (purple dots) and GMM defined AOI (white polygons)..... 16
- Figure 16: West AOI Complete Bouguer Gravity Anomaly (CBA) for Bouguer Density 2.67g/cm^3 . Gravity sites are indicated by grey dots. Contour interval is 0.04 , 0.2 and 1.0 g/cm^3 . Mapped geologic faults (dashed white lines) are plotted. Background is drone DEM grid. 17
- Figure 17: West AOI Complete Bouguer Gravity Anomaly (CBA) for Bouguer Density 2.67g/cm^3 . Gravity sites are indicated by grey dots. Contour interval is 0.1 , 0.5 and 2.5 g/cm^3 . Mapped geologic faults (dashed white lines) are plotted. Background is drone DEM grid. 18
- Figure 18: West AOI 1VD of the Complete Bouguer Gravity Anomaly (CBA) for Bouguer Density 2.67g/cm^3 . Gravity sites are indicated by grey dots. Mapped geologic faults (dashed white lines) are plotted. Background contours ($50/250/1000\text{ m}$) are elevations from the drone DEM grid in units of masl. 20
- Figure 19: West AOI Analytic Signal of the Complete Bouguer Gravity Anomaly (CBA) for Bouguer Density 2.67g/cm^3 . Gravity sites are indicated by grey dots. Mapped geologic faults (dashed white lines) are plotted. Background contours ($50/250/1000\text{ m}$) are elevations from the drone DEM grid in units of masl. 21
- Figure 20: West AOI Tilt derivative of the Complete Bouguer Gravity Anomaly (CBA) for Bouguer Density 2.67g/cm^3 . Gravity sites are indicated by grey dots. Mapped geologic faults (dashed white lines) are plotted. Background contours ($50/250/1000\text{ m}$) are elevations from the drone DEM grid in units of masl. 22
- Figure 21: West AOI Reduced to the Pole (RTP) total magnetic intensity (TMI) from the airborne survey with contour overlay of the CBA 2.67g/cm^3 . Gravity sites are indicated by grey dots. Mapped geologic faults (dashed white lines) are plotted..... 23
- Figure 22: West AOI airborne radiometric ternary plot with contour overlay of the CBA 2.67g/cm^3 .. 24
- Figure 23: West AOI airborne radiometric Potassium (K) plot with contour overlay of the CBA 2.67g/cm^3 25
- Figure 24: West AOI airborne radiometric Thorium (Th) plot with contour overlay of the CBA 2.67g/cm^3 26
- Figure 25: West AOI airborne radiometric Uranium (U) plot with contour overlay of the CBA 2.67g/cm^3 27
- Figure 26: 3D Voxi inversion of the CBA 2.67g/cm^3 data. View is looking northeast. The iso-surface/shell for a density contrast of 0.075 g/cm^3 (corresponding to a density of 2.745 g/cm^3) is shown. Topographic surface (drone DEM) is plotted in addition to surface mapped faults (yellow lines), gravity measurement sites (grey dots), DCIP lines (purple) and GMM defined AOI (red polygon). 28

Figure 27: 3D Voxi inversion of the CBA 2.67g/cm^3 data. View is looking northeast. The iso-surface/shell for a density contrast of 0.15 g/cm^3 (corresponding to a density of 2.82 g/cm^3) is shown. Topographic surface (drone DEM) is plotted in addition to surface mapped faults (yellow lines), gravity measurement sites (grey dots), DCIP lines (purple) and GMM defined AOI (red polygon)..... 29

Figure 28: 3D Voxi inversion of the CBA 2.67g/cm^3 data. View is looking northeast. The iso-surface/shell for a density contrast of 0.05 g/cm^3 (corresponding to a density of 2.72 g/cm^3) is shown. Magnetic susceptibility iso-surface (0.002 SI ; grey surfaces) are shown. Topographic surface (drone DEM) is plotted in addition to surface mapped faults (yellow lines), gravity measurement sites (grey dots), DCIP lines (purple) and GMM defined AOI (red polygon)..... 30

Figure 29: Central AOI Complete Bouguer Gravity Anomaly (CBA) for Bouguer Density 2.67g/cm^3 . Gravity sites are indicated by grey dots. Contour interval is $0.1, 0.5$ and 2.5 g/cm^3 . Mapped geologic faults (dashed white lines) are plotted. Background is drone DEM grid. 32

Figure 30: West AOI Complete Bouguer Gravity Anomaly (CBA) for Bouguer Density 2.67g/cm^3 . Gravity sites are indicated by grey dots. Contour interval is $0.01, 0.5$ and 2.5 g/cm^3 . Mapped geologic faults (dashed white lines) are plotted. Background is drone DEM grid. 33

Figure 31: Central AOI 1VD of the Complete Bouguer Gravity Anomaly (CBA) for Bouguer Density 2.67g/cm^3 . Gravity sites are indicated by grey dots. Mapped geologic faults (dashed white lines) are plotted. Background contours ($50/250/1000\text{ m}$) are elevations from the drone DEM grid in units of masl. 34

Figure 32: Central AOI Analytic Signal of the Complete Bouguer Gravity Anomaly (CBA) for Bouguer Density 2.67g/cm^3 . Gravity sites are indicated by grey dots. Mapped geologic faults (dashed white lines) are plotted. Background contours ($50/250/1000\text{ m}$) are elevations from the drone DEM grid in units of masl. 35

Figure 33: Central AOI Tilt derivative of the Complete Bouguer Gravity Anomaly (CBA) for Bouguer Density 2.67g/cm^3 . Gravity sites are indicated by grey dots. Mapped geologic faults (dashed white lines) are plotted. Background contours ($50/250/1000\text{ m}$) are elevations from the drone DEM grid in units of masl. 36

Figure 34: Central AOI Reduced to the Pole (RTP) total magnetic intensity (TMI) from the airborne survey with contour overlay of the CBA 2.67g/cm^3 . Gravity sites are indicated by grey dots. Mapped geologic faults (dashed white lines) are plotted..... 37

Figure 35: Central AOI airborne radiometric ternary plot with contour overlay of the CBA 2.67g/cm^3 38

Figure 36: Central AOI airborne radiometric Potassium (K) plot with contour overlay of the CBA 2.67g/cm^3 39

Figure 37: Central AOI airborne radiometric Thorium (Th) plot with contour overlay of the CBA 2.67g/cm^3 40

Figure 38: Central AOI airborne radiometric Uranium (U) plot with contour overlay of the CBA 2.67g/cm^3 41

- Figure 39: 3D Voxi inversion of the CBA 2.67g/cm^3 data for the Central AOI. View is looking north. The iso-surface/shell for a density contrast of 0.075 g/cm^3 (corresponding to a density of 2.745 g/cm^3) is shown. Topographic surface (drone DEM) is plotted in addition to surface mapped faults (yellow lines), gravity measurement sites (grey dots) and GMM defined AOI (red polygon). 42
- Figure 40: 3D Voxi inversion of the CBA 2.67g/cm^3 data for the Central AOI. View is looking north. The iso-surface/shell for a density contrast of 0.15 g/cm^3 (corresponding to a density of 2.82 g/cm^3) is shown. Topographic surface (drone DEM) is plotted in addition to surface mapped faults (yellow lines), gravity measurement sites (grey dots) and GMM defined AOI (red polygon). 43
- Figure 41: 3D Voxi inversion of the CBA 2.67g/cm^3 data for the Central AOI. View is looking north. The iso-surface/shell for a density contrast of 0.05 g/cm^3 (corresponding to a density of 2.72 g/cm^3) is shown. Magnetic susceptibility iso-surface (0.0024 SI ; grey surfaces) are shown. The 2D magnetic modelling completed in the past is shown in dark blue. Topographic surface (drone DEM) is plotted in addition to surface mapped faults (yellow lines), gravity measurement sites (grey dots) and GMM defined AOI (red polygon). 44
- Figure 42: East AOI Complete Bouguer Gravity Anomaly (CBA) for Bouguer Density 2.67g/cm^3 . Gravity sites are indicated by grey dots. Contour interval is $0.1, 0.5$ and 2.5 g/cm^3 . Mapped geologic faults (dashed white lines) are plotted. Background is drone DEM grid. 46
- Figure 43: East AOI Complete Bouguer Gravity Anomaly (CBA) for Bouguer Density 2.67g/cm^3 . Gravity sites are indicated by grey dots. Contour interval is $0.1, 0.5$ and 2.5 g/cm^3 . Mapped geologic faults (dashed white lines) are plotted. Background is drone DEM grid. 47
- Figure 44: East AOI 1VD of the Complete Bouguer Gravity Anomaly (CBA) for Bouguer Density 2.67g/cm^3 . Gravity sites are indicated by grey dots. Mapped geologic faults (dashed white lines) are plotted. Background contours ($50/250/1000\text{ m}$) are elevations from the drone DEM grid in units of masl. 48
- Figure 45: East AOI Analytic Signal of the Complete Bouguer Gravity Anomaly (CBA) for Bouguer Density 2.67g/cm^3 . Gravity sites are indicated by grey dots. Mapped geologic faults (dashed white lines) are plotted. Background contours and image ($50/250/1000\text{ m}$) are elevations from the drone DEM grid in units of masl. 49
- Figure 46: East AOI Tilt derivative of the Complete Bouguer Gravity Anomaly (CBA) for Bouguer Density 2.67g/cm^3 . Gravity sites are indicated by grey dots. Mapped geologic faults (dashed white lines) are plotted. Background colour/contours ($50/250/1000\text{ m}$) are elevations from the drone DEM grid in units of masl. 50
- Figure 47: East AOI Reduced to the Pole (RTP) total magnetic intensity (TMI) from the airborne survey with contour overlay of the CBA 2.67g/cm^3 . Gravity sites are indicated by grey dots. Mapped geologic faults (dashed white lines) are plotted. 51
- Figure 48: East AOI airborne radiometric Ternary plot with contour overlay of the CBA 2.67g/cm^3 ... 52
- Figure 49: East AOI airborne radiometric Potassium (K) plot with contour overlay of the CBA 2.67g/cm^3 53

Figure 50: East AOI airborne radiometric Thorium (Th) plot with contour overlay of the CBA 2.67g/cm ³	54
Figure 51: East AOI airborne radiometric Uranium (U) plot with contour overlay of the CBA 2.67g/cm ³	55
Figure 52: 3D Voxi inversion of the CBA 2.67g/cm ³ data for the East AOI. View is looking west. The iso-surface/shell for a density contrast of 0.01 g/cm ³ (corresponding to a density of 2.77 g/cm ³) is shown. Topographic surface (drone DEM) is plotted in addition to surface mapped faults (yellow lines), gravity measurement sites (grey dots), DCIP Lines (black) and GMM defined AOI (red polygon).	56
Figure 53: 3D Voxi inversion of the CBA 2.67g/cm ³ data for the East AOI. View is looking west. The iso-surface/shell for a density contrast of 0.015 g/cm ³ (corresponding to a density of 2.82 g/cm ³) is shown. Topographic surface (drone DEM) is plotted in addition to surface mapped faults (yellow lines), gravity measurement sites (grey dots), DCIP Lines (black) and GMM defined AOI (red polygon).	57
Figure 54: 3D Voxi inversion of the CBA 2.67g/cm ³ data for the East AOI. View is looking west. The iso-surface/shell for a density contrast of 0.01 g/cm ³ (corresponding to a density of 2.77 g/cm ³) is shown. Magnetic susceptibility iso-surface (0.0024 SI; grey surfaces) are shown. The 2D magnetic modelling completed in the past is shown in dark blue. Topographic surface (drone DEM) is plotted in addition to surface mapped faults (yellow lines), gravity measurement sites (grey dots) and GMM defined AOI (red polygon).....	58

LIST OF TABLES

Table 1 – Rock Physical Properties from 2001-2002 (After Doherty and Tyjaklo, 2003).....	6
Table 2 – Rock Physical Properties from 2018/19 (from GMM).....	7

LIST OF APPENDICES

Appendix A: Precision Airborne Survey Report
--

ABBREVIATIONS

Ωm	ohm metres (unit of resistivity)
2D	two-dimensional
3D	three-dimensional
CBA	Complete Bouguer Anomaly
DCIP	Direct current resistivity and induced polarisation
DEM	digital elevation model
GIS	Geographic Information System
GPS	Global Positioning System
IP	induced polarisation
kVA	kilovolt amperes (unit of power)
mGal	milliGals (unit of gravity)
mV/V	millivolts per volt (unit of chargeability)
QC	quality control
RTP	reduced-to-pole
SGC	Southern Geoscience Consultants
TMI	Total Magnetic Intensity
UTM	Universal Transverse Mercator

SUMMARY

From the limited rock physical property data available it is apparent that the Wernecke Breccia covers a wide range of possibilities with respect to density and magnetisation. The average density of the Wernecke Breccia on which the most recent sampling is largely based is 2.58 g/cm^3 . A broader rock physical property study is required including rocks of the Gillespie and Quartet Groups to be able to better determine if and how the Wernecke Breccia can be better identified. The assumption in this study was that the denser materials producing the gravity anomalies are Wernecke Breccia.

The regional 3D inversion of the gravity data and previous magnetic data inversions shows three main areas of high potential for Wernecke Breccia which are similar to the three areas identified by GMM as areas of interest (AOI) but have been defined as significantly larger in area in this study.

There is a high degree of correlation between the gravity data and mapped faults strongly suggesting that the Wernecke Breccia extent is indicated by fault controlled high density blocks and fault trends.

The magnetic inversion data is arguably less effective, in part due to a lack of magnetic contrast in the rocks. A common relationship between the magnetic inversion and gravity inversion models is that the magnetic bodies are often shallower and flanked by high density bodies. Small features in the magnetic signal related to thin magnetic dikes are not imaged well by the 3D modelling. The strikes and dips of the inverted data for the magnetic and gravity data often differ particularly in the East and Central AOIs. The introduction of a geologic model and/or drill hole data into the inversion process would be advantageous to improving the interpretability of the results.

A fairly high degree of correlation of between the gravity anomalies and the airborne radiometric data was noted in almost all AOIs with the most common correlation being with potassium being more dominant than thorium or uranium with dense bodies, particularly on slope sides in the East and Central AOIs.

The greatest degree of correlation between the magnetic and gravity data is in the West AOI where the central anomaly is both a magnetic high and a gravity high anomaly and at the intersection of NNW-SSE fault that offsets an ENE-WSW striking fault. An apparent ring structure around this anomaly is also of interest and worthy of further investigation. The inversion modelling suggests that the magnetic and gravimetric sources are very shallow.

In the Central AOI, two intersecting dominant gravity trends ranging in width from 200m to 500m have been identified. There are weak associations with both the radiometrics and the magnetics suggesting that these may alteration zones related to faulting. There is also a partially overlapping shallow gravity and magnetic feature bisected by a NNW striking fault which is worthy of further work and follow-up.

The East AOI is interesting as the gravity modelling highs appears to flank the magnetic inversion highs in almost all cases. This could indicate an intrusive centre (the magnetics) and surrounding alteration into the surrounding rock (density high). The magnetic core appears to be deep whereas the gravity inversion suggests that the dense rocks are very shallow. A separate shallow fault controlled correlation between the magnetic and the gravity features is worthy of follow-up. A final target of interest is a correlation between high potassium and a gravity high density anomaly along the slope of a cirque wall.

1 INTRODUCTION

1.1 BACKGROUND

Southern Geoscience Consultants Pty Ltd (SGC) has been contracted by Go Metals Mining (GMM) for enhanced gravity data processing, 3D modelling and interpretation utilizing historic and recently acquired ground gravity data acquired over the Monster Project, Yukon Territory, Canada. Included in this study are the historic magnetic data including 3D inversion modelling along with the recently acquired DC resistivity and IP data completed over parts of the Monster Project.

The Monster property is located approximately 85 km north-northwest of Dawson City, at the headwaters of Coal Creek and the Monster River. Both watercourses are tributaries to the Yukon River. Access to the area is typically by helicopter. Elevation ranges from 900 m Above Sea Level in the coal creek valley to over 2000 m Above Sea Level. Of importance to note, the region was unaffected by continental glaciation during the Pleistocene resulting in rounded mountainous terrain and steep alpine glaciation related cirques and ridges. The implication of this is that the weathering has predominately been in-situ, with highly localised down slope transport if at all.

The project area encompasses part of the Wernecke Breccia belt, an east-west trending belt of hematitic iron oxide, copper and gold (IOCG) mineralized breccia zones. The mineralisation of interest is hosted within and adjacent to the hematitic breccia zones with the Cu occurring in pods, veins accompanied by disseminated bornite and chalcopyrite and anomalous Co, Au, Ag, Pb and Zn. (Doherty and Verbaas, 2018).

1.2 PREVIOUS WORK

Recorded exploration work in the Ogilvie Mountains of the Yukon Territory dates from the 1970's. Original target being explored for was red bed copper, Sullivan-style sedex deposits and in some cases unconformity associated uranium deposits. Recent work has concentrated on the Wernecke Breccia and their perceived potential to host IOCG deposits.

Extensive sampling throughout the late 1970's and into the 1990's defined a belt of Cu in soil and grab samples of 1% to 5% or greater (Figure 1). In the 2000's the pulps of the soil and rock samples collected during the campaigns of the 1990's were analysed for U. The highest recorded values were 32ppm in the grab samples and 20 ppm in the soil samples.

A detailed summary of geological mapping and field work can be found in assessment report 094430 (Setterfield and Tykajlo, 2003) and the 43-101 report (Doherty and Verbaas, 2018).

Geophysical surveying of the property area commenced in 1996 when Blackstone Resources Inc. completed an airborne magnetic and radiometric survey over the North and South Belts of the Wernecke Breccia as outlined in Figure 1. Regional flight lines were widely spaced at 1 km intervals with 250 m spacing used over the Monster claims. The survey was coarse and the flight lines irregular due to topography, the data quality, although degraded, was deemed acceptable. Conclusions from the interpretation of the survey data were:

- The radiometric data could outline the major lithological units;
- Within the Wernecke Breccia, zones of variable potassic alteration were identifiable and generally correlated to areas of known mineralisation. In the area covered by the 250 m spaced flight lines, potential areas of high potassic alteration were visible;

- Broad structural zones and regional structures were discernible from the aeromagnetic coverage;
- Magnetic highs were locally correlatable to zones of increased mineralization;
- Density of the coverage was insufficient for drill hole targeting.

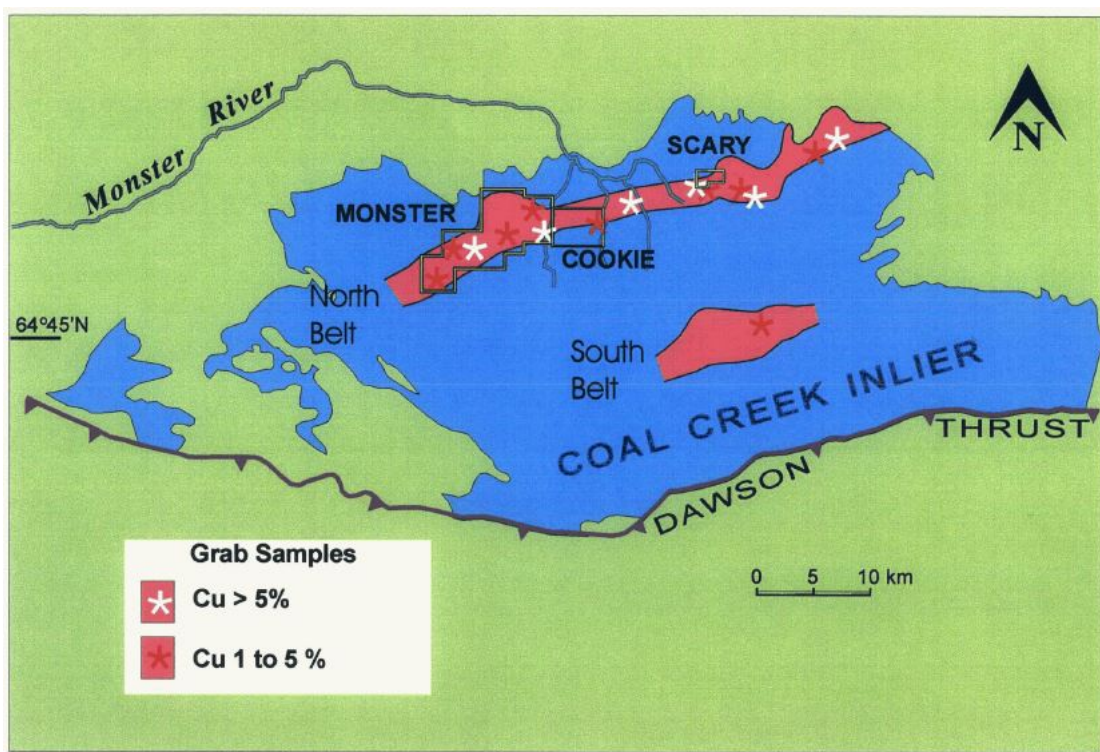


Figure 1: Location of belts of Wernecke Breccia (red), original Monster Project properties (grey outline) and area of known Cu mineralization within the Coal Creek Inlier of the Ogilvie Mountains (after Setterfield and Tykajlo, 2003).

The period of 2001 to 2003 was dominated by ground gravity surveys completed by MWH Geo-surveys (MWH). During this period, rock physical property measurements were completed on samples of the Wernecke Breccia and surrounding shale country rocks yielding a mean density of about 2.75 g/cm³. Several interesting density anomalies were identified by the gravity surveys, however the one drill hole completed failed to test the density anomaly targeted (Doherty and Verbaas, 2018).

In 2018, geophysical exploration was again taken up in the form of a high resolution helicopter-borne aeromagnetic and radiometric survey over the Monster survey block for Go Cobalt Mining Corp. (now GMM). The survey consisted of 901 line-km flown using a 75m m line spacing on a heading of 165°/345° with tie lines flown at 750 m intervals on a heading of 075°/255°. Terrain clearance for the survey was nominally 42 m. The magnetic data was inverted in 3D and accompanied by selected discrete modelling of 2D vein/dyke features in addition to a deeper discrete magnetic source.

The aeromagnetic survey was followed up with additional gravity surveying by MWH Geo-survey in 2018 and 2019. MWH also reprocessed all previously acquired gravity data to ensure consistency in the handling of the data and calculation of the terrain effect using the latest drone based DEM. The inner circle (near station terrain effects) was calculated using the high resolution drone derived DEM.

During 2019 a DC resistivity-IP (DCIP) survey was completed over a total of 8 lines (2 grids of 4 lines each) for Go Cobalt Mining (now GMM). The location of the DCIP lines was primarily driven by the

3D magnetic inversion results. A total of 4 lines were completed over each of the West and East target areas as identified from the high resolution magnetic data 3D inversion modelling. The survey was completed by GroundTruth Exploration using the Super Sting system with a transmit dipole of 30 m and receiver dipole size of 10 m in a dipole-dipole type of configuration. Up to 84 dipoles were deployed and kept stationary on the line during the survey. The transmit dipole was walked through the receiver dipole array. Results from the DCIP survey suggest that there are two discrete responses to the known mineralization:

- Zones of low resistivity and low chargeability; and
- Zones of high-grade Co and Cu correlating to high chargeability and low resistivity.
- Both above observed DCIP responses correlate to magnetically anomalous susceptibility 3D inversion anomalies.

1.3 SCOPE

The aim of the current work is to improve upon the current modelling of the gravity data taking into consideration magnetic structures and IP conductivity where appropriate for the drill targeting of possible areas of enrichment of massive base metals consistent with an IOCG deposit.

1.4 OBJECTIVES

The objectives of the study are to:

- Delineate and classify gravity and magnetic units;
- Identify structures and potential controls on the mineralization inferred from the gravity and magnetic data
- Integrated interpretation of the gravity, aeromagnetic, DCIP and radiometric data sets with reference to previous work.

2 GEOLOGICAL SETTING

The following discussion is condensed from Doherty and Verbaas (2018).

The Monster property contains several Wernecke Breccia zones that are emplaced within the Wernecke Supergroup. In this area, the Wernecke Supergroup is comprised of members of the Quartet Group and Gillespie Lake Group.

Comprised of coarse quartzite to conglomerate, black shale, grey to black siltstone and grey mudstone, the Quartet Group is the dominate geology noted on the Monster property. The conglomerates tend to be highly variable, comprised of well sorted to sub-angular 2 cm or smaller pebbles of mudstone, chert and quartz. The shales and siltstones are often well bedded, cleaved and interbedded with quartzite.

The Gillespie Group consists primarily of silty dolostone and dolostone. In brecciated areas, the bedding is deformed and contorted.

Mineralisation on the Monster project is within or adjacent to the Wernecke Breccia. The Breccia can be divided into three zones that are elongated along a 15km strike length and elongated in a northeast – southwest direction. The Breccia zones range from tabular to ellipsoidal and circular in shape. Clasts present within the Wernecke Breccia are thought to be sourced from formerly overlying igneous and sedimentary lithologies. Diorites are most likely transported clasts within the Breccia zones. Similarly the maroon and green mudstone and siltstone clasts are thought to be derived from

overlying sediments, possibly derived from what is the Gawler Craton in Australia (Doherty and Verbaas, 2018).

The Breccia zones on the Monster property are majorly heterolithic containing a variety of clast types ranging from siltstone, shale, dolostone, diorite, banded iron formation, chert and quartzite. The matrix of the Breccia is composed of clastic or soft sediments.

Alteration within the Wernecke Breccia is related to the immediate wall-rock and breccia clasts. Iron rich dolomite is common in the breccia zones and suggests some assimilation of the wall rock Gillespie Lake Group. Similarly, siderite is commonly associated with silica alteration in the dolomites and clastic Quartet Group rocks.

Hematite is present as both earthy hematite and specular hematite. Earthy hematite is common on the margins of the breccia zones with specular hematite occurring towards the centre and associated with diorite clasts.

Layered silica and carbonate is a common alteration style localised to dolomitic host rock. Magnetite is uncommon but when encountered occurs as blebs and may be locally massive within beds of dolomite clasts.

Mineralization occurs within and adjacent to the Wernecke Breccia and tends to be stringers of sulphide mineralization and/or disseminated sulphides. Mineralization is often associated with potassic alteration but can also occur in areas that have not undergone extensive or increased alteration.

3 STUDY DATA SET DETAILS

The data provided for this study included the following historical and recent data as illustrated by Figure 2.

3.1 AEROMAGNETIC AND RADIOMETRIC DATA

The 2018 aeromagnetic and radiometric survey completed by Precision Surveys and reprocessed and modelled by SGC was supplied by GMM for the study. This data included 3D inversion of the magnetic data using the UBC_GIF magnetic inversion software, and 2D magnetic modelling completed over a central magnetic high.

The radiometric data included the normal suite of radiometric processes, K, U, Th, K/Th, K/U, U/Th and a ternary plot of the data.

Details of the survey can be obtained from Appendix A.

3.2 GRAVITY DATA

Ground gravity data provided by GMM consisted of the data surveyed by GWH Resurvey over the period of 2001 to 2019. During this period approximately 1454 gravity readings were obtained including 70 repeat readings. All data, including historical data was reprocessed by MWH to current standards to ensure consistency within the data for the period of acquisition. As part of this program a detailed topographic survey was completed using drone technology. The drone DEM was then used to calculate the terrain correction and used in all subsequent 3D modelling.

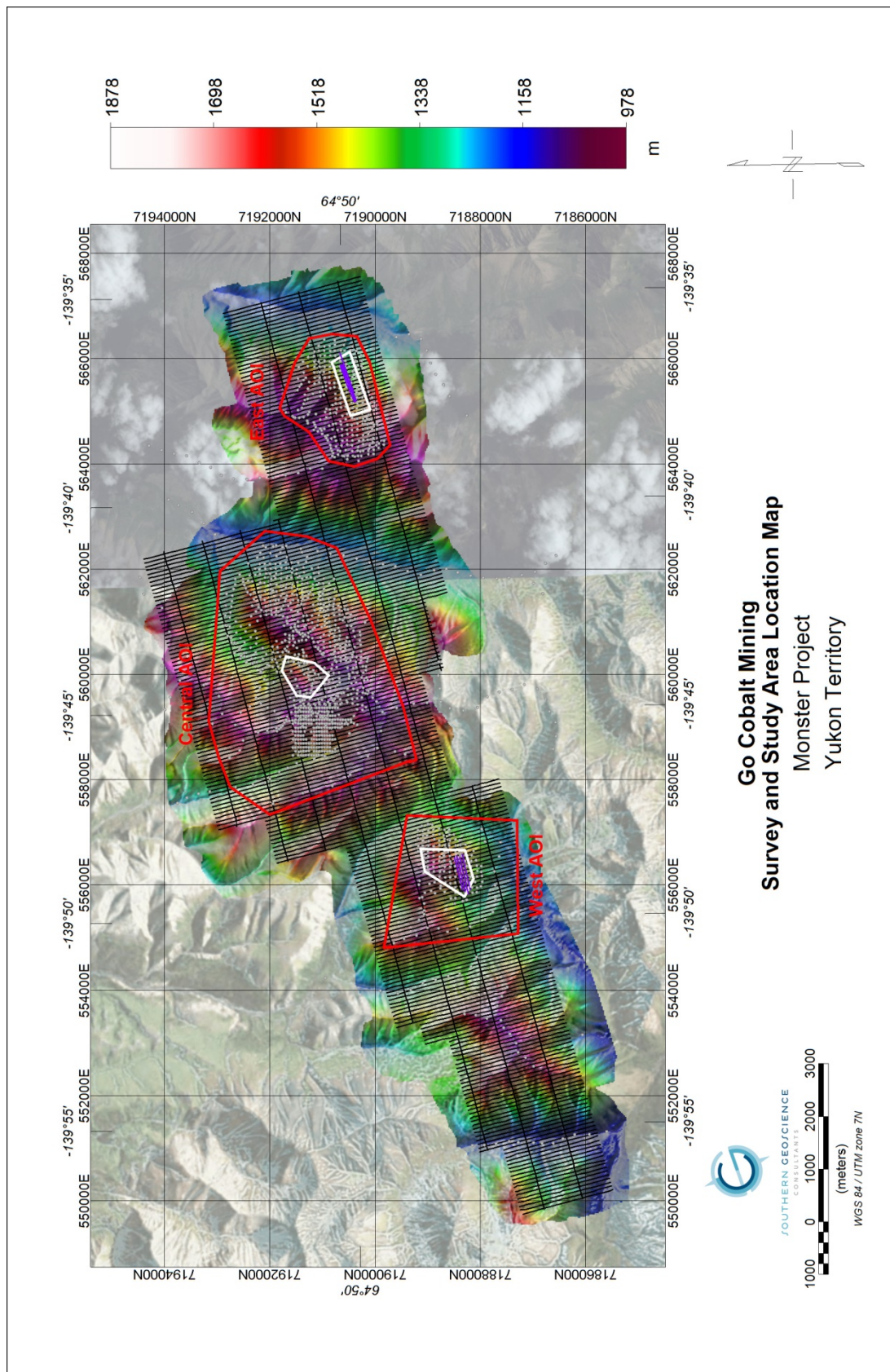


Figure 2: Survey and Study Area Location Map – Location of the various datasets used in the study are illustrated. Airborne survey flight (black), gravity sites (grey dots), DCIP lines (purple), GMM Areas Of Interest (AOI) (white), gravity detail study areas (red) on a drone DEM (masl) with a Bing satellite imagery background.

3.3 DC RESISTIVITY AND INDUCED POLARISATION DATA (DCIP)

DC resistivity and induced polarisation (DCIP) data for eight short test lines (two grids of four lines) and accompanying 3D inversions were provided by GMM. Verification of the inversion results was completed by SGC. The survey was completed by GroundTruth Exploration Inc. of Dawson City, YT using the Super Sting system utilizing a 30 m TX dipole and 10 m Rx dipole.

Four lines were completed in the West AOI and 4 Lines were completed in the East AOI. The design of the survey was optimized for the centre of the array used. In general, the results were such that the survey did not look deep enough over a broad enough area to effectively sample the magnetic and or density anomalies in these areas

3.4 ROCK PHYSICAL PROPERTY DATA

During the 2001 and 2002 field season drill core samples were obtained and density measurements were completed. This data was supplemented by more recent grab/float sampling by GMM. There is a major discrepancy in the two data sets collected. The historical data collected by Monster Copper from the one drill hole completed tends to have a higher average density (2.73 g/cm^3 ; Table 1) whereas the average density of the rock samples collected by GMM have an average density of 2.58 g/cm^3 (Table 2). The discrepancy could largely be due to selective sampling methodology used by the various companies and the methodology applied for the determination of the properties. As a result, for the 3D gravity modelling applied in this study a background density of 2.67 g/cm^3 .

Table 1 – Rock Physical Properties from 2001-2002 (After Setterfield and Tykajlo, 2003)

Depth (m)	Rock Type	Density gcm^{-3}	Magnetic Susceptibility	Depth (m)	Rock Type	Density gcm^{-3}	Magnetic Susceptibility
12.5	Shale	2.73	0.10	114.63	Wernecke Bx	2.70	0.54
28.66	Shale	2.71	0.10	123.78	Wernecke Bx	2.77	0.27
44.51	Shale	2.72	0.07	129.84	Diorite	2.86	3.12
50.61	Shale	2.67	0.03	137.16	Wernecke Bx	2.80	0.21
56.71	Shale	2.70	0.07	142.65	Wernecke Bx	3.13	0.20
56.71	Wernecke Bx	2.69	0.07	145.39	Wernecke Bx	2.74	0.16
70.27	Wernecke Bx	2.73	1.00	148.44	Wernecke Bx	2.77	0.91
73.48	Wernecke Bx	2.65	0.34	160.32	Wernecke Bx	2.72	0.54
79.12	Wernecke Bx	2.79	1.15	166.42	Wernecke Bx	2.77	0.16
85.06	Wernecke Bx	2.75	0.21	170.08	Wernecke Bx	2.76	0.67
88.11	Wernecke Bx	2.70	0.14	178.00	Wernecke Bx	2.68	0.38
96.34	Wernecke Bx	2.73	0.16	181.05	Wernecke Bx	2.86	0.32
101.52	Wernecke Bx	2.80	1.09	184.4	Wernecke Bx	2.84	0.21
107.32	Wernecke Bx	2.84	2.45	188.98	Wernecke Bx	2.87	03.2
107.32	Wernecke Bx	2.84	2.45	194.46	Wernecke Bx	2.82	0.25

Table 2 – Rock Physical Properties from 2018/19 (from GMM)

Field Sample ID	Sample ID	Location Type (Borehole/Outcrop/Subcrop/Float)	Lithological_Unit	Bulk Density (ρB, ρB') [g/cm ³]	Magnetic Susceptibility
19MO-001A	1795901	Float/Subcrop	WBX	2.32	0.0634
19MO-001B	1795902	Float/Subcrop	WBX	2.45	0.4032
19MO-001C	1795903	Float/Subcrop	WBX	2.73	0.026
19MOJ-01	1795904	Float/Subcrop	WBX	2.46	0.1084
19MOJ-02	1795905	Float/Subcrop	WBX	2.23	0.3832
19MO-003	1795906	Float/Subcrop	INT	2.82	2.968
19MOJ-03	1795907	Float/Subcrop		2.51	0.3508
19MOJ-04	1795908	Float/Subcrop	WBX	2.59	0.189
19MOJ-05	1795909	Float/Subcrop		2.58	58.76
19MO-05	1795910	Float/Subcrop		2.56	0.2568
19MOJ-06	1795911	Float/Subcrop		2.57	0.2508
19MOJ-07	1795912	Float/Subcrop	WBX	2.28	0.1804
19MO-007	1795913	Float/Subcrop		2.57	0.1908
19MOJ-08	1795914	Float/Subcrop	WBX	2.73	0.2508
19MOJ-09	1795915	Float/Subcrop	WBX	2.69	0.2664
19MOJ-10	1795916	Float/Subcrop	WBX	2.61	0.2056
19MOJ-11	1795917	Float/Subcrop	WBX	2.71	0.3188
19MOJ-12	1795918	Float/Subcrop	WBX	2.71	0.1626
19MOJ-13	1795919	Float/Subcrop	WBX	2.72	7.506
19MOJ-14	1795920	Float/Subcrop		2.66	0.191
19MOJ-15	1795921	Float/Subcrop		2.50	0.203
19MOJ-16	1795922	Float/Subcrop		2.70	0.1526
19MO-16	1795923	Float/Subcrop		2.72	0.3838
19MOJ-17	1795924	Float/Subcrop		2.61	0.1004
19MOJ-18	1795925	Float/Subcrop		2.40	0.0426
19MOJ-19	1795926	Float/Subcrop		2.65	0.37
19MO-025	1795927	Float/Subcrop	INT	2.62	5.372
19MO-63	1795928	Float/Subcrop		2.68	0.2086

4 GRAVITY DATA INVERSION

The data was inverted using the Geosoft™ VOXI gravity inversion program. The VOXI inversion uses a right rectangular prism method whereby prisms are increased in thickness with depth based on the rate of fall off with distance from the source of the parameter being inverted. In the case of gravity, this fall-off rate is $1/r^2$ where “r” is the distance from the measurement device. This results in the increasing voxel element size with depth in VOXI. The inputs into the VOXI inversion process are the residual gravity and digital elevation model for a given area. The output is a 3D representation of the spatial distribution and amplitude of the density. The reported values are the difference from the Bouguer density used to reduce the input data (i.e. Bouguer density = 2.67 g/cc, VOXI will report the difference in density from the Bouguer density).

An unconstrained inversion, allowing for the inversion routine to complete a “best fit” smooth model to the gravity data was completed on the gravity data. A total of four gravity inversion models were completed as follows:

1. Inversion on a regional scale of the contiguous portion of the collected gravity data
2. Three smaller detail inversion areas referred to as the:
 - a. East Area Of Interest
 - b. Central Area of Interest
 - c. West Area of Interest

The valid depth limit for all inversions is approximately -1500m asl. Below this depth higher frequency noise is observed in the inversion.

For the entire project area, the voxel X, Y dimensions were 52.5 m; for the detail study area analysis, the voxel X, Y dimensions were variable dependent on the size of the area to be inverted and ranged 11 m to 22 m. The vertical discretization started with a voxel thickness of 25 m for the regional inversion and 5 m for the detailed inversions and expanded logarithmically with depth.

5 RESULTS AND INTERPRETATION

The following discussion will consist of a discussion of the results of property wide data and inversions followed by a discussion of each of the Areas of Interest (AOI) as defined by GMM.

It is important to note that there is no evidence that this part of the Yukon Territory has undergone glaciation in the last 60,000 years. As a result, the weathering of the rock is accepted as occurring in-situ with mobility down slope and existing drainage.

5.1 PROPERTY COVERAGE

The property wide coverage of the ground gravity data is illustrated by Figure 3. Due to the topography, the more “regional” transects are confined to valley floors and/or mountain ridges and peaks. The overall topographic dynamic range is approximately 1100 m, from a low of 905 masl to a high of 2030 masl. The topography is dominated in places by cirques carved by local alpine glaciers into the Wernecke mountain range although the area was not covered by continental glaciers. A higher density of gravity sites was often facilitated by these cirques.

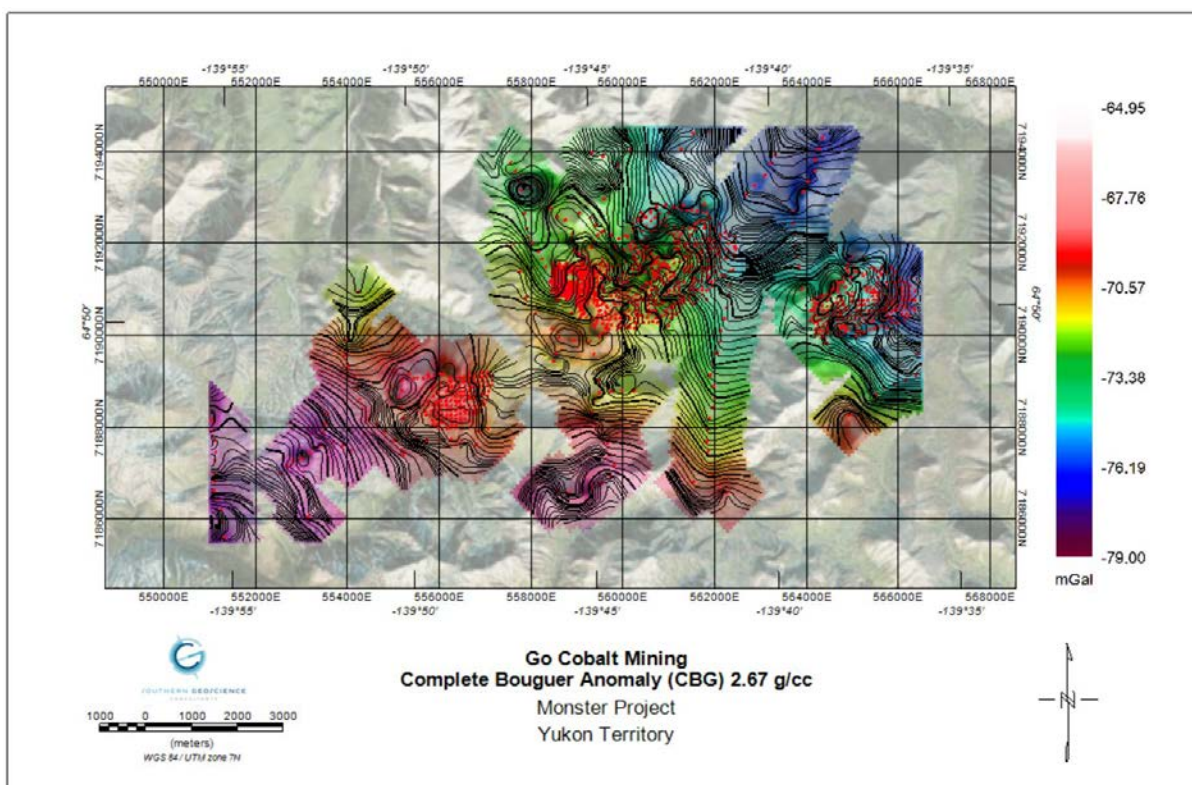


Figure 3: Complete Bouguer Gravity Anomaly (CBA) for Bouguer Density 2.67g/cm^3 . Gravity sites are indicated by red dots. Contour interval is 0.04, 0.2 and 1.0g/cm^3 . On a Bing satellite image base.

Overlaying the Complete Bouguer Gravity Anomaly (CBA) contours onto the drone DEM topographic base (Figure 4), there is a positive correlation between gravity local gravity highs with peaks and ridges and gravity lows with the incised valleys and watercourses. Terrain corrections applied for the near gravity site area from 0 m to 2500 m account for up to 30% of the CBA. On the project scale there is potentially a significant terrain effect present in the data.

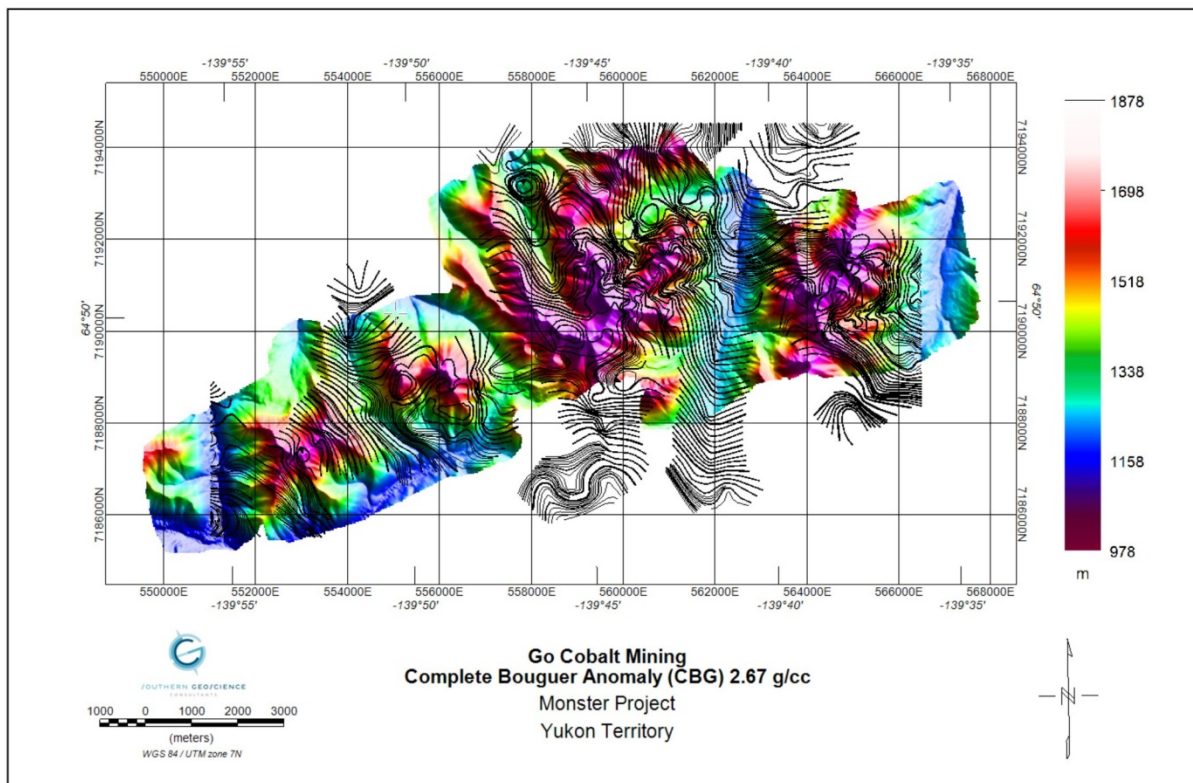


Figure 4: CBA 2.67g/cm³ contours (0.04, 0.2 and 1.0 g/cm³) overlain on drone DEM image.

The first vertical derivative (1VD) of the CBA, when displayed with DEM contours (Figure 5), particularly in areas of more dense gravity sampling, appears to be reflecting lithology in the near surface that is outcropping/sub-cropping at a given elevation. The central area appears to have 1VD lineations that are cross-cutting to the topography.

Examination of the analytic signal of the CBA (Figure 6) in comparison to the DEM contours also exhibits lineations that are cross-cutting to the topography, particularly in areas where the density of gravity sites is high. The analytic signal image also exhibits edge effects and some aliasing of the gravity signal in areas of low gravity site density.

The Tilt Derivative of the CBA (TDR) results in a similar presentation as the 1VD in that it appears to be indicating lithology in the near surface that is outcropping/sub-cropping at a given elevation (Figure 7). In areas of dense gravity sites, the TDR is defining several short and discrete positive features that are at times cross-cutting the topography. In the sparsely sampled areas there is a strong aliasing effect visible in the image (stipple-like texture). This is an artefact related to the data sample density and can be ignored.

Comparing the CBA contours with the RTP TMI of the airborne survey (Figure 8), there is correlation between discrete magnetic highs and CBA highs, suggesting that not all of the gravity anomalies are

unduly influenced by the topography. There is also some correlation between magnetic lows and gravity lows, particularly in the west and north of the project area. A strong correlation of a broad magnetic high with the pronounced gravity low (52000E, 7186000N to 562500E, 71892000N) is visible. This feature correlates to a well-developed valley in the DEM topography.

Combining the airborne radiometric data (Figures 9, 10, 11 and 12) with the CBA contours, it is apparent that areas of steep gravity gradient correspond to areas where the rocks appear to be depleted in Thorium. This is in contrast to the valley floors and watercourses that tend to be enriched in Thorium. Ridges tend to be higher in Potassium than the surrounding slopes. Uranium appears to be enriched along a NW-SE trend in the extreme west of the CBA coverage. A similar, more E-W oriented trend is observed and a gravity low in the eastern half of the area, transected by a strong U and Th feature in the valley is defined by the gravity traverse and gravity low running from 52000E, 7186000N to 562500E, 71892000N.

The 3D inversion of the CBA data was completed using the drone DEM windowed to the extent of the gravity surveys. The voxel size used for the inversion was 52.5 m in X and Y and thickness increasing logarithmically with depth from 25 m to 215 m over a vertical extent of ~4km. The 25 m voxel thickness was maintained for the topographic dynamic range of ~ 1000 m. Density iso-surfaces have been prepared at an increment of 0.05g/cm³ over the range 2.67 g/cm³ to 3.07 g/cm³. A 3D perspective image of the 0.05g/cm³ iso-surface (density of 2.72 g/cm³ and greater; Figure 10) illustrates the potential extent of the Wernecke Breccia from surface to depth. The iso-surface correlates well to the mapped fault structures provided by GMM. Offsetting faults mapped at surface correspond to offsets in the iso-surface. The inversion suggests, in general, that in the near surface the N-S to NNW-SSE family of faults are sub-vertical to E-NE dipping and the E-W to ENE-WSW family of faults are sub-vertical to south dipping. As the density contrast is increased, the iso-surfaces contract, becoming smaller in extent, but are still in the near surface and may in places outcrop (Figure 11).

There appears to be three (3) main density anomalous zones correlating to the three AOI as defined by GMM. The zones have been designated as East AOI, Central AOI (formerly the west AOI in earlier documents) and the West AOI. All three density zones appear to be sub-vertical, potentially outcropping/subcropping in the very near-surface. The three density zones have been inverted individually using a significantly tighter voxel size and will be discussed in the following sections.

In the East AOI area, the project wide gravity inversion appears to flank the AOI to the north. In the Central AOI area, the density anomalies appear to envelope the AOI. The West AOI differs from the East AOI and Central AOI in that it is the smallest of three, at the lowest apparent elevation and has density anomalies (two) within the original bounds of the AOI.

Adding the 2D magnetic modelling and 3D susceptibility iso-surfaces to the CBA inversion is illustrated by Figure 12. The 3D susceptibility inversion may be more stratigraphically constrained than the gravity iso-surfaces as the magnetic iso-surfaces appear to be more sub-horizontal in the central part of the project area (Central AOI). In the area of the East AOI, there is some overlap between the 2D model results and the 3D inversion iso-surfaces; however the density anomalies

appear to flank the magnetic anomaly. In the West AOI, there is very good correlation to the gravity and magnetic iso-surfaces.

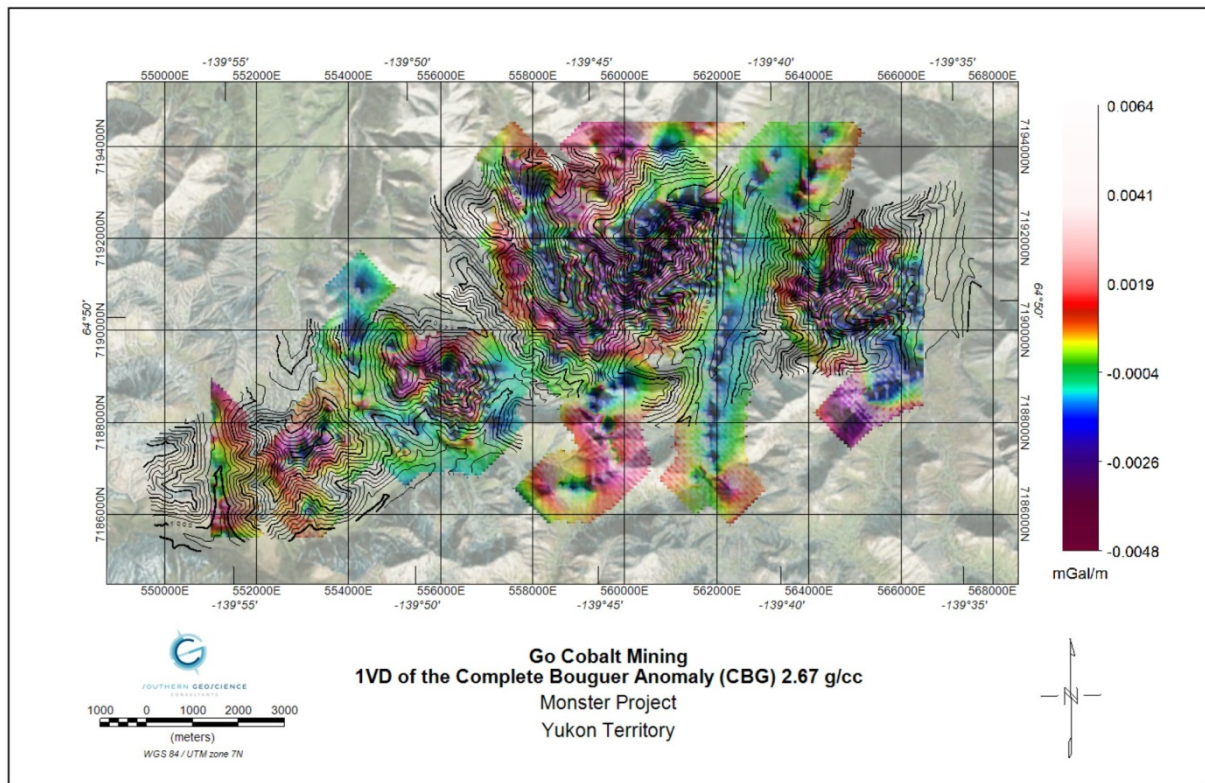


Figure 5: 1VD of the CBA 2.67 g/cm^3 overlain with drone DEM contours (50/250/1000 m) ON a Bing satellite image base.

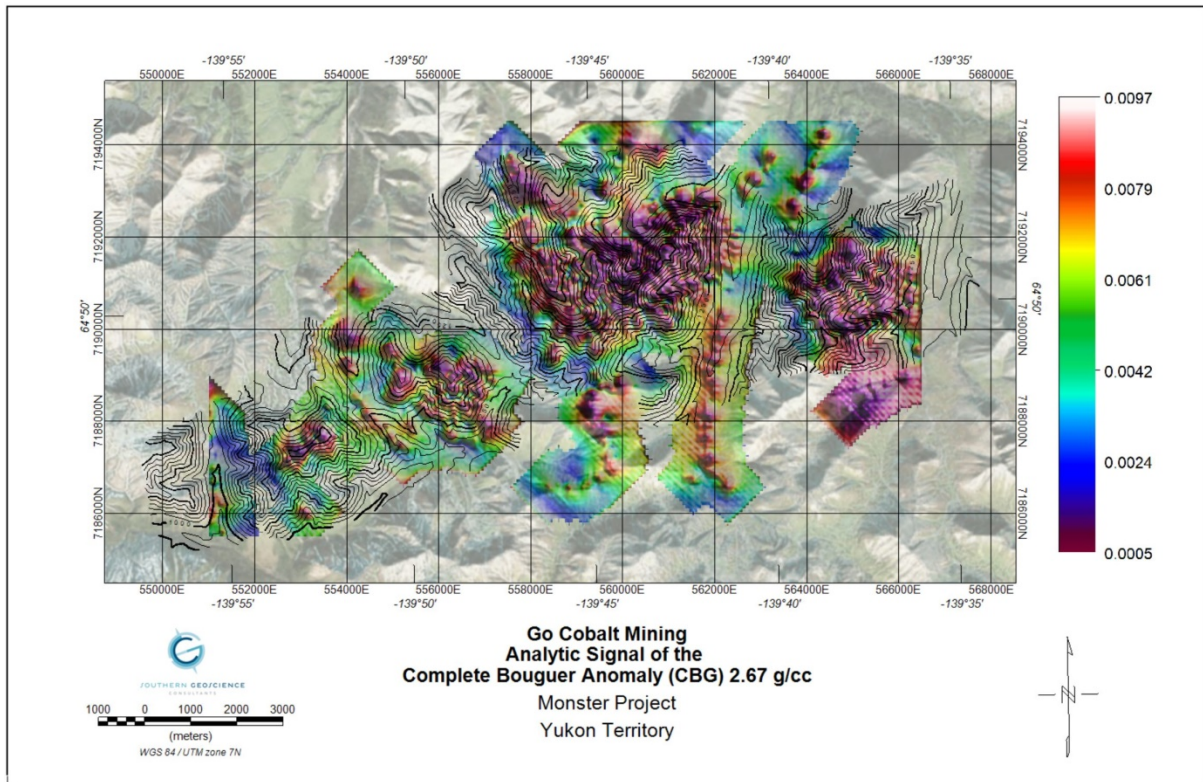


Figure 6: Analytic Signal of the CBA 2.67 g/cm^3 overlain with drone DEM contours (50/250/1000 m) ON a Bing satellite image base.

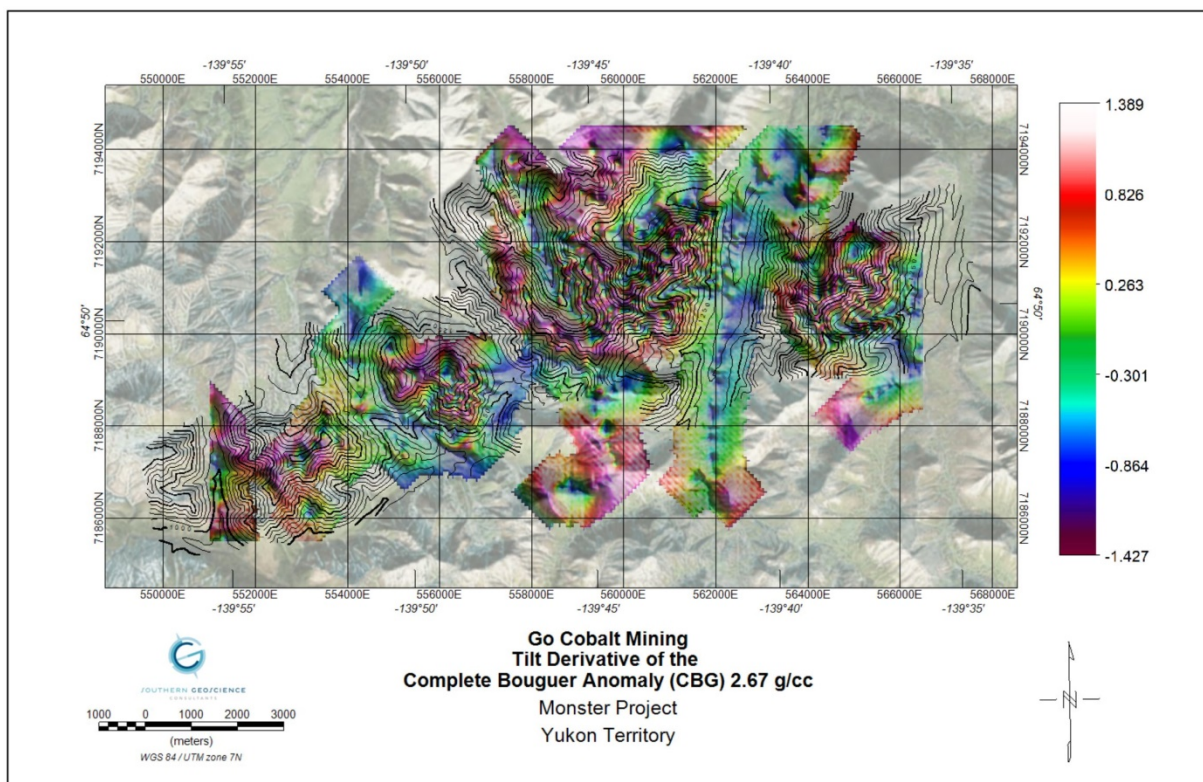


Figure 7: Tilt Derivative of the CBA 2.67 g/cm^3 overlain with drone DEM contours (50/250/1000 m) on a Bing satellite image base.

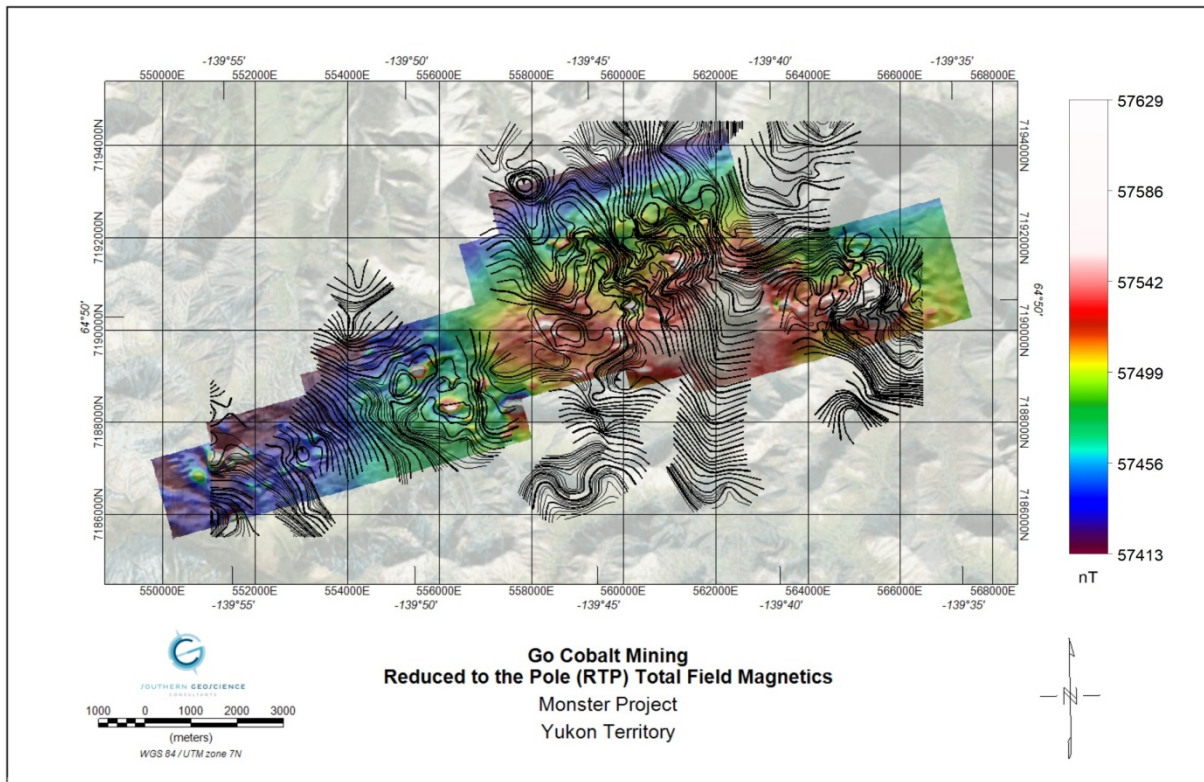


Figure 8: Reduced to the Pole (RTP) total magnetic intensity (TMI) from the airborne survey with contour overlay of the CBA $2.67\text{g}/\text{cm}^3$ on a Bing satellite image base.

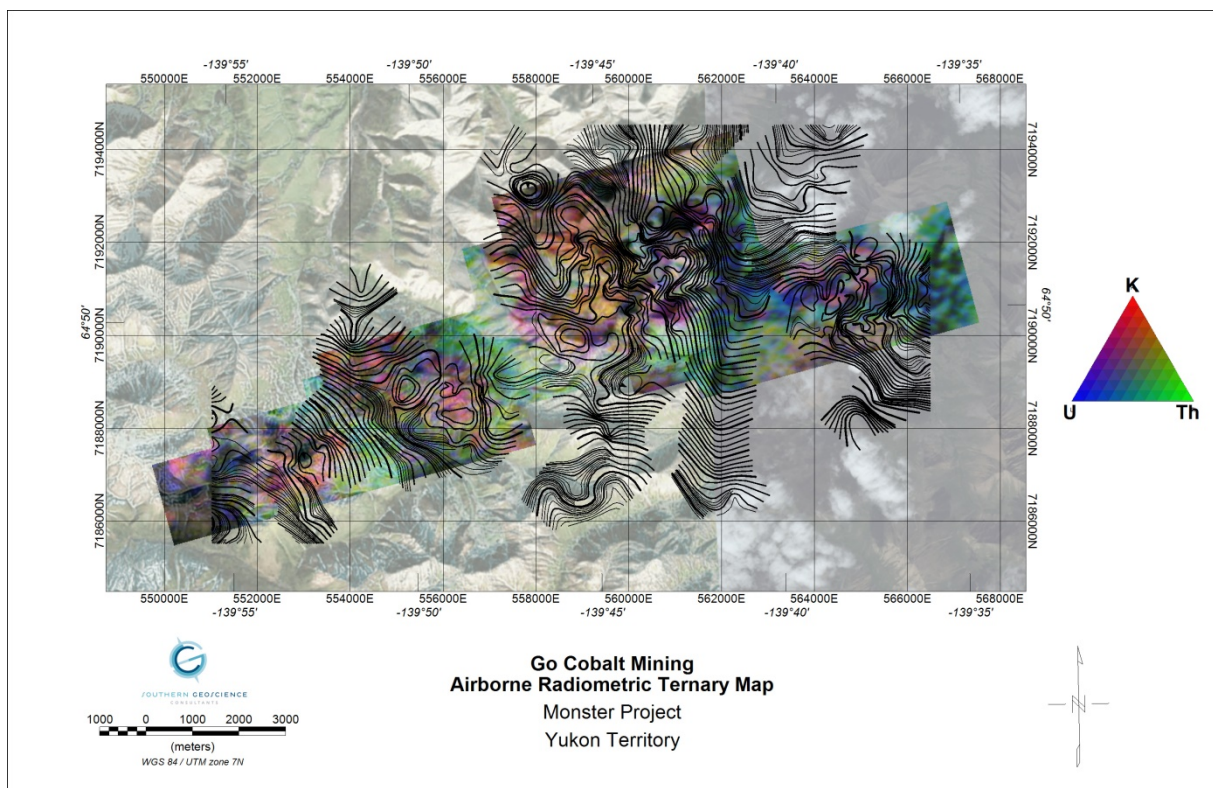


Figure 9: Airborne radiometric ternary plot with contour overlay of the CBA $2.67\text{g}/\text{cm}^3$ on a Bing satellite image base.

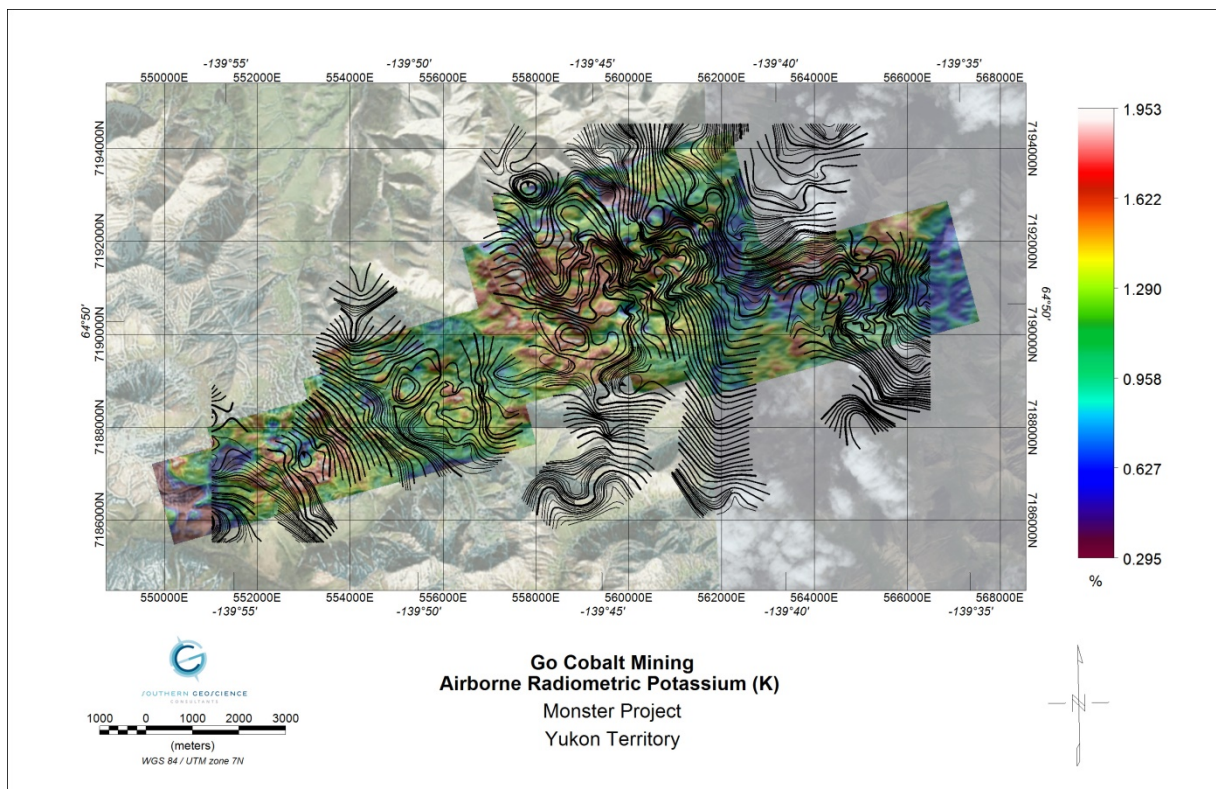


Figure 10: Airborne radiometric Potassium (K) with contour overlay of the CBA 2.67g/cm^3 on a Bing satellite image base.

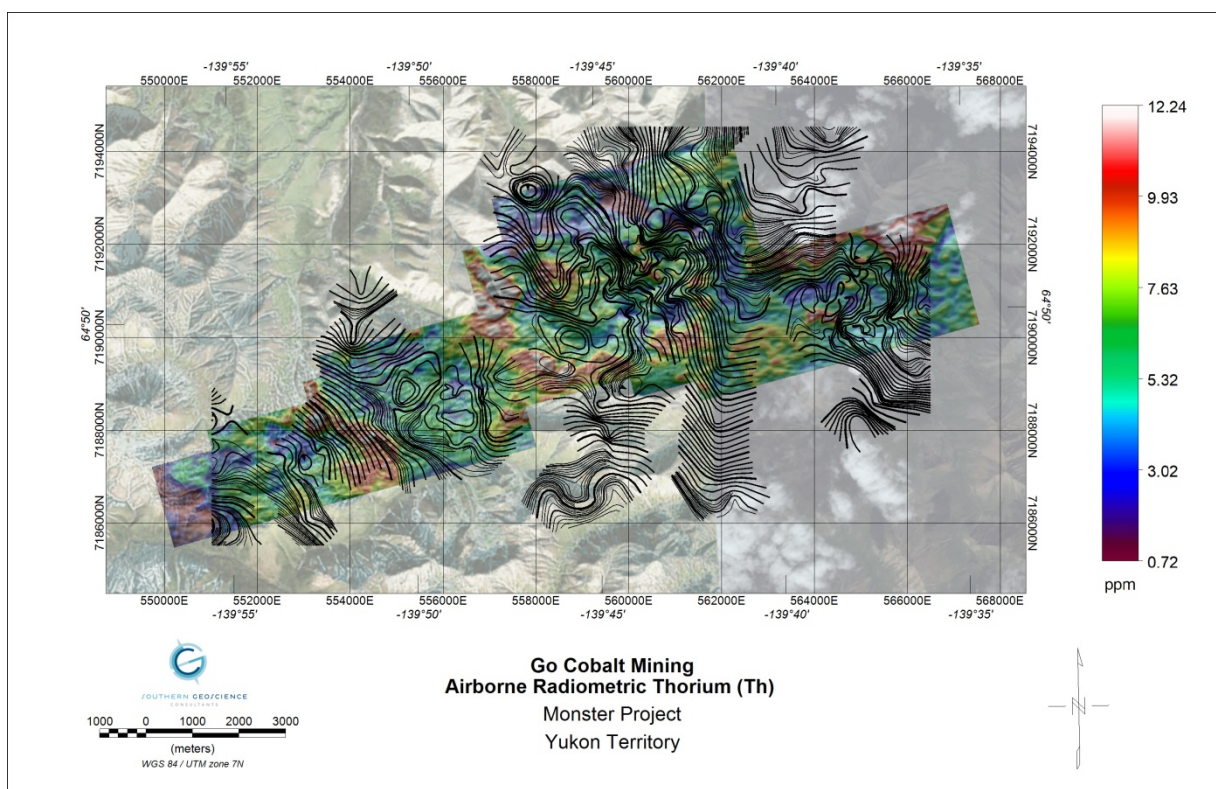


Figure 11: Airborne radiometric Thorium (Th) with contour overlay of the CBA 2.67g/cm^3 on a Bing satellite image base.

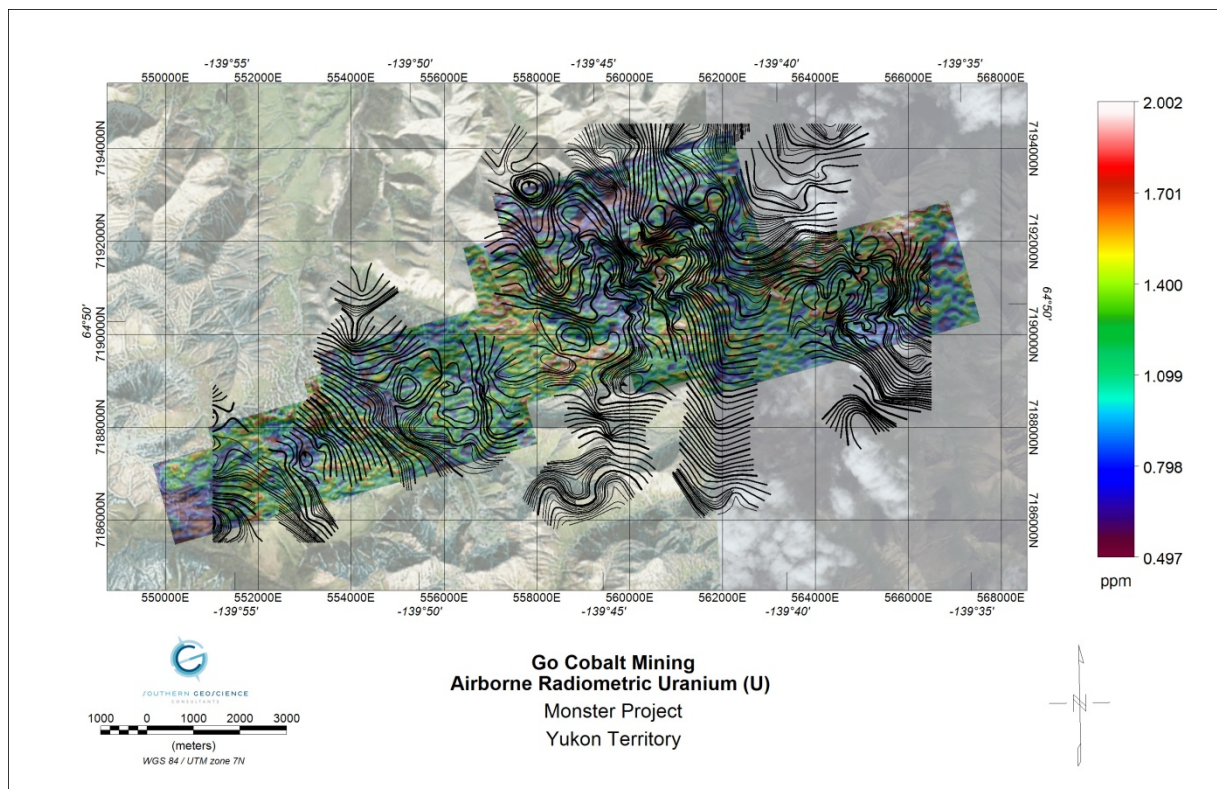


Figure 12: Airborne radiometric Uranium (U) with contour overlay of the CBA 2.67g/cm^3 on a Bing satellite image base.

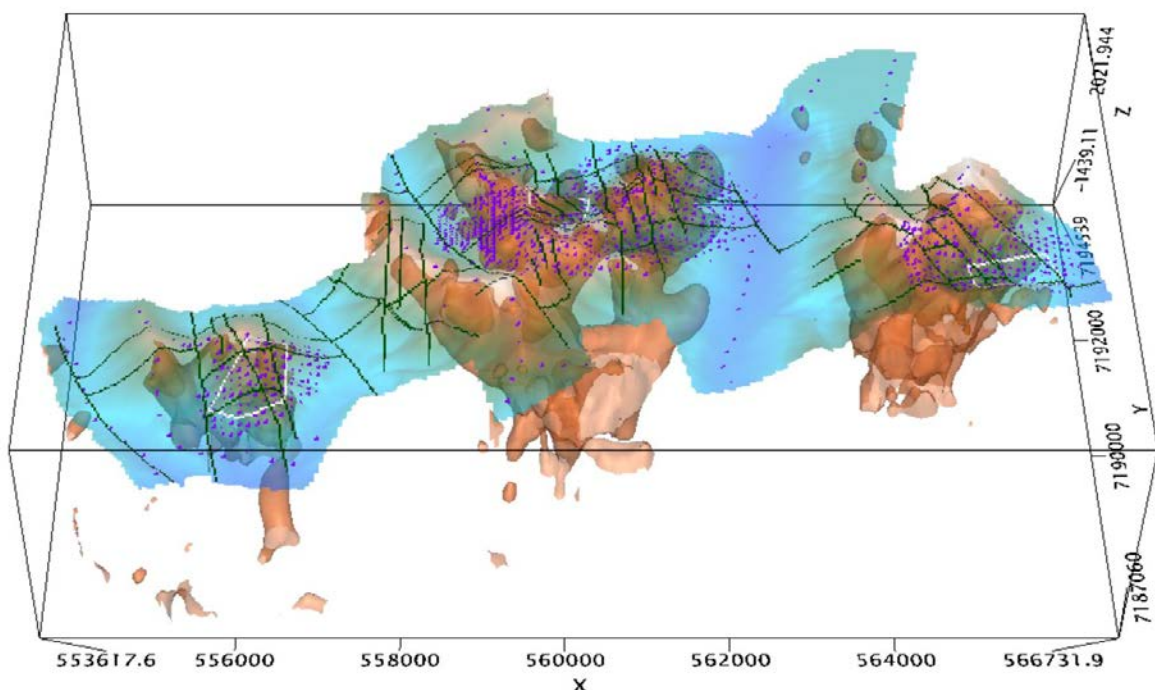


Figure 13: 3D Voxi inversion of the CBA 2.67g/cm^3 data. View is looking north. The iso-surface/shell for a density contrast of 0.05 g/cm^3 (corresponding to a density of 2.72 g/cm^3) shown. Topographic surface (drone DEM) is plotted in addition to surface mapped faults (green lines), gravity measurement sites (purple dots) and GMM defined AOI (white polygons).

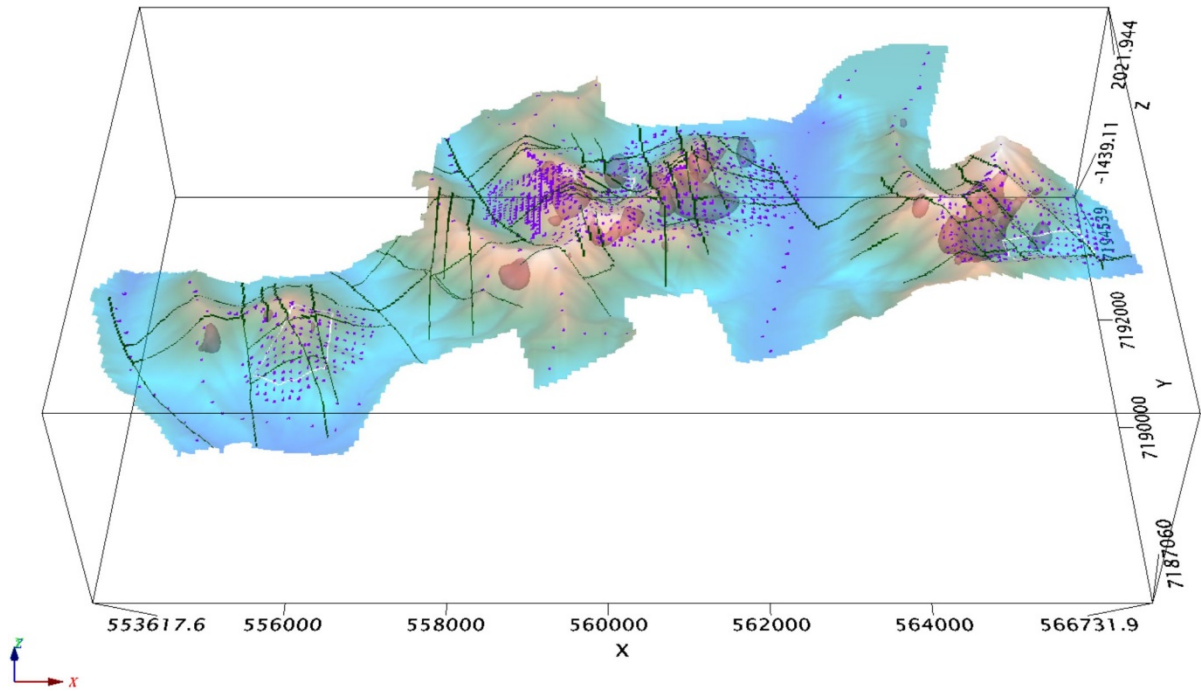


Figure 14: 3D Voxi inversion of the CBA 2.67g/cm³ data. View is looking north. The iso-surface/shell for a density contrast of 0.15 g/cm³ (corresponding to a density of 2.82 g/cm³) shown. Topographic surface (drone DEM) is plotted in addition to surface mapped faults (green lines), gravity measurement sites (purple dots) and GMM defined AOI (white polygons).

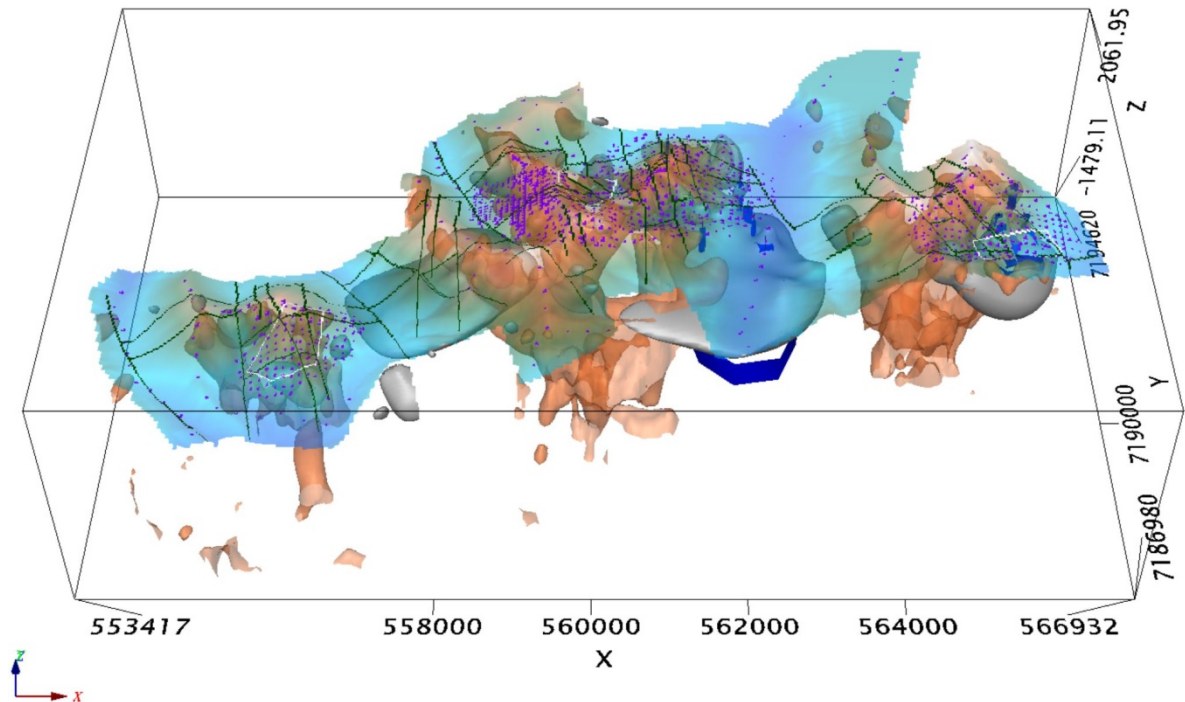


Figure 15: 3D Voxi inversion of the CBA 2.67g/cm³ data. View is looking north. The iso-surface/shell for a density contrast of 0.05 g/cm³ (corresponding to a density of 2.72 g/cm³) shown. Magnetic susceptibility iso-surface (0.0028 SI; grey surfaces) and 2D modelling results (dark blue) are plotted. Topographic surface (drone DEM) is plotted in addition to surface mapped faults (green lines), gravity measurement sites (purple dots) and GMM defined AOI (white polygons).

5.2 WEST AREA OF INTEREST

The West AOI is defined by a central, discrete CBA anomaly of approximately 1.4 mGal amplitude (Figure 16). The anomaly is EW striking and is fault controlled, bounded by mapped geologic faults to the west, east and north. The main anomaly has been covered by a loose grid of gravity sites on a nominally 100m grid of stations. The AOI was enlarged beyond the detail grid in order to minimize aliasing during the 3D inversion process.

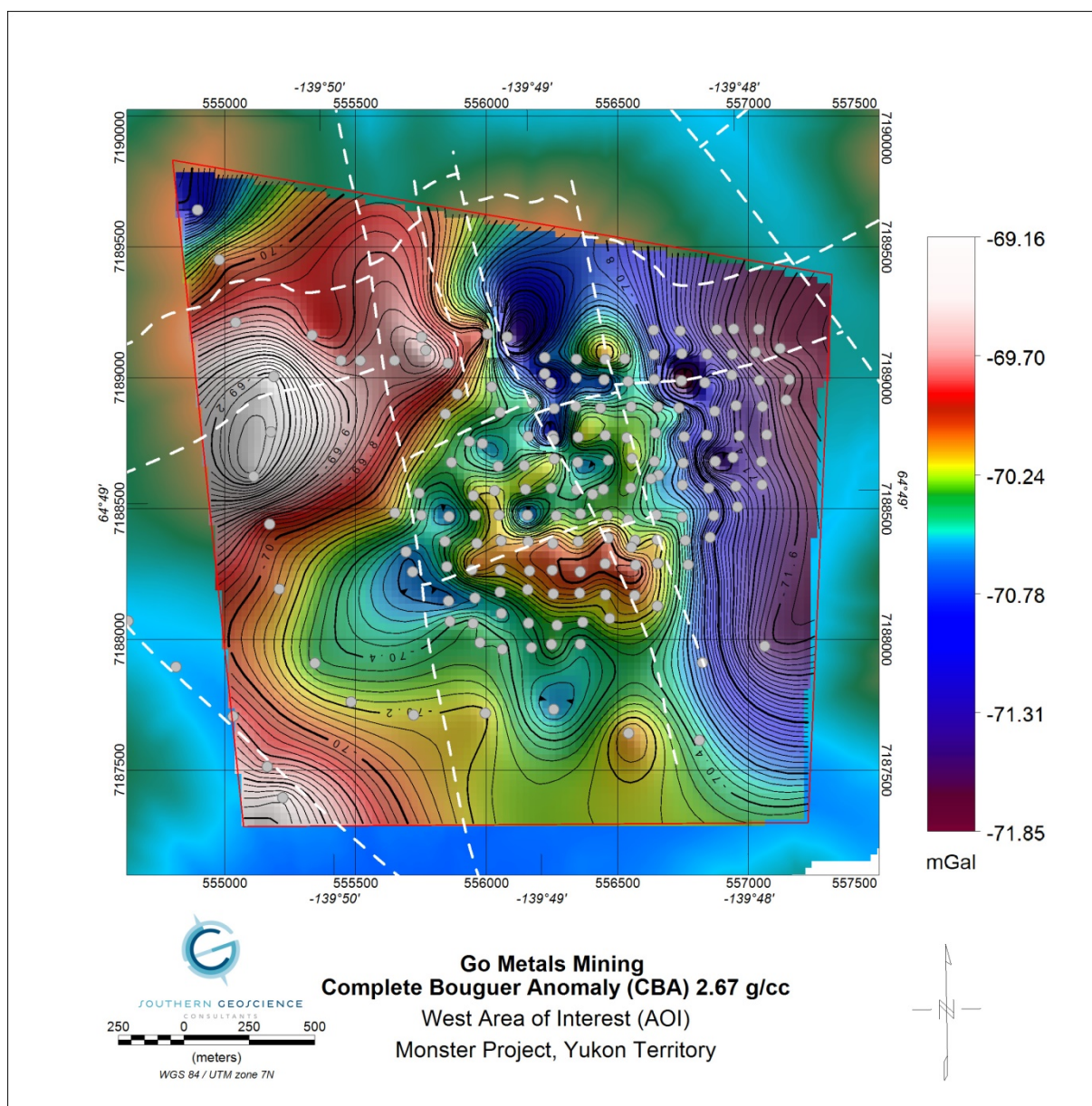


Figure 16: West AOI Complete Bouguer Gravity Anomaly (CBA) for Bouguer Density 2.67g/cm^3 . Gravity sites are indicated by grey dots. Contour interval is 0.04, 0.2 and 1.0g/cm^3 . Mapped geologic faults (dashed white lines) are plotted. Background is drone DEM grid.

Topographically, the central portion of the AOI is a high (Figure 17). The central gravity anomaly is coincident with a small topographic shelf on the south side of a small mountain. The crest of the mountain is coincident with several smaller, lower amplitude gravity anomalies defined by three to

five gravity sites. The density body associated with these anomalies is thought to be in the shallow sub-surface.

The first vertical derivative of the CBA (Figure 18) highlights the correlation between the density anomaly and the mapped geologic faults. The general NNE-SSW trend of the main set of faults is mimicked by the trend of the 1VD. The set of ENE-WSW mapped faults correlates to offsets observed in the 1VD data. This suggests the density anomalies may be the product of metamorphic activity and related alteration products.

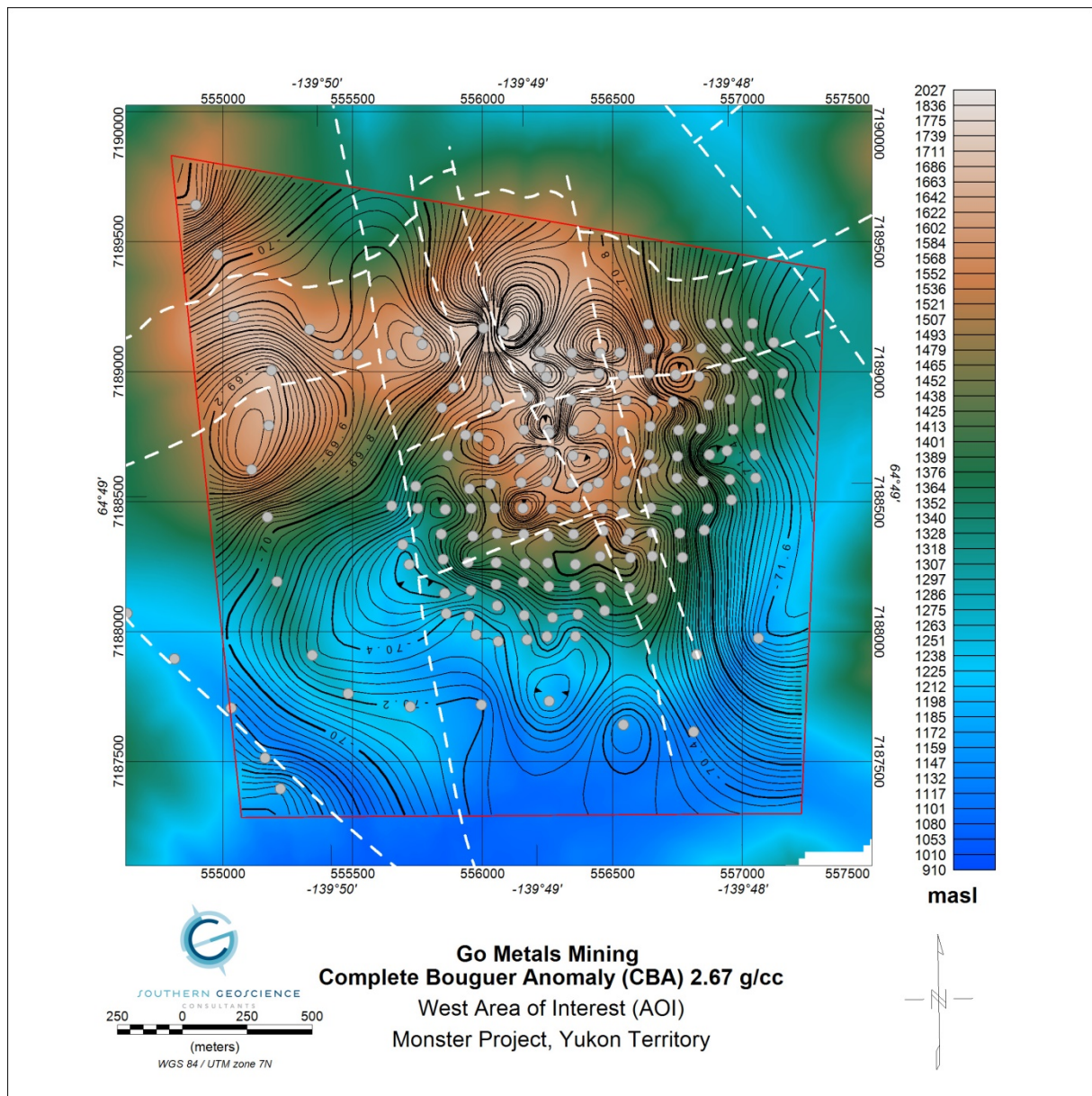


Figure 17: West AOI Complete Bouguer Gravity Anomaly (CBA) for Bouguer Density 2.67g/cm^3 . Gravity sites are indicated by grey dots. Contour interval is 0.1, 0.5 and 2.5g/cm^3 . Mapped geologic faults (dashed white lines) are plotted. Background is drone DEM grid.

The analytic signal of the CBA (Figure 19) highlights the fault controlled, square to circular aspect of the cluster of near surface density anomalies predominately on the south slope of the mountain.

The tilt derivative (Figure 20) further reinforces that the sources of the density anomalies are in the near-surface. There is the suggestion that the density bodies are not only fault controlled, but also may have undergone folding.

There is very good correlation between the RTP magnetics and the CBA (Figure 21). There are three dominant magnetic anomalies for which there is a coincident or slightly offset CBA anomaly. Implication is that there is some zonation and/or a unit that is both dense and magnetic.

The airborne radiometric survey data (Figures 22 to 25) indicates a strong Potassium component to the gravity anomalies observed in this AOI. Thorium is dominant along the NE slope of the AOI. A relatively strong uranium response is observed sub-parallel to and to the NE of the mapped fault striking NW-SE in the SW corner of the AOI.

The 3D inversion of the CBA data for the West AOI was completed using the drone DEM windowed to the extent of the AOI polygon. The voxel size used for the inversion was 10.5 m in X and Y and thickness increasing logarithmically with depth from 5 m to 93 m over a vertical extent of ~2.6km. The 5 m voxel thickness was maintained for the topographic dynamic range of ~1000 m. Density iso-surfaces have been prepared at an increment of 0.025g/cm³ over the range 2.67 g/cm³ to 2.82 g/cm³ and by increments of 0.05 g/cm³ over the range from 2.82 g/cm³ to 2.97 g/cm³. A 3D perspective image of the 0.075g/cm³ iso-surface (density of 2.745 g/cm³ and greater; Figure 26) illustrates the potential extent of the Wernecke Breccia from surface to depth. The iso-surface correlates well to the mapped fault structures provided by GMM, which tend to bound and divide the iso-surface. Offsetting faults mapped at surface correspond to offsets in the iso-surface. The inversion suggests, in general, that in the near surface the N-S to NNW-SSE family of faults are sub vertical and the E-W to ENE-WSW family of faults are sub vertical to south dipping. As the density contrast is increased, the iso-surfaces contract, becoming smaller in extent, but are still in the near surface and may in places outcrop (Figure 27).

Adding the 2D magnetic modelling and 3D susceptibility iso-surfaces to the CBA inversion is illustrated by Figure 28. The 3D susceptibility inversion bodies tend to flank or be flanked by the density inversion bodies. The main difference between the 3D inversion models is that the susceptibility inversion models tend to be restricted to within the near surface whereas the CBA inversion models are suggesting that the anomalous density material extends to depth.

The DCIP survey conducted over the central part of the AOI did not look deep enough to be able to definitively sample the magnetic body in this area. The lines were also too short (at each end) to sample the dense gravity anomalies present at the ends of the lines. The survey was further hampered by the fact the northerly lines were subparallel to a mapped fault cutting through the DCIP grid.

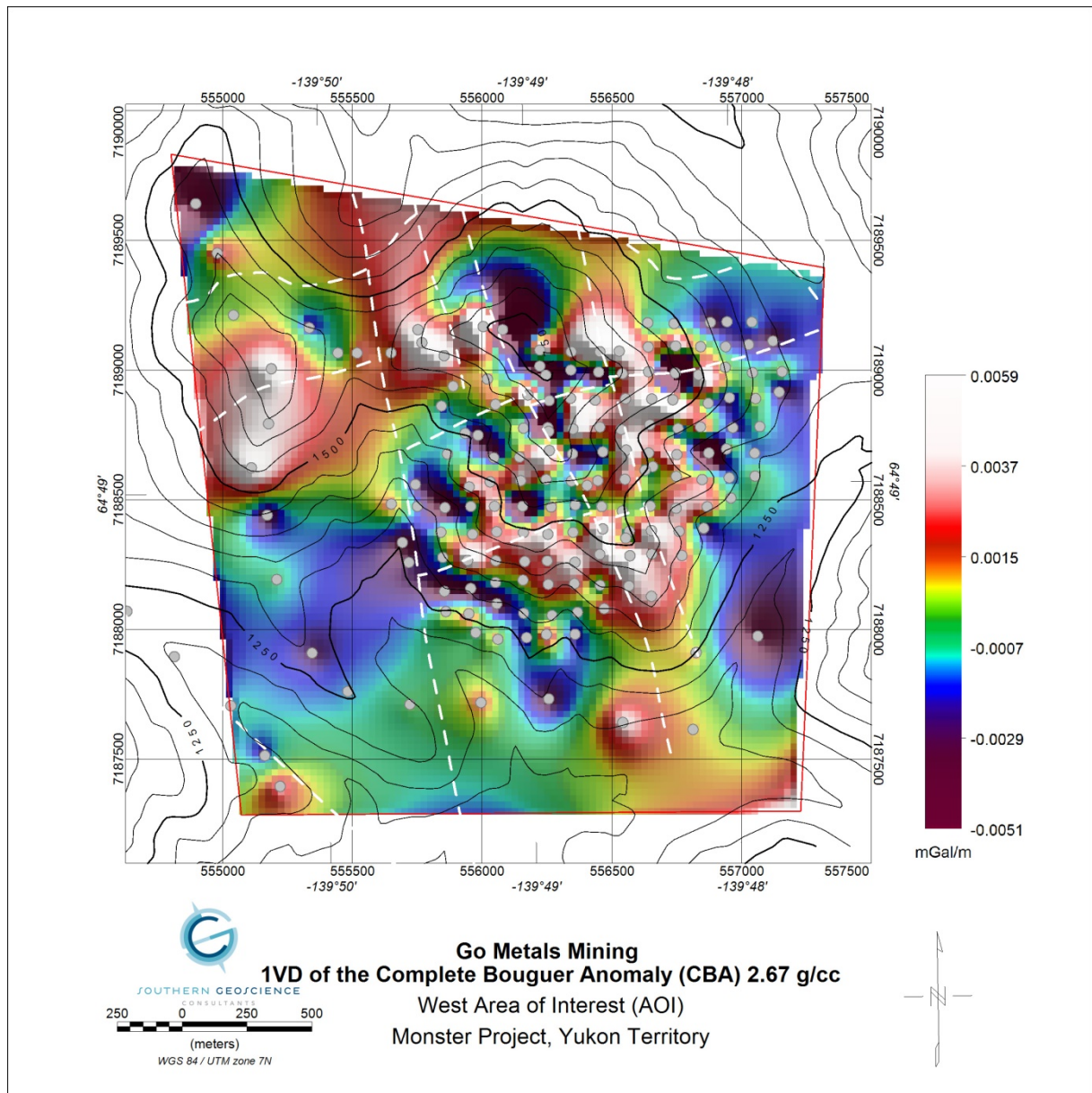


Figure 18: West AOI 1VD of the Complete Bouguer Gravity Anomaly (CBA) for Bouguer Density 2.67g/cm^3 . Gravity sites are indicated by grey dots. Mapped geologic faults (dashed white lines) are plotted. Background contours (50/250/1000 m) are elevations from the drone DEM grid in units of masl.

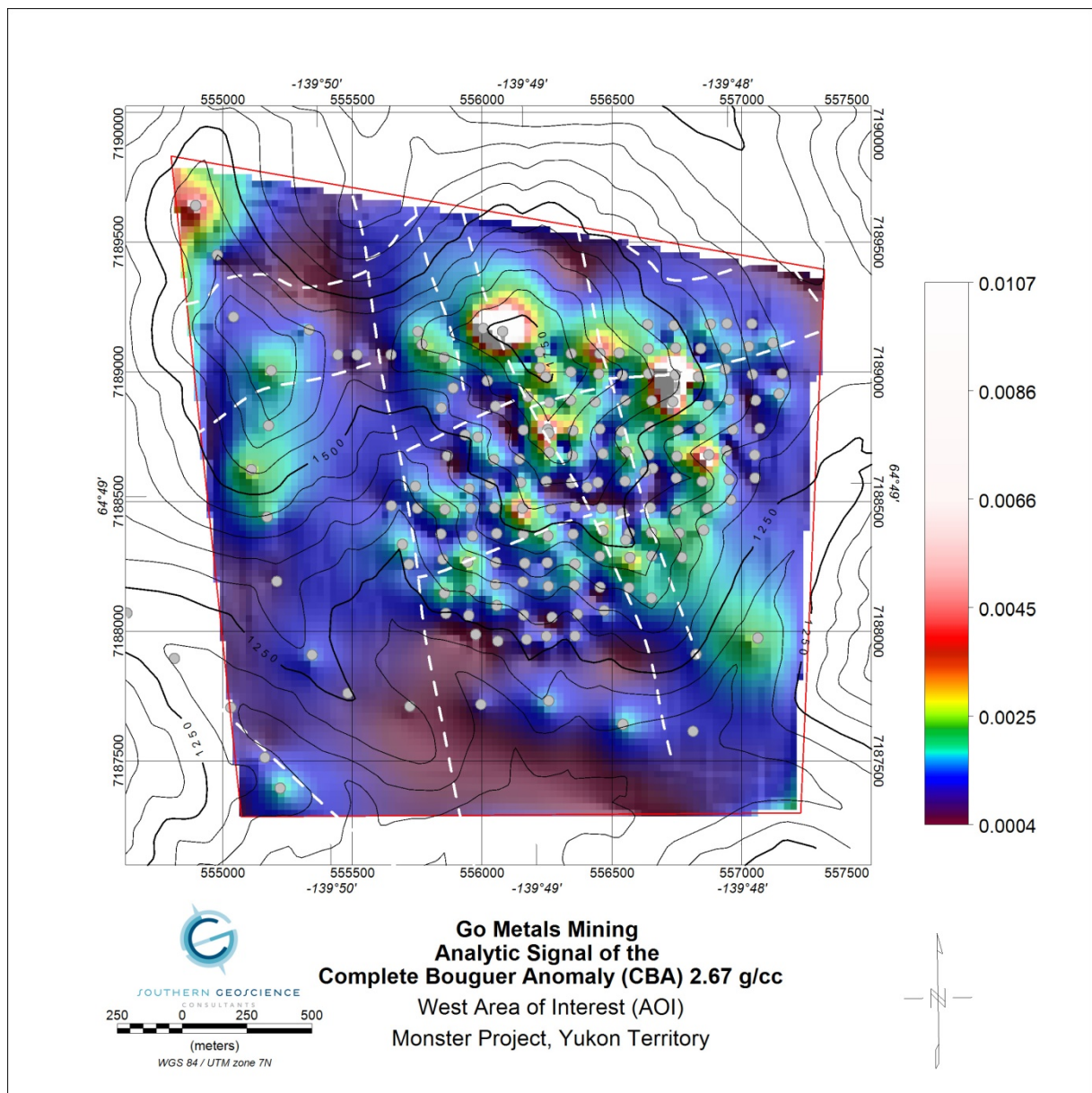


Figure 19: West AOI Analytic Signal of the Complete Bouguer Gravity Anomaly (CBA) for Bouguer Density 2.67g/cm³. Gravity sites are indicated by grey dots. Mapped geologic faults (dashed white lines) are plotted. Background contours (50/250/1000 m) are elevations from the drone DEM grid in units of masl.

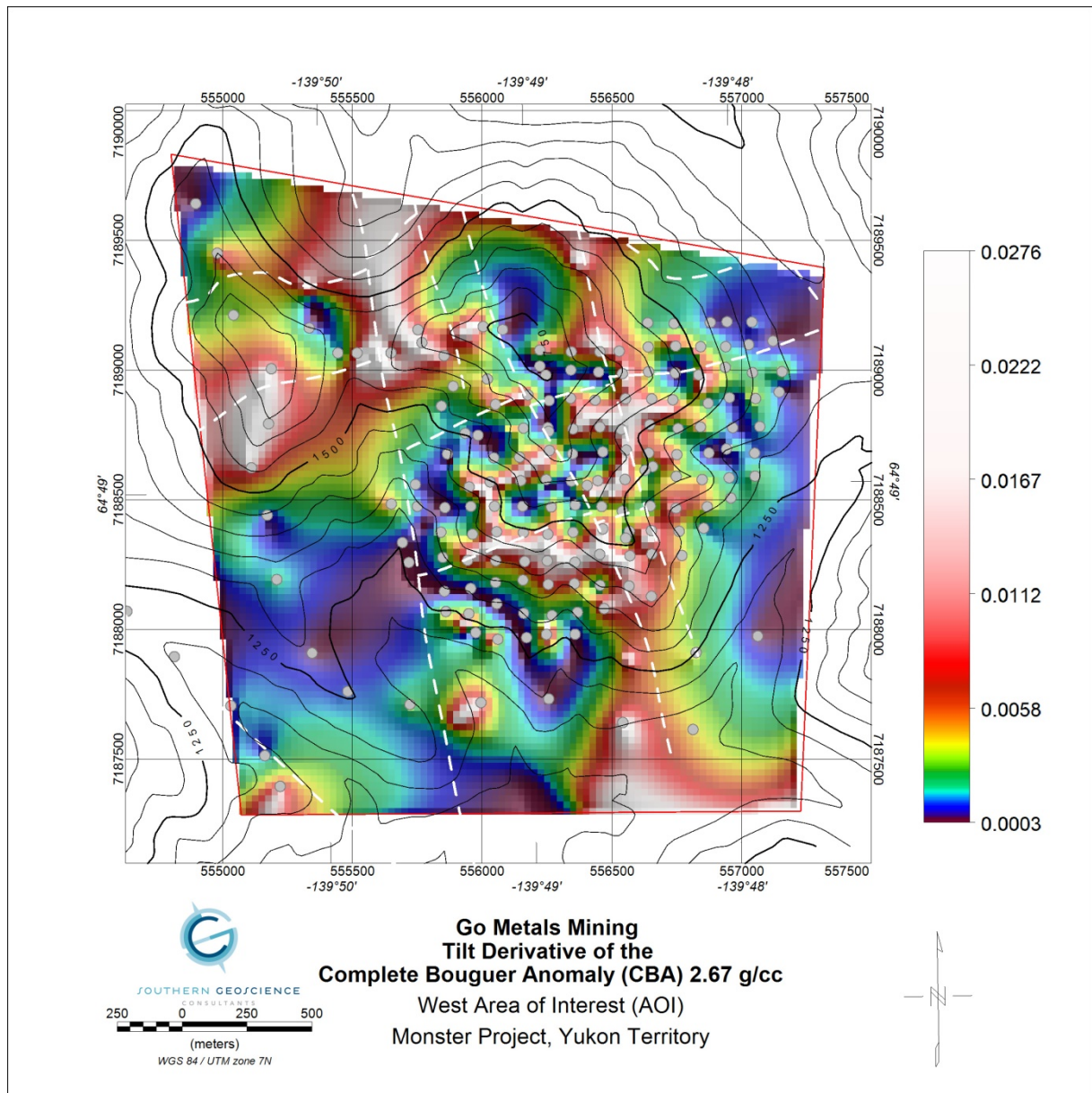


Figure 20: West AOI Tilt derivative of the Complete Bouguer Gravity Anomaly (CBA) for Bouguer Density 2.67g/cm^3 . Gravity sites are indicated by grey dots. Mapped geologic faults (dashed white lines) are plotted. Background contours (50/250/1000 m) are elevations from the drone DEM grid in units of masl.

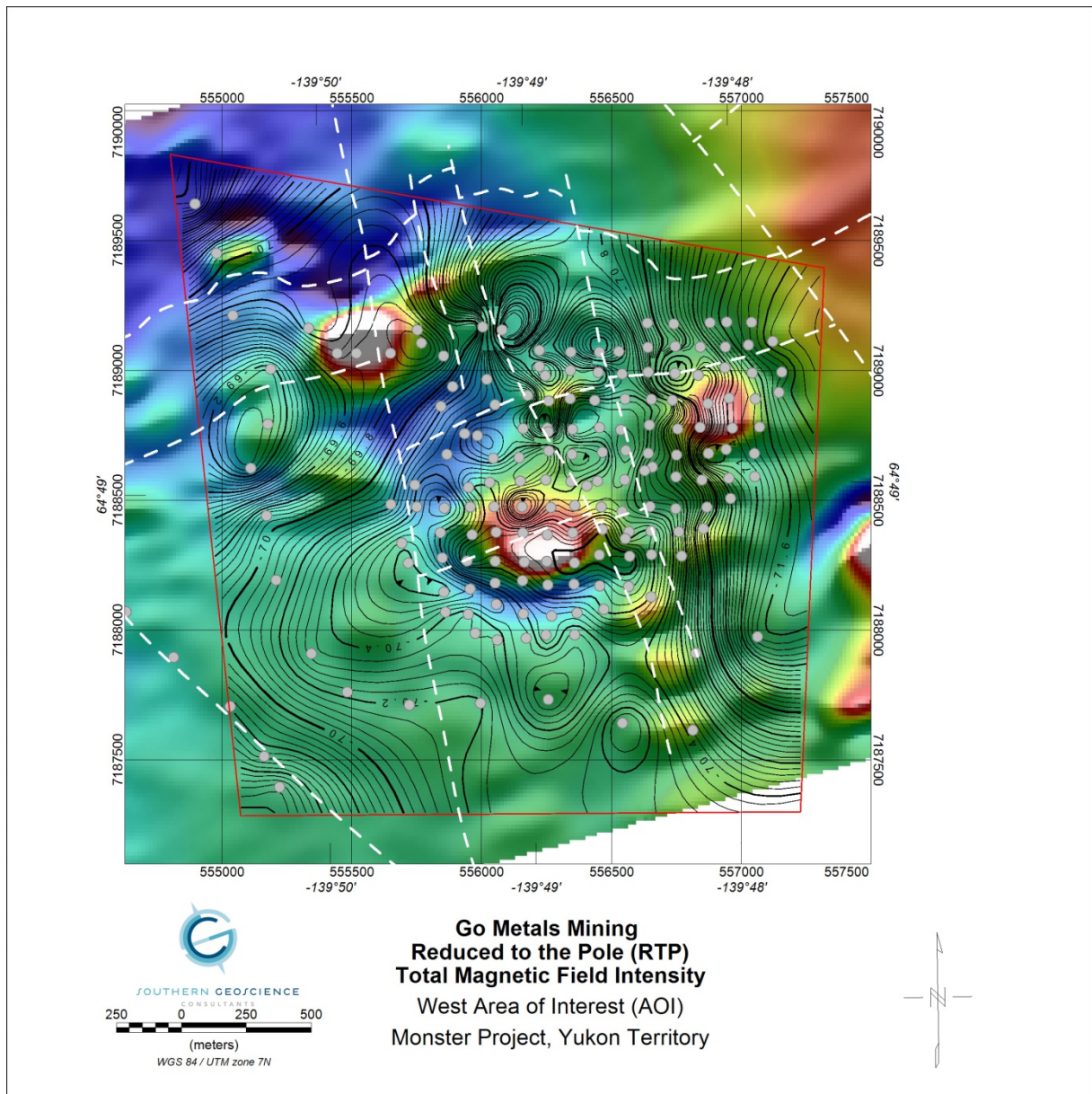


Figure 21: West AOI Reduced to the Pole (RTP) total magnetic intensity (TMI) from the airborne survey with contour overlay of the CBA 2.67g/cm³. Gravity sites are indicated by grey dots. Mapped geologic faults (dashed white lines) are plotted.

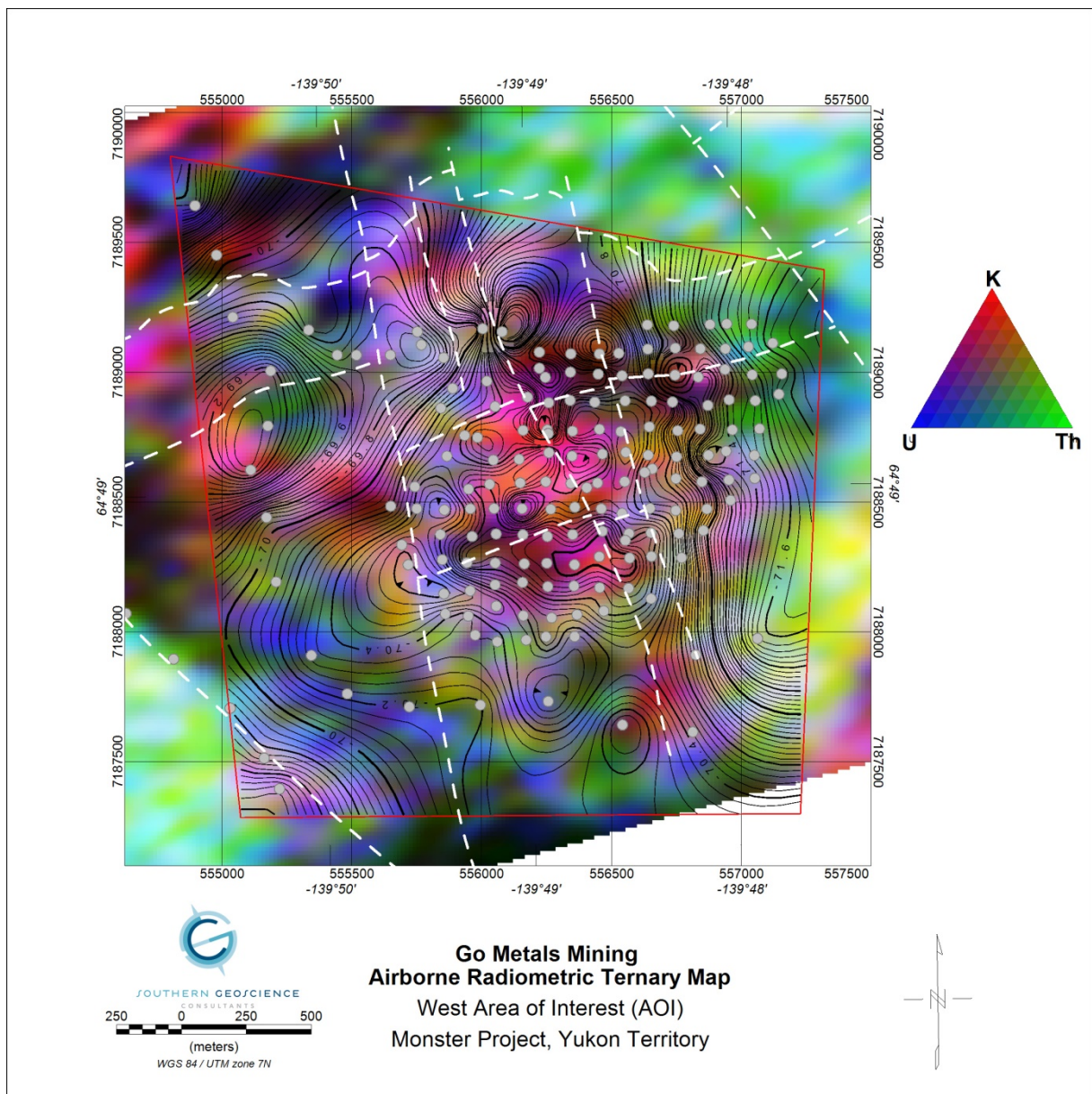


Figure 22: West AOI airborne radiometric ternary plot with contour overlay of the CBA 2.67g/cm^3 .

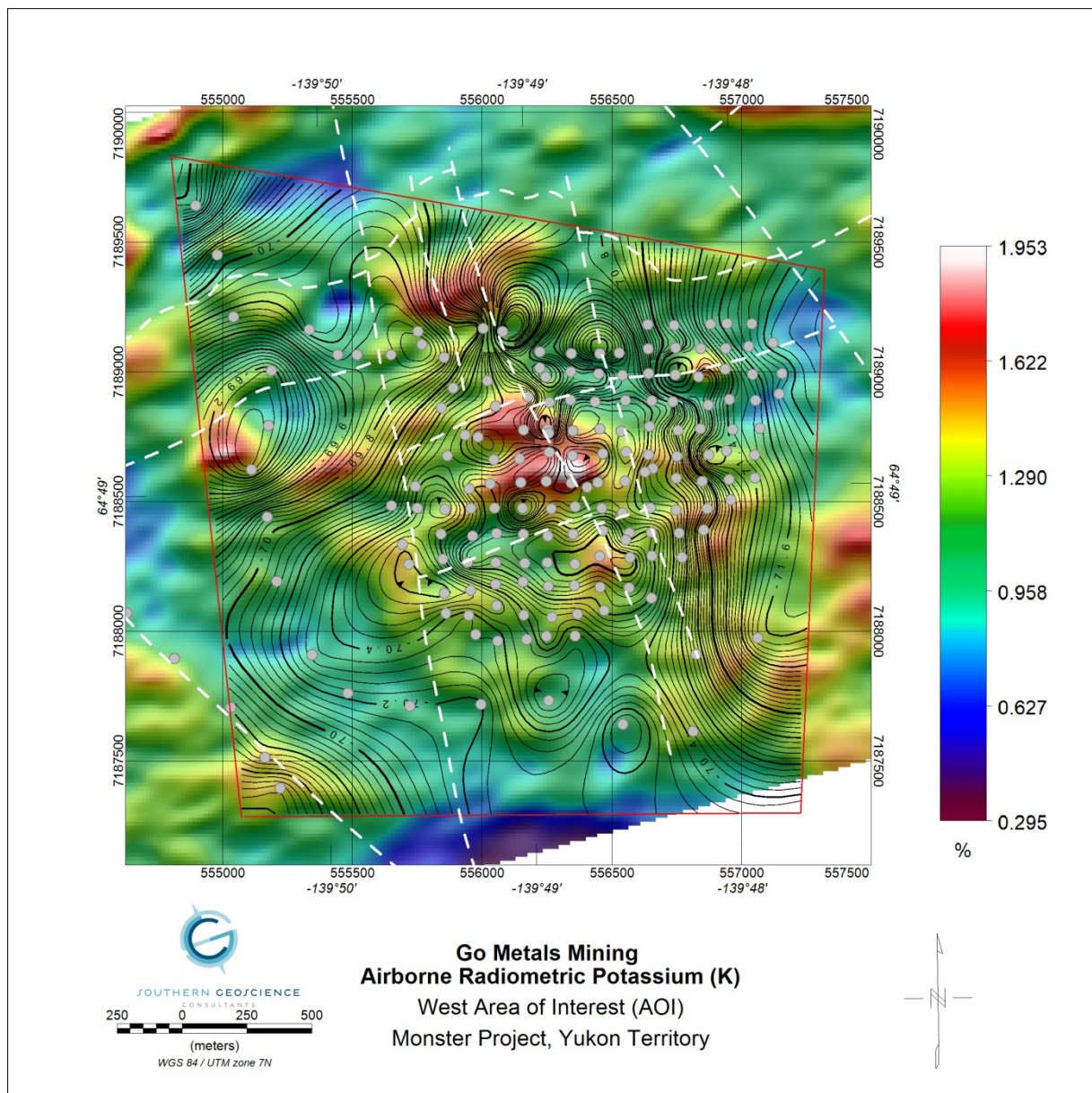


Figure 23: West AOI airborne radiometric Potassium (K) plot with contour overlay of the CBA 2.67g/cm^3 .

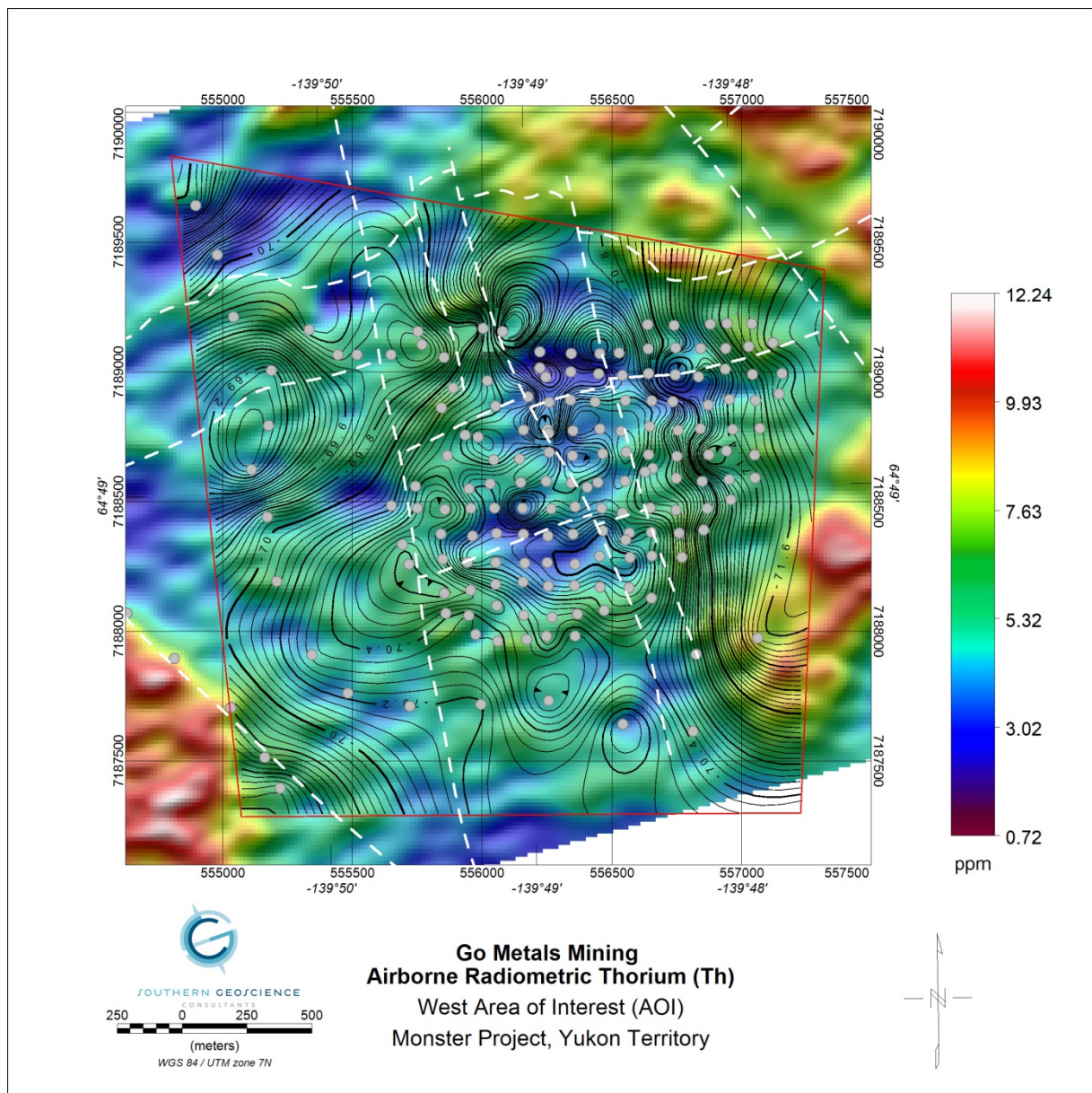


Figure 24: West AOI airborne radiometric Thorium (Th) plot with contour overlay of the CBA 2.67g/cm^3 .

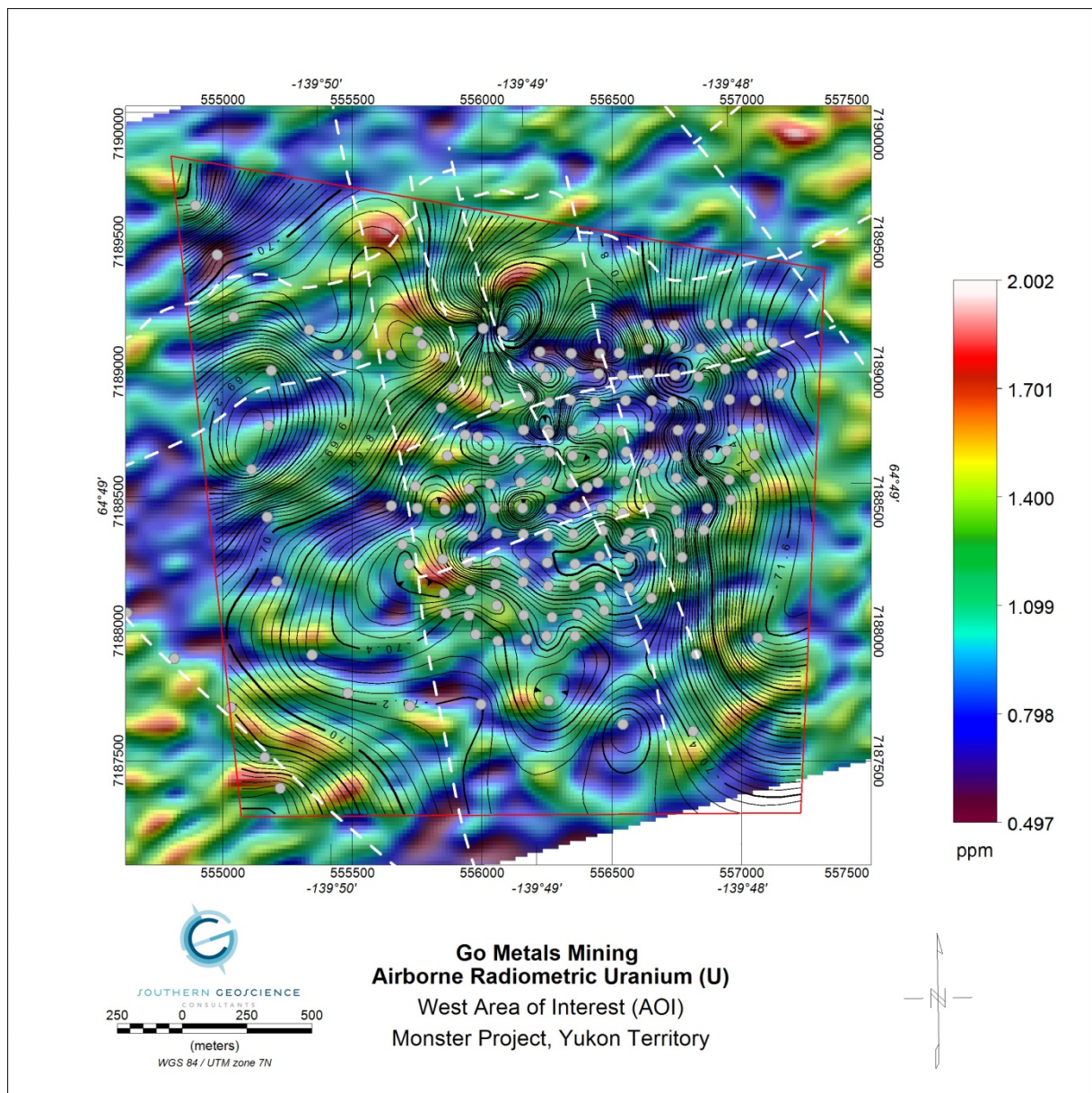


Figure 25: West AOI airborne radiometric Uranium (U) plot with contour overlay of the CBA $2.67\text{g}/\text{cm}^3$.

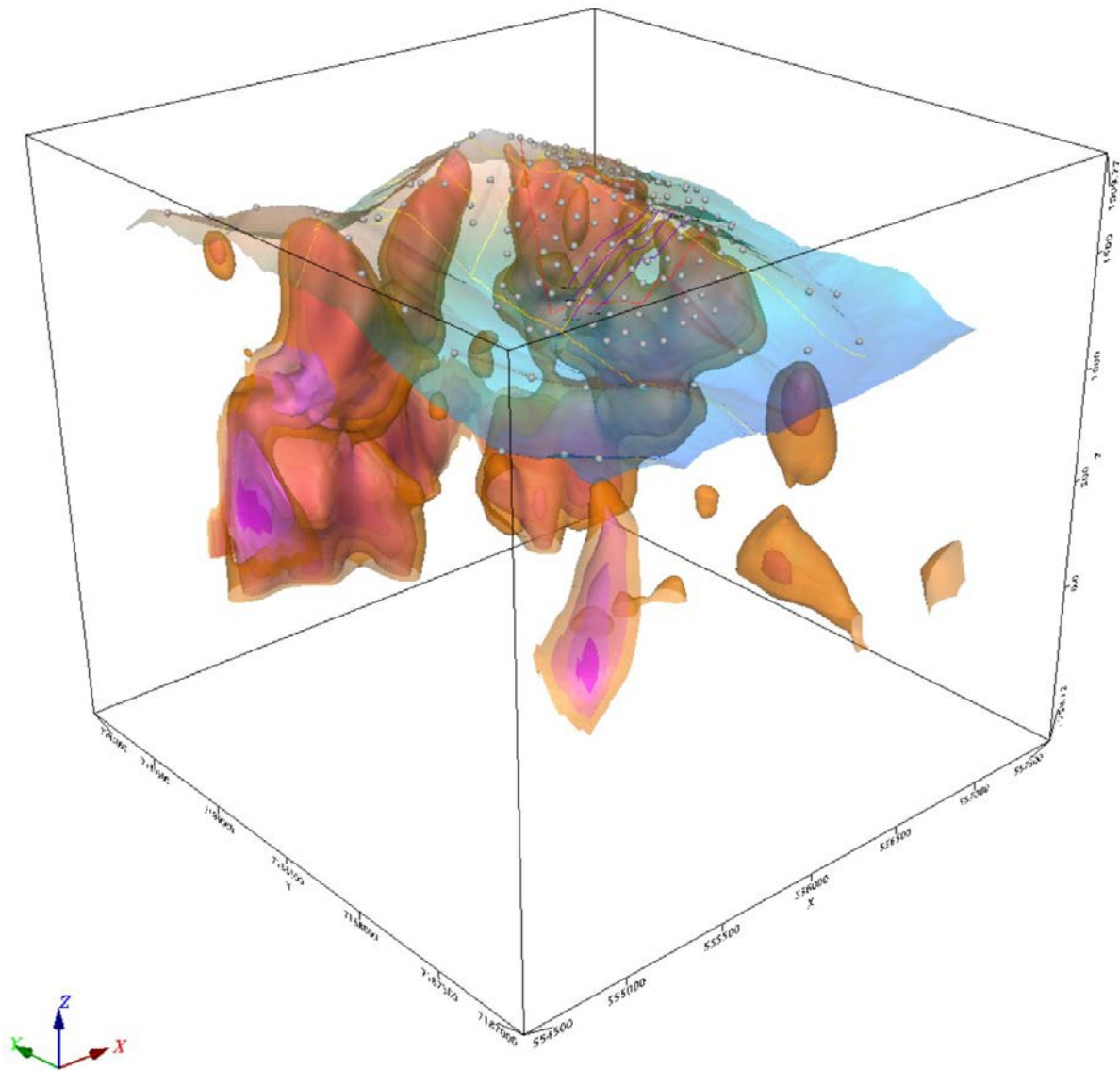


Figure 26: 3D Voxi inversion of the CBA 2.67g/cm³ data. View is looking northeast. The iso-surface/shell for a density contrast of 0.075 g/cm³ (corresponding to a density of 2.745 g/cm³) is shown. Topographic surface (drone DEM) is plotted in addition to surface mapped faults (yellow lines), gravity measurement sites (grey dots), DCIP lines (purple) and GMM defined AOI (red polygon).

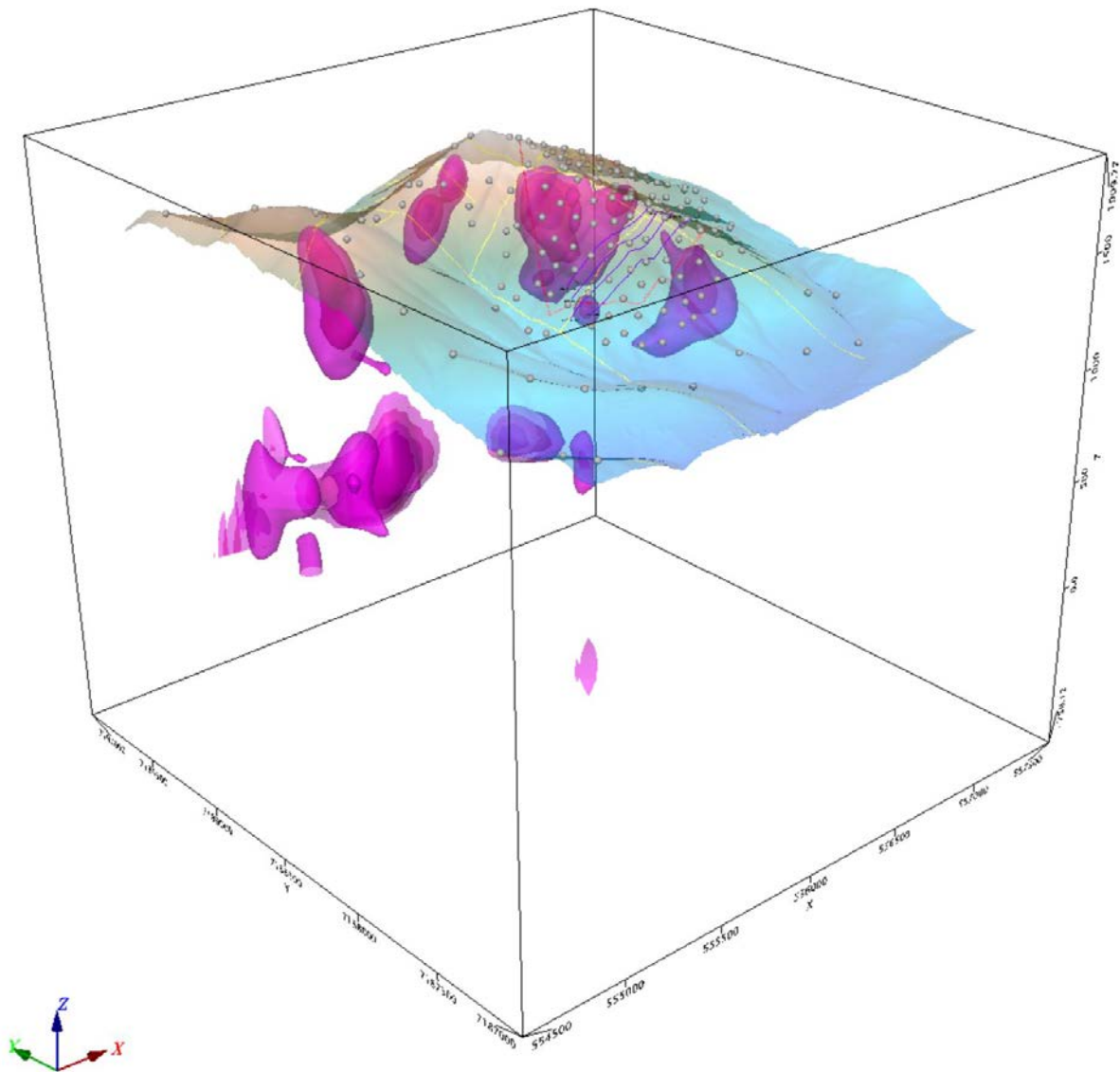


Figure 27: 3D Voxi inversion of the CBA 2.67g/cm³ data. View is looking northeast. The iso-surface/shell for a density contrast of 0.15 g/cm³ (corresponding to a density of 2.82 g/cm³) is shown. Topographic surface (drone DEM) is plotted in addition to surface mapped faults (yellow lines), gravity measurement sites (grey dots), DCIP lines (purple) and GMM defined AOI (red polygon).

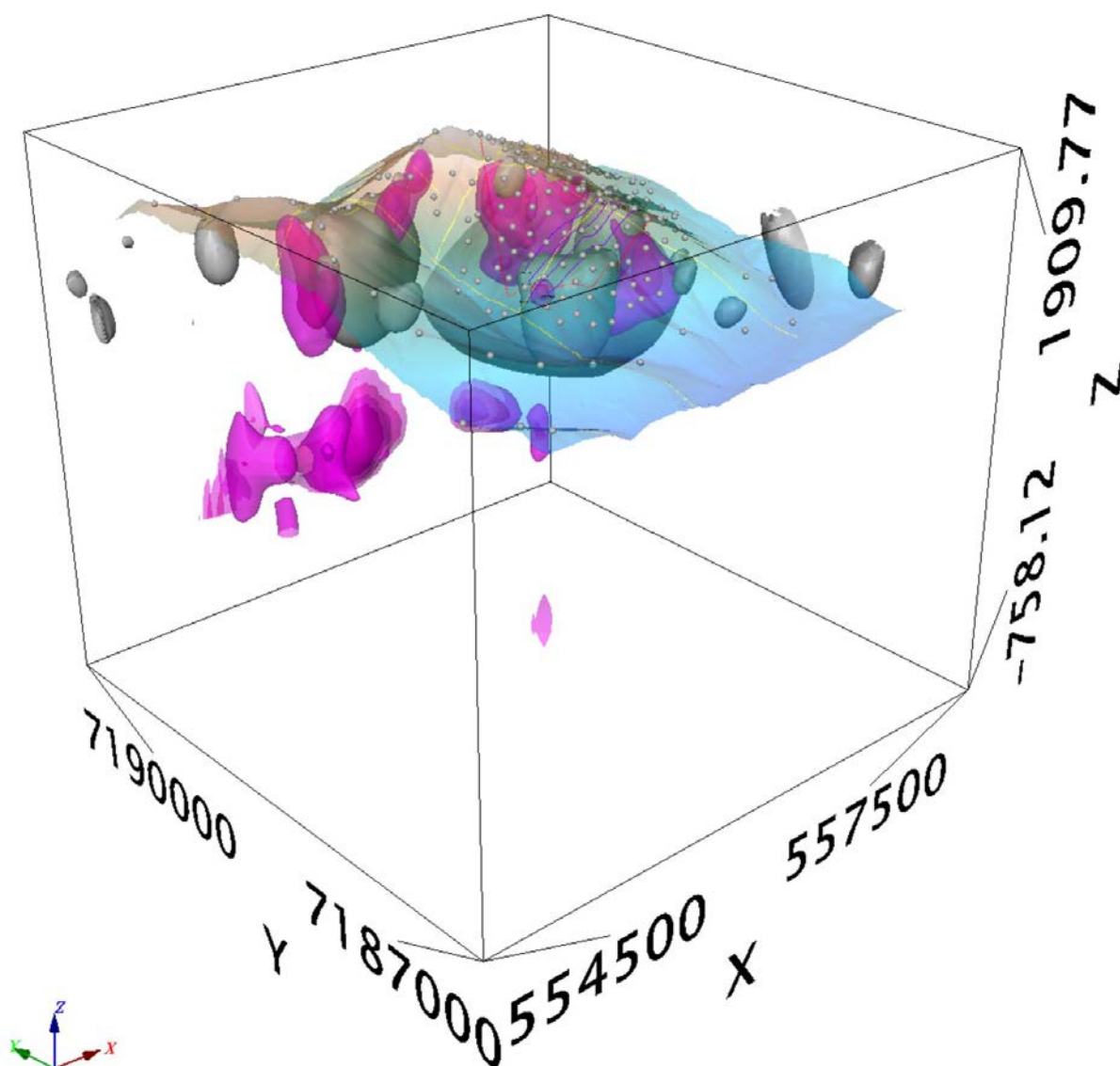


Figure 28: 3D Voxi inversion of the CBA 2.67g/cm³ data. View is looking northeast. The iso-surface/shell for a density contrast of 0.05 g/cm³ (corresponding to a density of 2.72 g/cm³) is shown. Magnetic susceptibility iso-surface (0.002 SI; grey surfaces) are shown. Topographic surface (drone DEM) is plotted in addition to surface mapped faults (yellow lines), gravity measurement sites (grey dots), DCIP lines (purple) and GMM defined AOI (red polygon).

5.3 CENTRAL AREA OF INTEREST

Topographically, the central portion of the AOI is a high (Figures 29 and 30) and dominated potentially by two cirques at altitude. The topography is dominated by knife edge ridges and steep inclined watercourses/valleys. The gravity anomalies are mostly confined to the ridges and flatter high altitude areas. Gravity sites in the central part of the area are nominally acquired on a loose 50 m grid.

The 1VD of the CBA, when viewed in conjunction with the mapped faults (Figure 31), presents a complex image. The mapped faults correlate very well with disruptions and breaks in the 1VD anomalies. As in previous examples, the dense body sources appear in some cases to follow the

topographic contours, possibly mapping a more dense and hence more resistant to weathering geologic unit along the side of the mountains. The images suggest that the source of the density anomalies are constrained by the N-S and E-W family of faults and hence tied to alteration products associated with the fault systems.

There is the appearance of a circular, zoned density feature centred on the topographic and density high located at 561000E, 7191750N as defined by the analytic signal response (Figure 32). This feature is situated at the intersection of an N-S fault that is offsetting an ENE-WSW trending fault. To the south, east and northeast of this anomaly, a series of concentric ring features (potentially three rings) are visible and crosscut the topography. To the north the ring structure is less obvious; suggesting that the ENE-WSW striking fault may be controlling the density features. This fault that runs along the southern edge of a broad accurate valley starting at altitude from appears to be cirque with a localised density anomaly.

The tilt derivative (Figure 33) presents a similar but more tightly constrained perspective to the analytic signal (Figure 32). The ring structure is slightly less obvious on the tilt derivative; however the tilt derivative suggests much of the signal may be formational in origin as there is a much tighter correlation with tilt derivative peaks and constant topographic elevation.

Overlaying the CBA gravity contours on the RTP TMI image (Figure 34) shows that there is some local correlation between high magnetisation and positive gravity anomalies. The ring structure suggested by the gravity data is less obvious in the magnetics, the magnetics being more angular and influenced by the ENE-WSW family of mapped faults. There is a magnetic anomaly associated with the gravity anomaly observed at 561000E, 7191750N; however the magnetic anomaly is offset to the east and south by approximately 200 m. The main magnetic anomaly centre lying on the east side of a NS fault whereas the gravity centre is located on the west side of the fault. There are many ENE-WSW, short strike length magnetic anomalies that are potentially dikes and have been modelled as such in the past (Figure 39). These magnetic features have weak to no gravity response.

A high Potassium response in respect to Thorium and Uranium is associated with the topographic ridges (Figures 35 to 38). Thorium enrichment in comparison to Uranium and Potassium is visible in the valleys and watercourses. Moderate Uranium enrichment is visible on the northeast and east slopes from the ridge centred on 561500E, 7191500N. There is some suggestion from the radiometric data that there is a large, zoned circular feature coincident with the feature seen on the analytic signal (Figure 32).

The 3D inversion of the CBA has resulted in the definition of two dominate trends of density enhancement (Figure 39 and Figure 40). The NNE-SSW trend is running parallel to and under the topographic ridge extending from approximately 559800E, 7189600N to 558600E, 7139000N. The density trend is to the east of and subparallel to, an identified fault in the base of the topographic valley on the west flank of the anomaly. There is an EW splay off of this trend that extends into and covers the northern half of the original AOI polygon. Offsets in the strike of the density feature correlate to the mapped faults.

The second density trend strikes NE-SW from approximately 659500E, 7190150N to 561800E, 7192500N. There is no subparallel mapped fault associated with this feature; however offsets in the strike do correlate to NS faulting suggesting an on-echelon or staircase type of faulting along strike.

The correlation with the magnetic susceptibility modelling tends to be poor as evidenced from Figure 41. The susceptibility iso-surfaces tend to be large and horizontal. If the geology is essentially horizontal, then the magnetic response may be stratigraphic in source. Where there is limited correlation is when the magnetic iso-surface shallows, the gravity iso-surface appears to flank and marginally overlap with the edge of the susceptibility isosurfaces. The magnetic surfaces tend not to intersect density features and may be indicating an additional control on the placement of denser material.

2D magnetic modelling was completed in the east part of the AOI in the past. There is little associated gravity effect associated with the magnetic features modelled.

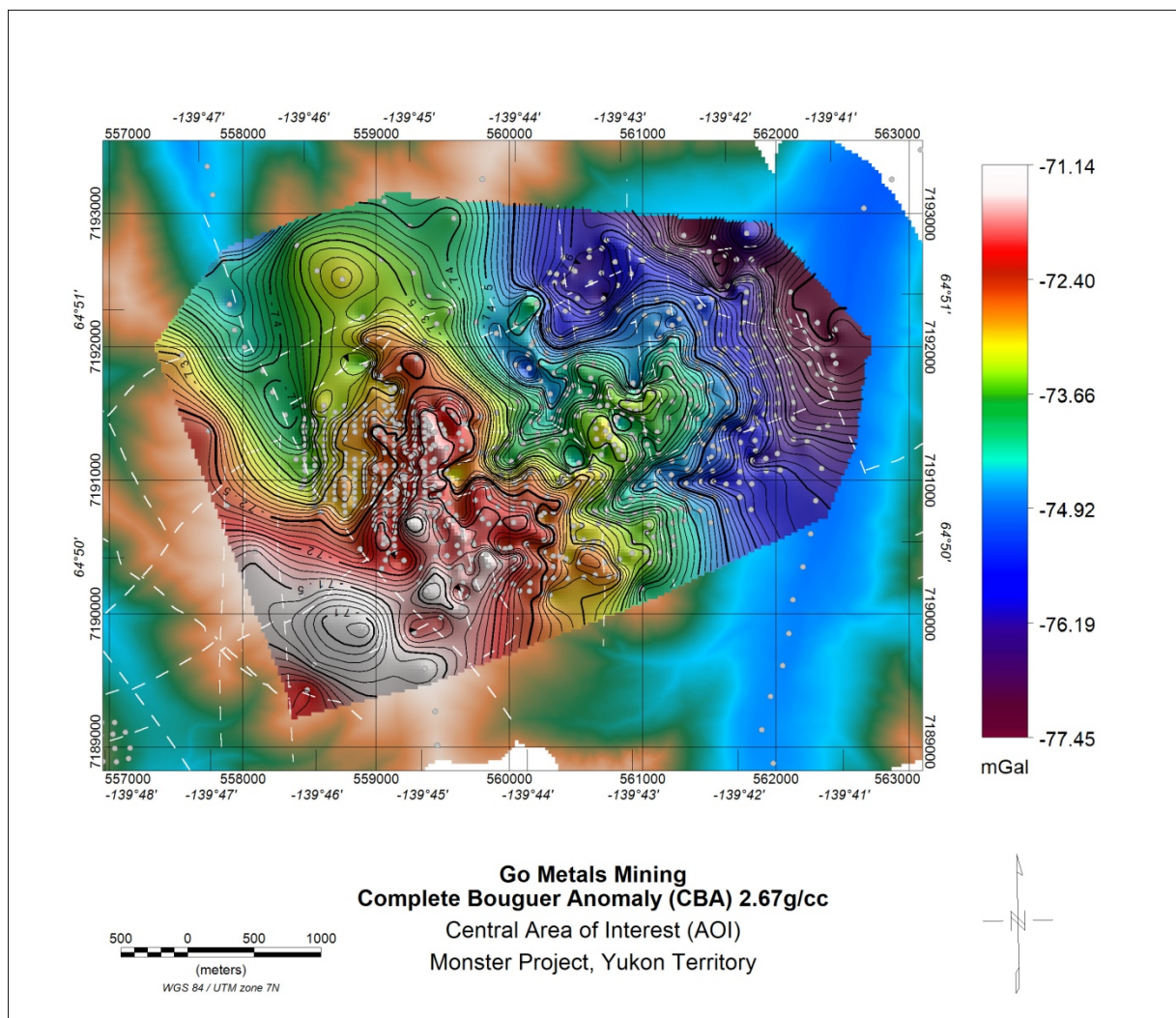


Figure 29: Central AOI Complete Bouguer Gravity Anomaly (CBA) for Bouguer Density 2.67g/cm³. Gravity sites are indicated by grey dots. Contour interval is 0.1, 0.5 and 2.5 g/cm³. Mapped geologic faults (dashed white lines) are plotted. Background is drone DEM grid.

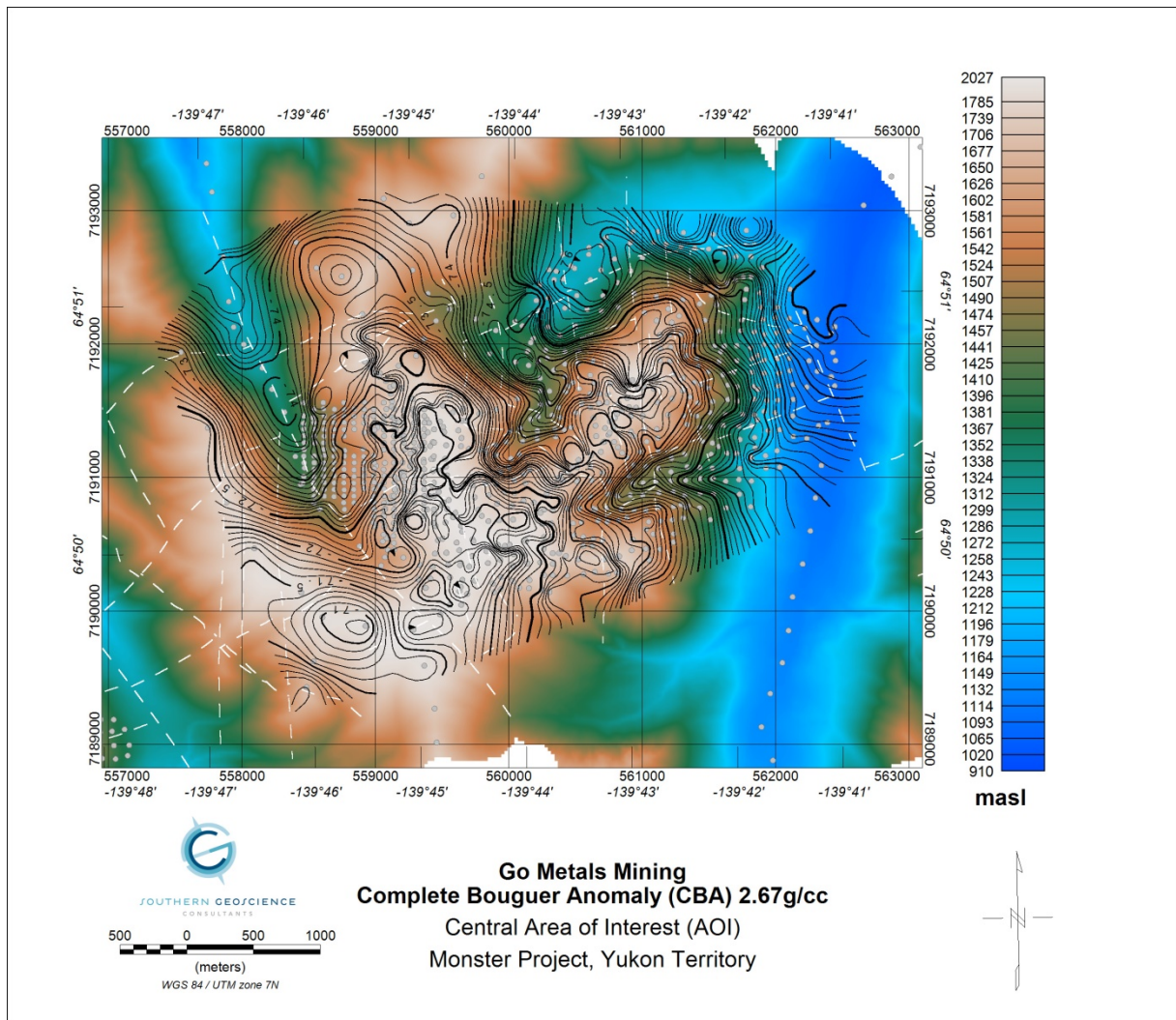


Figure 30: West AOI Complete Bouguer Gravity Anomaly (CBA) for Bouguer Density 2.67g/cm^3 . Gravity sites are indicated by grey dots. Contour interval is 0.01, 0.5 and 2.5g/cm^3 . Mapped geologic faults (dashed white lines) are plotted. Background is drone DEM grid.

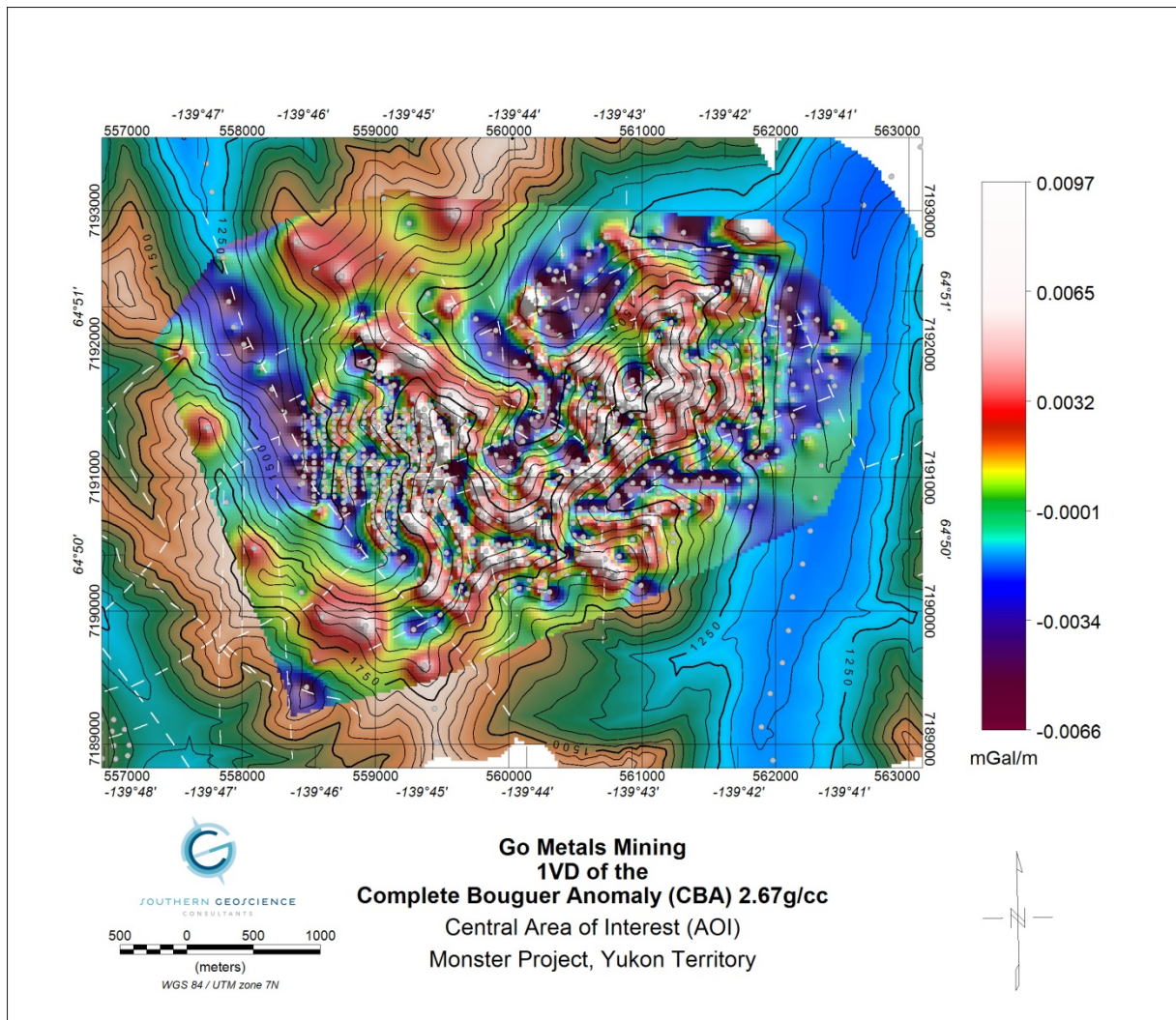


Figure 31: Central AOI 1VD of the Complete Bouguer Gravity Anomaly (CBA) for Bouguer Density 2.67g/cm³. Gravity sites are indicated by grey dots. Mapped geologic faults (dashed white lines) are plotted. Background contours (50/250/1000 m) are elevations from the drone DEM grid in units of masl.

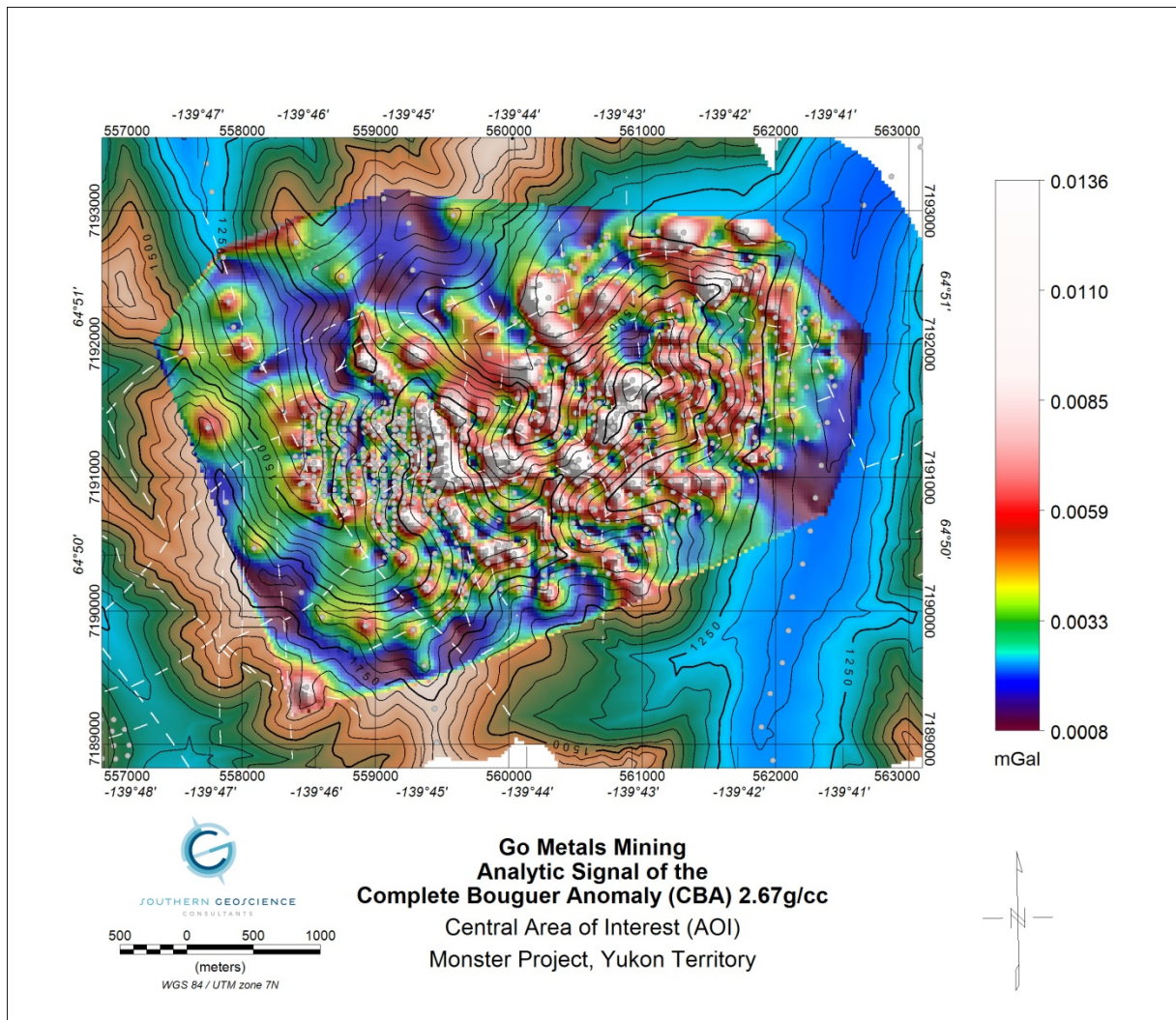


Figure 32: Central AOI Analytic Signal of the Complete Bouguer Gravity Anomaly (CBA) for Bouguer Density 2.67g/cm³. Gravity sites are indicated by grey dots. Mapped geologic faults (dashed white lines) are plotted. Background contours (50/250/1000 m) are elevations from the drone DEM grid in units of masl.

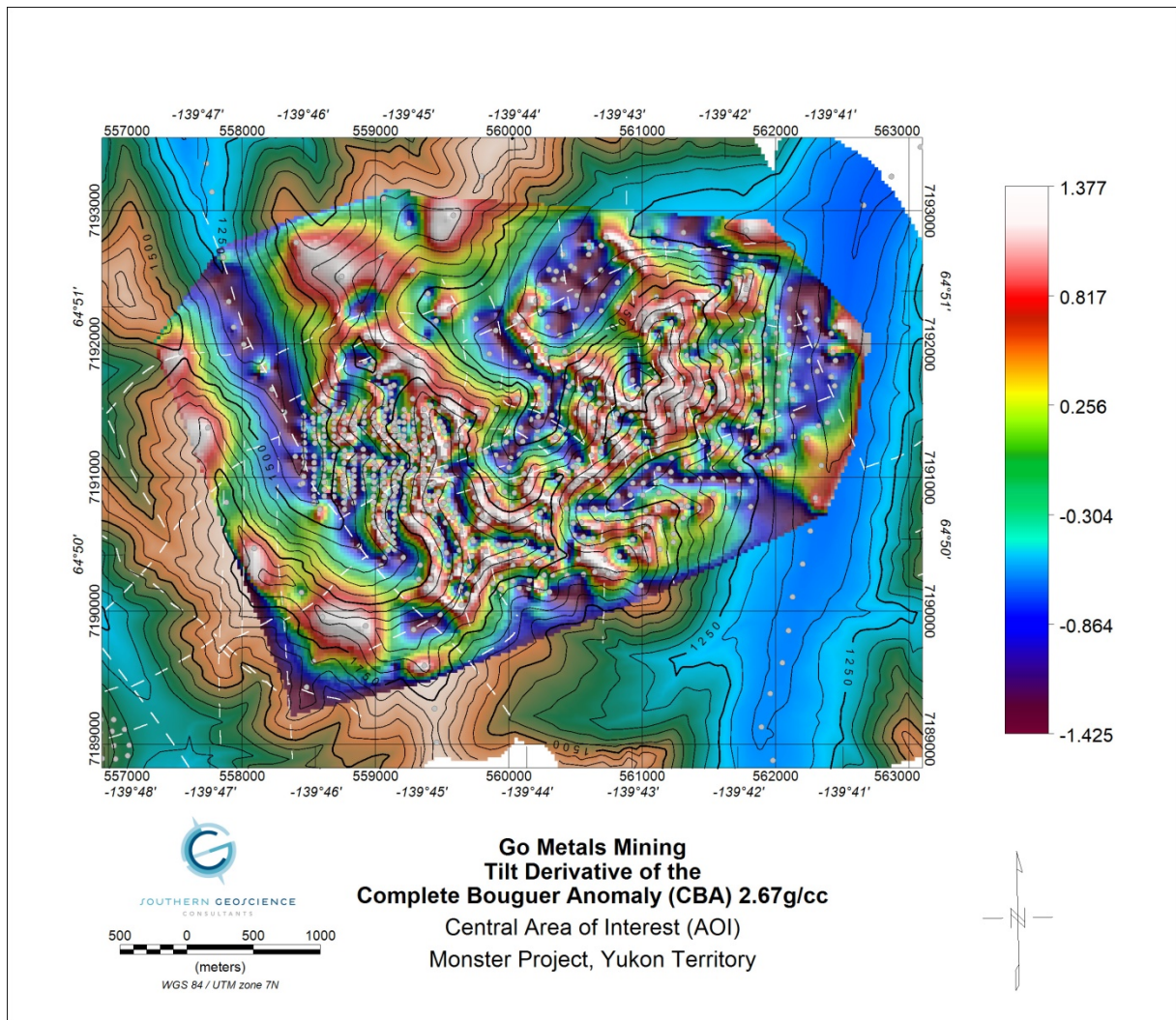


Figure 33: Central AOI Tilt derivative of the Complete Bouguer Gravity Anomaly (CBA) for Bouguer Density 2.67g/cm^3 . Gravity sites are indicated by grey dots. Mapped geologic faults (dashed white lines) are plotted. Background contours (50/250/1000 m) are elevations from the drone DEM grid in units of masl.

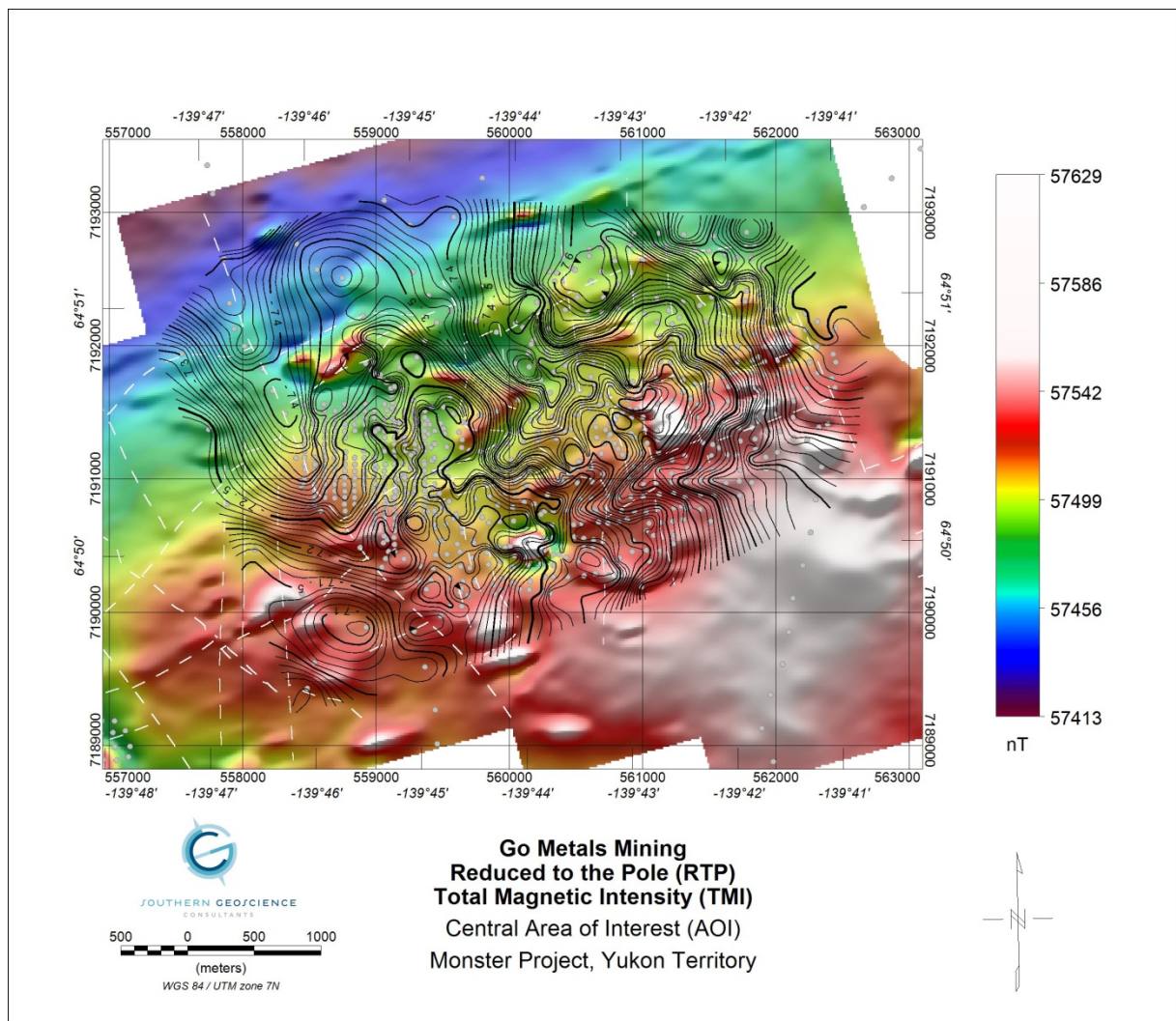


Figure 34: Central AOI Reduced to the Pole (RTP) total magnetic intensity (TMI) from the airborne survey with contour overlay of the CBA 2.67g/cm³. Gravity sites are indicated by grey dots. Mapped geologic faults (dashed white lines) are plotted.

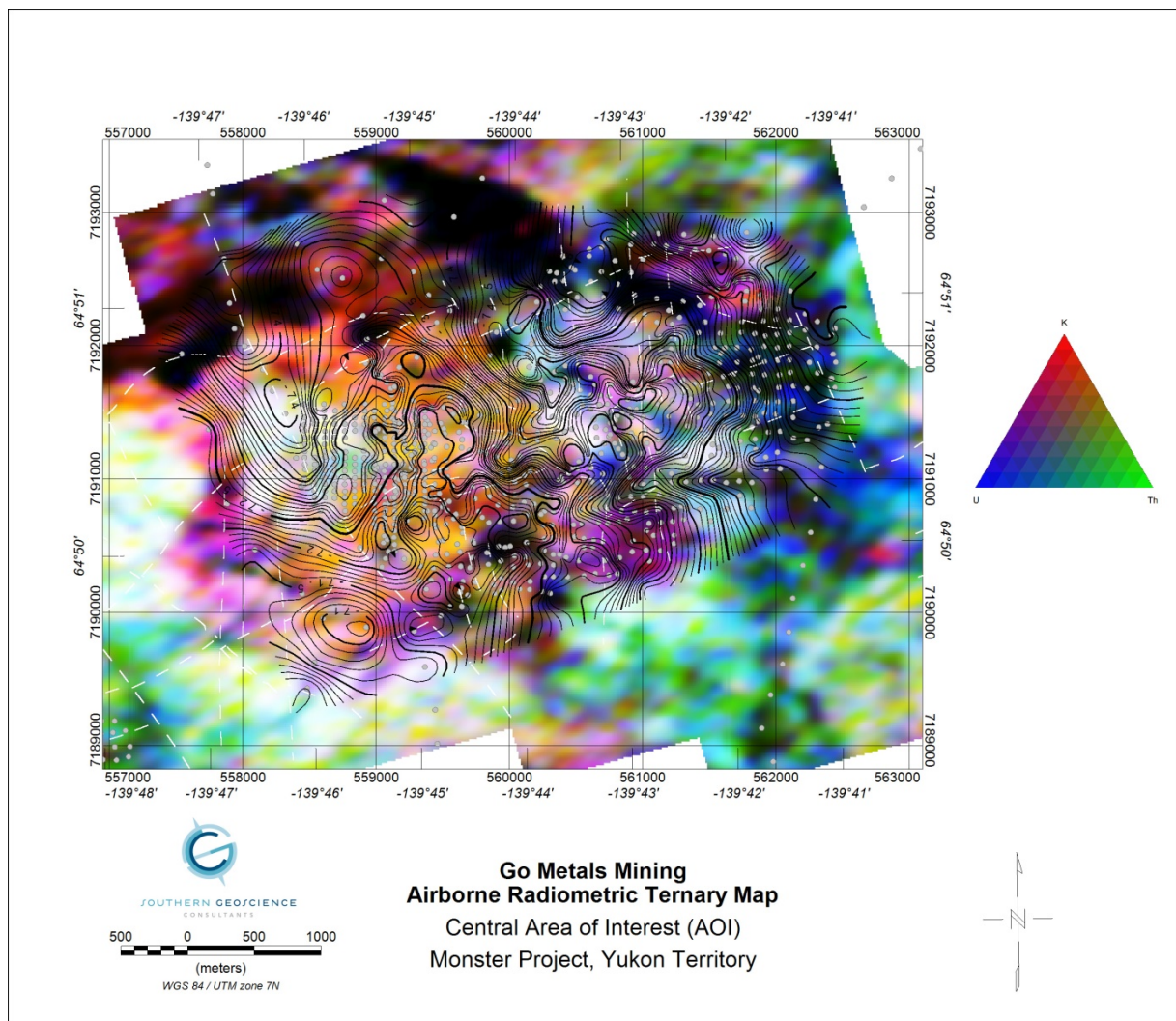


Figure 35: Central AOI airborne radiometric ternary plot with contour overlay of the CBA 2.67g/cm³.

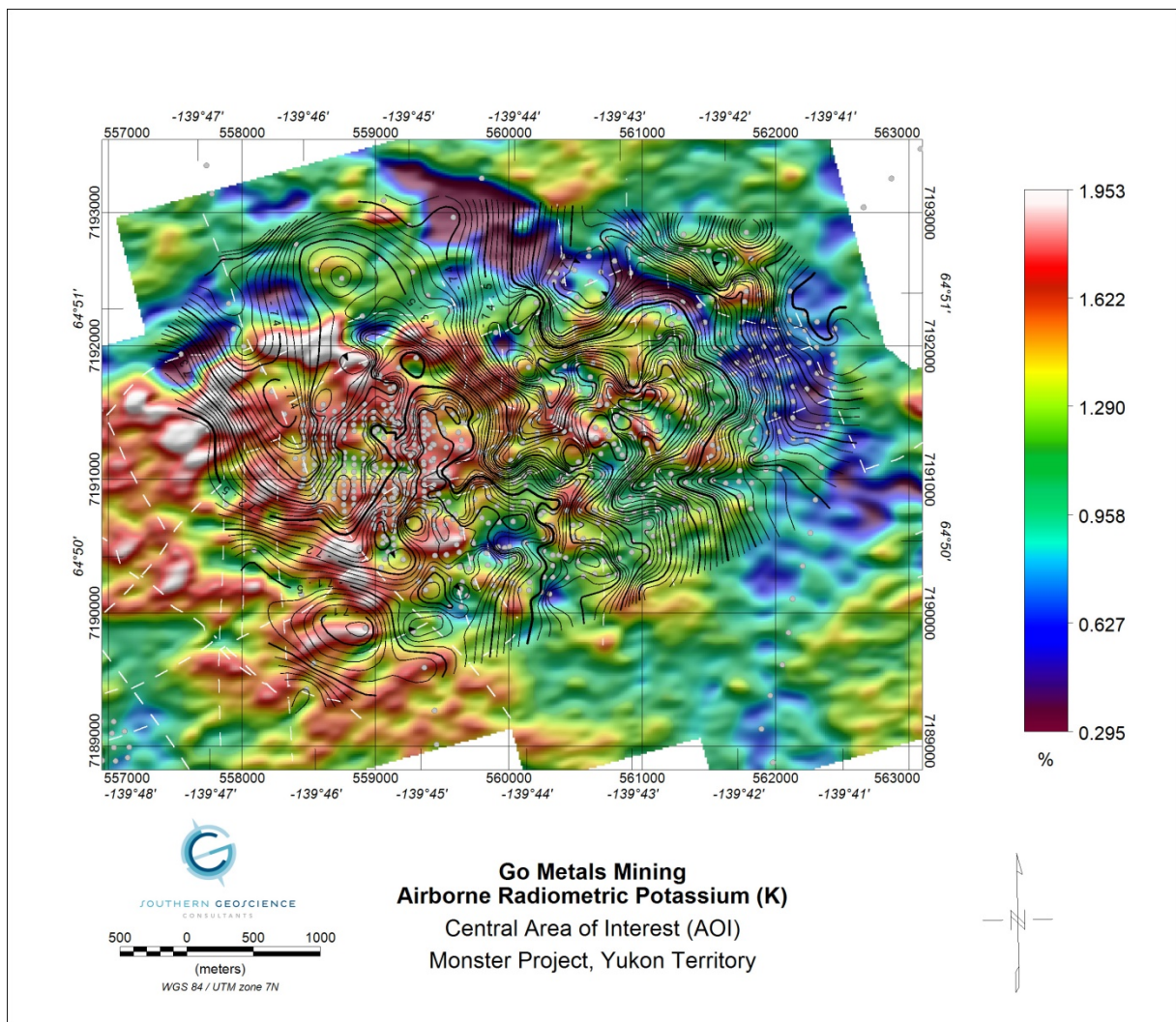


Figure 36: Central AOI airborne radiometric Potassium (K) plot with contour overlay of the CBA 2.67g/cm³.

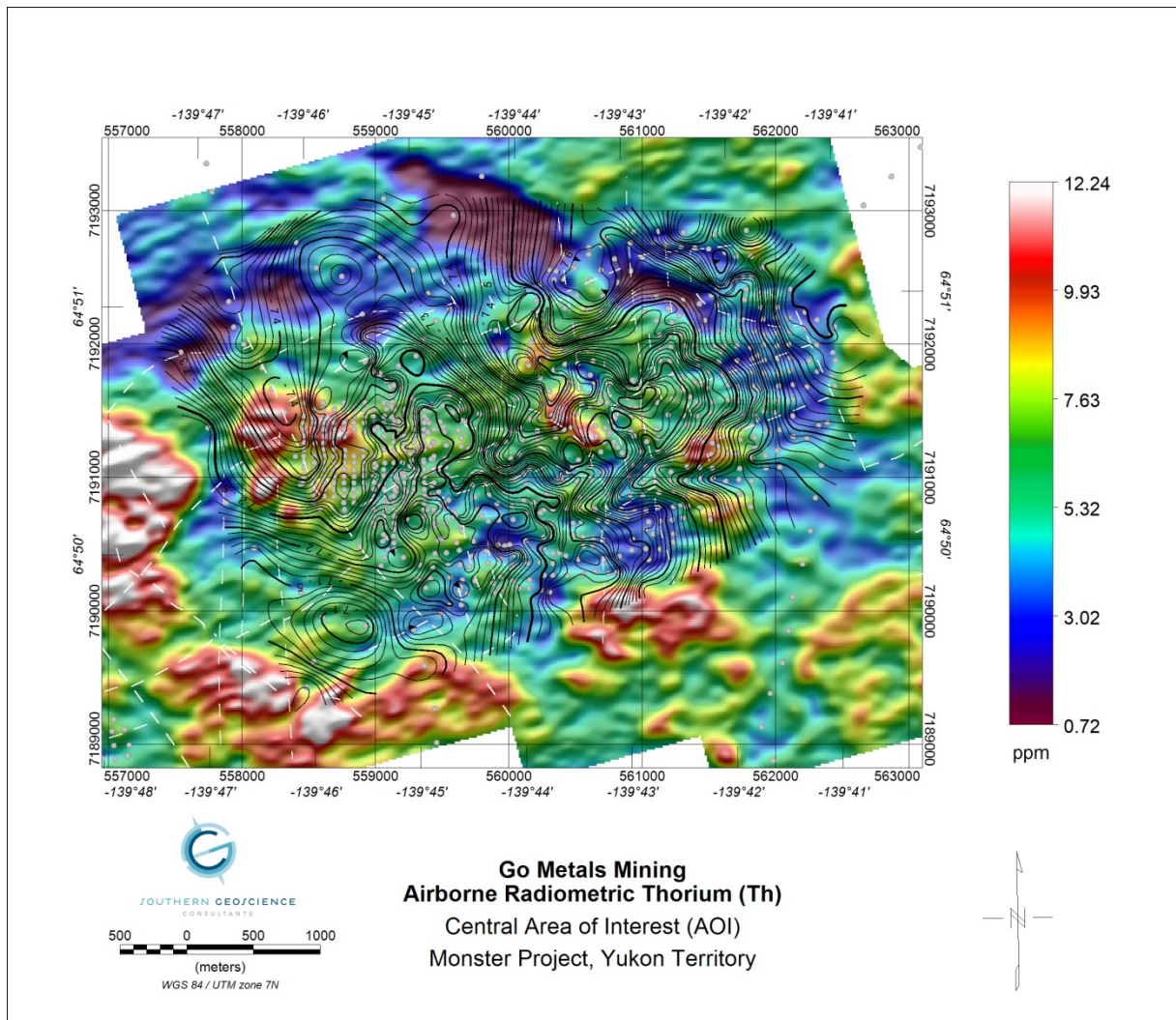


Figure 37: Central AOI airborne radiometric Thorium (Th) plot with contour overlay of the CBA 2.67g/cm³.

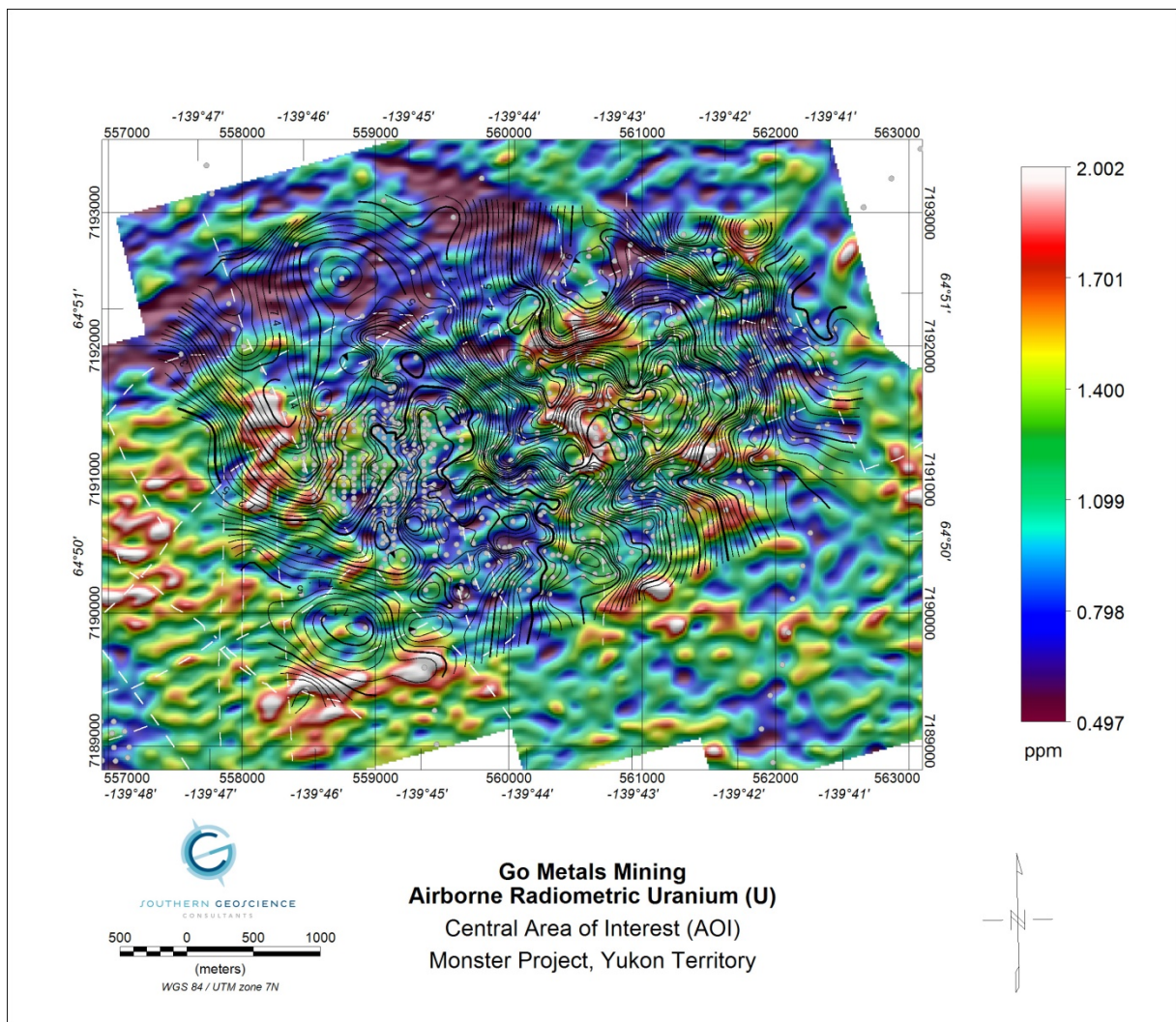


Figure 38: Central AOI airborne radiometric Uranium (U) plot with contour overlay of the CBA 2.67g/cm³.

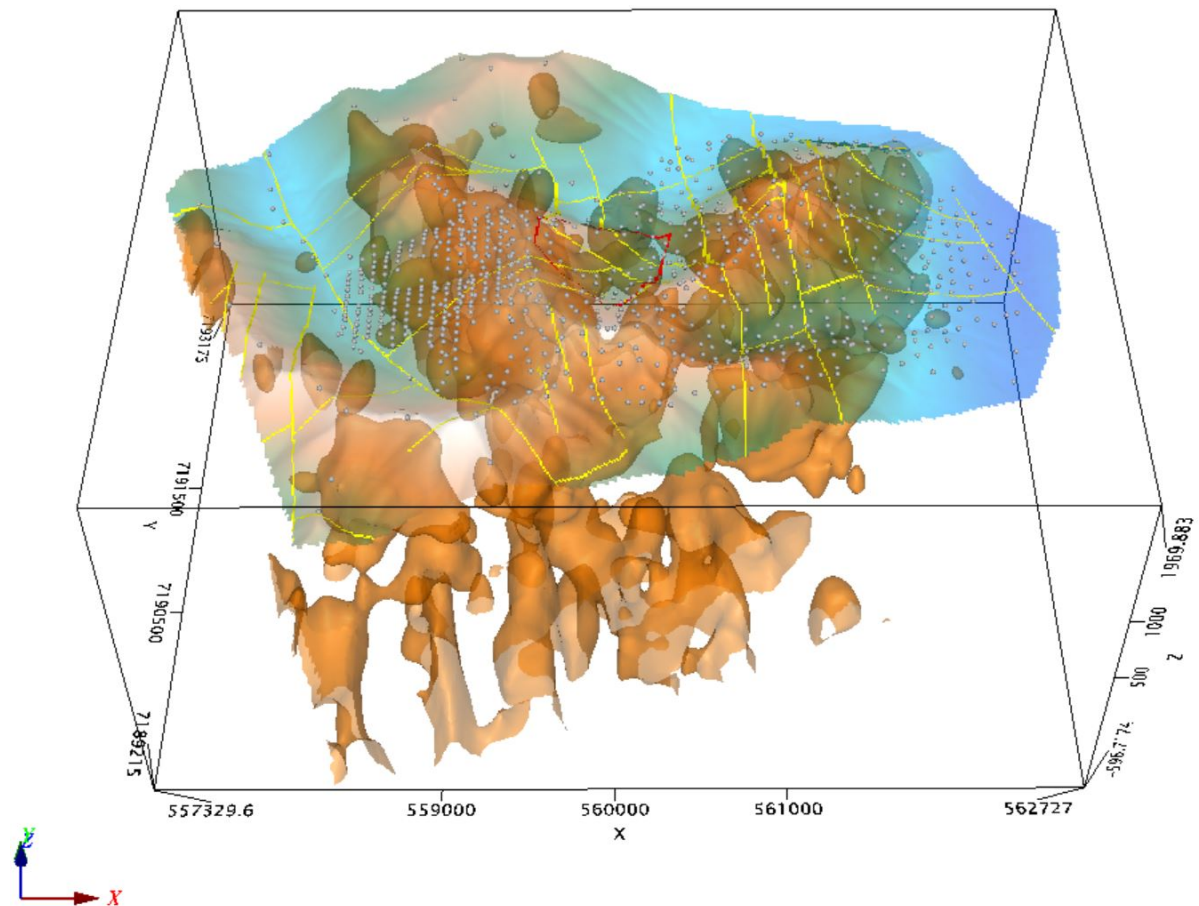


Figure 39: 3D Voxi inversion of the CBA 2.67g/cm^3 data for the Central AOI. View is looking north. The iso-surface/shell for a density contrast of 0.075 g/cm^3 (corresponding to a density of 2.745 g/cm^3) is shown. Topographic surface (drone DEM) is plotted in addition to surface mapped faults (yellow lines), gravity measurement sites (grey dots) and GMM defined AOI (red polygon).

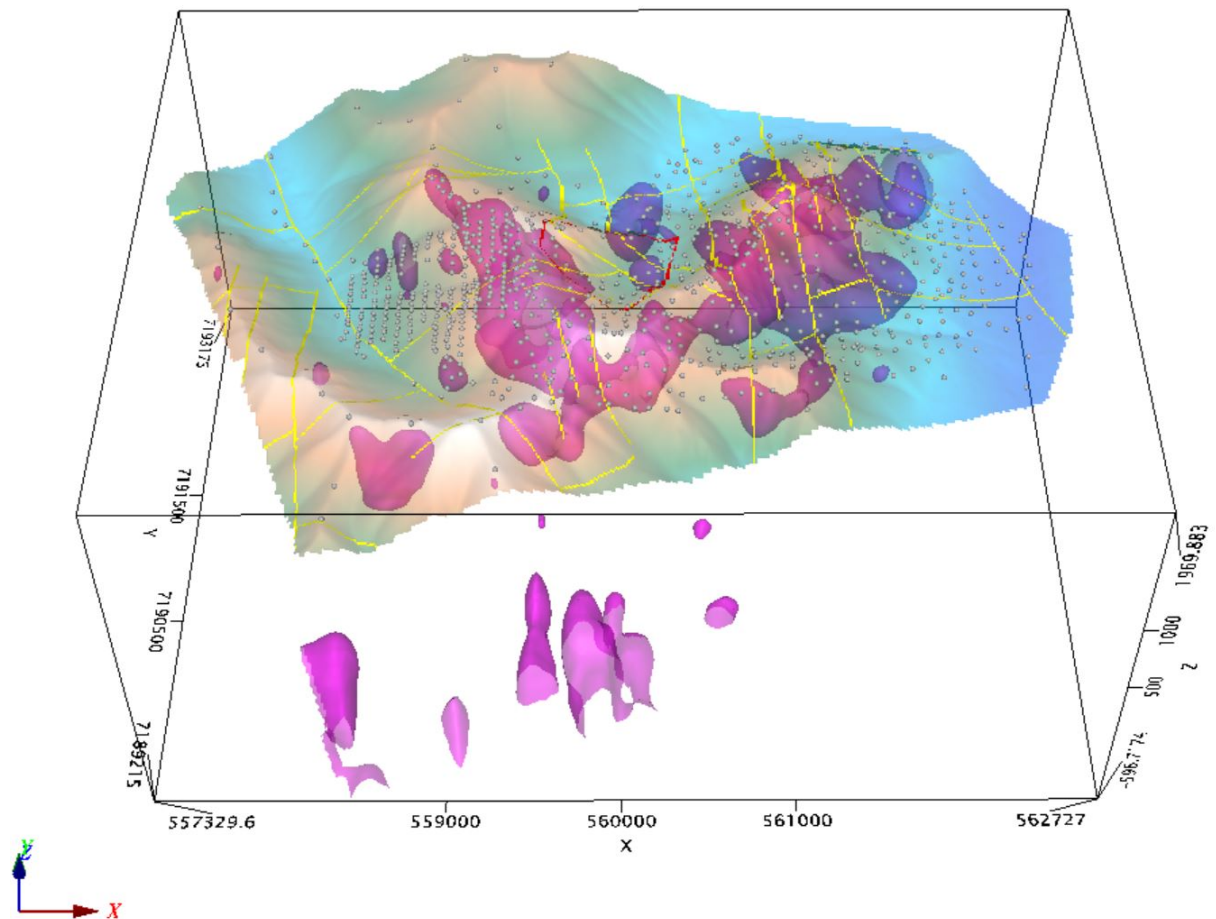


Figure 40: 3D Voxi inversion of the CBA 2.67g/cm^3 data for the Central AOI. View is looking north. The iso-surface/shell for a density contrast of 0.15 g/cm^3 (corresponding to a density of 2.82 g/cm^3) is shown. Topographic surface (drone DEM) is plotted in addition to surface mapped faults (yellow lines), gravity measurement sites (grey dots) and GMM defined AOI (red polygon).

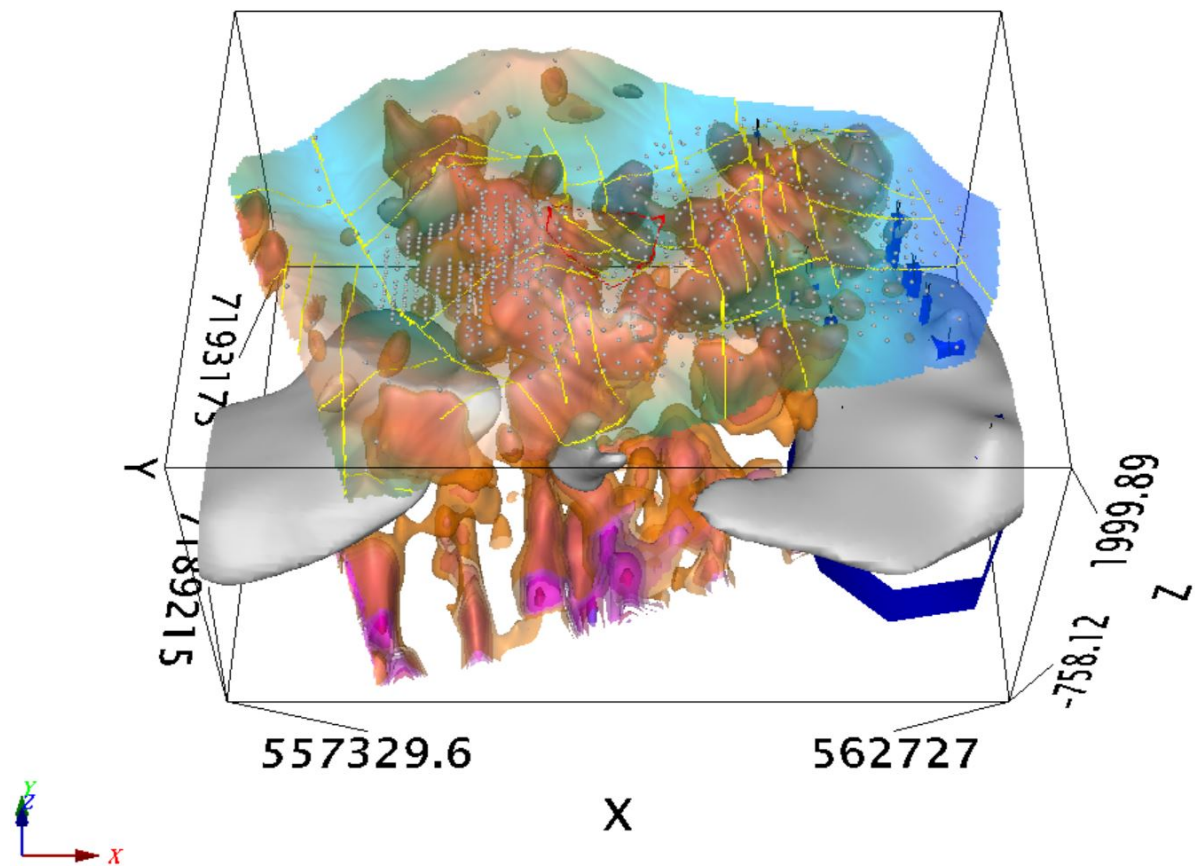


Figure 41: 3D Voxi inversion of the CBA 2.67g/cm³ data for the Central AOI. View is looking north. The iso-surface/shell for a density contrast of 0.05 g/cm³ (corresponding to a density of 2.72 g/cm³) is shown. Magnetic susceptibility iso-surface (0.0024 SI; grey surfaces) are shown. The 2D magnetic modelling completed in the past is shown in dark blue. Topographic surface (drone DEM) is plotted in addition to surface mapped faults (yellow lines), gravity measurement sites (grey dots) and GMM defined AOI (red polygon).

5.4 EAST AREA OF INTEREST

The East AOI (Figures 42 and 43) is dominated by a high ridge along the western edge striking NNW-SSE. The northwest limit is defined by an arcuate ridge coming off of the NNW-SSE ridge, curving first northeast then arcing northwards. The topographic effect is that of the high altitude western part of the AOI as cirque, valley extending downward to ENE across the AOI. The CBA positive gravity anomaly is not coincident with the ridge lines, but is at altitude and down slope from the peak on the East and south sides of the bounding ridges. The valley floor is a long and narrow string of ENE gravity lows, crosscut at intervals by NNW topographic and weaker gravity high anomaly trends.

This area was covered by a loose grid of nominally 100m spaced gravity sites.

The 1VD of the CBA (Figure 44) suggests that the on-slope gravity feature is not continuous and is somewhat controlled by a series of NW striking mapped faults. The 1VD suggests that the density distribution is controlled by the NW-SE striking family of faults, the faults marking zones of density destruction. At an area of shallower topographic slope centred at 565500E, 7190700N, the 1VD defines a large block, approximately 250m by 400m striking NE-SW of increased density. This anomalous area is crosscut by a NW-SE striking mapped fault.

The analytic signal (Figure 45) and the Tilt derivative (Figure 46) of the CBA offer differing perspectives. The analytic signal tends to accentuate bands of high amplitude material that are striking NW-SE and are controlled by the mapped geologic faults. This is contrast to the tilt derivative which presents trends similar to what is observed in the CBA of Figures 33 and 34. Of interest is the feature observed in the 1VD at 565500E, 7190700N which may be part of a larger, more circular density feature. The tilt derivative further supports the supposition that the density distribution is fault controlled.

Reviewing the RTP TMI of Figure 47, a positive discrete anomaly is associated with the south and east downslope region from the peak intersection of the ENE topographic trend and the topography arcing east and then north (centred on 564500E, 7190600N and striking ENE for ~250m). A much larger magnetic response is associated with the cirque and the north slope of the valley. This feature is ~ 1500m in strike length and 1000m in width (widest point). The gravity feature observed at 565500E, 7190700N is encompassed by this magnetic high. The overall shape of the magnetic feature appears to be fault controlled.

The radiometrics (Figure 48 to 51) exhibits a strong ENE-WSW bias. Higher potassium with respect to uranium and thorium is observed on the south slope of the north bounding arcuate ridge. This zone of potassium high flanks the north edge of the large central magnetic high and correlates with the gravity trend in this area. The on strike extent is fault limited. This feature extends from 564300E, 7190750N to 565500E, 7191250N. The central E-W topographic valley is depleted in potassium with respect to uranium and thorium. A preference for uranium is associated with the NW striking family of faults.

The original AOI for the East was significantly smaller in size than the area used for the 3D inversion of the CBA. In the original outline (as illustrated in Figures 52, 53 and 54) the original 3D magnetic susceptibility inversion and the current CBA 3D inversion do not indicate a source in the near surface. The 3D CBA inversion (Figures 52 and 53) indicates dense rocks surrounding the original AOI outline but none within it. The 3D magnetic susceptibility inversion (Figure 54) suggests a magnetic body, but at depth although the 2D inversion results place a magnetic source closer in the near surface but not outcropping. The 3D gravity inversion places a denser material surrounding and flanking the

magnetic features. It is doubtful if the limited test DCIP survey completed in this area looked sufficiently deep to reach the magnetic bodies.

The 3D CBA inversion suggests that denser material outcrops/subcrops along the sides of the cirque valley in addition to downslope into the valley from the valley wall peaks. There appears to be good correlation with the mapped faults, correlation between fault offsets and density offsets being observed. The gravity anomaly observed in the CBA (Figures 42 and 43) that is downslope from the ridge peaks into the cirque valley appears to be continuous with depth and sub-vertical in dip. Offsets in the 3D model correspond to mapped faults suggesting a staircase type of faulting along strike.

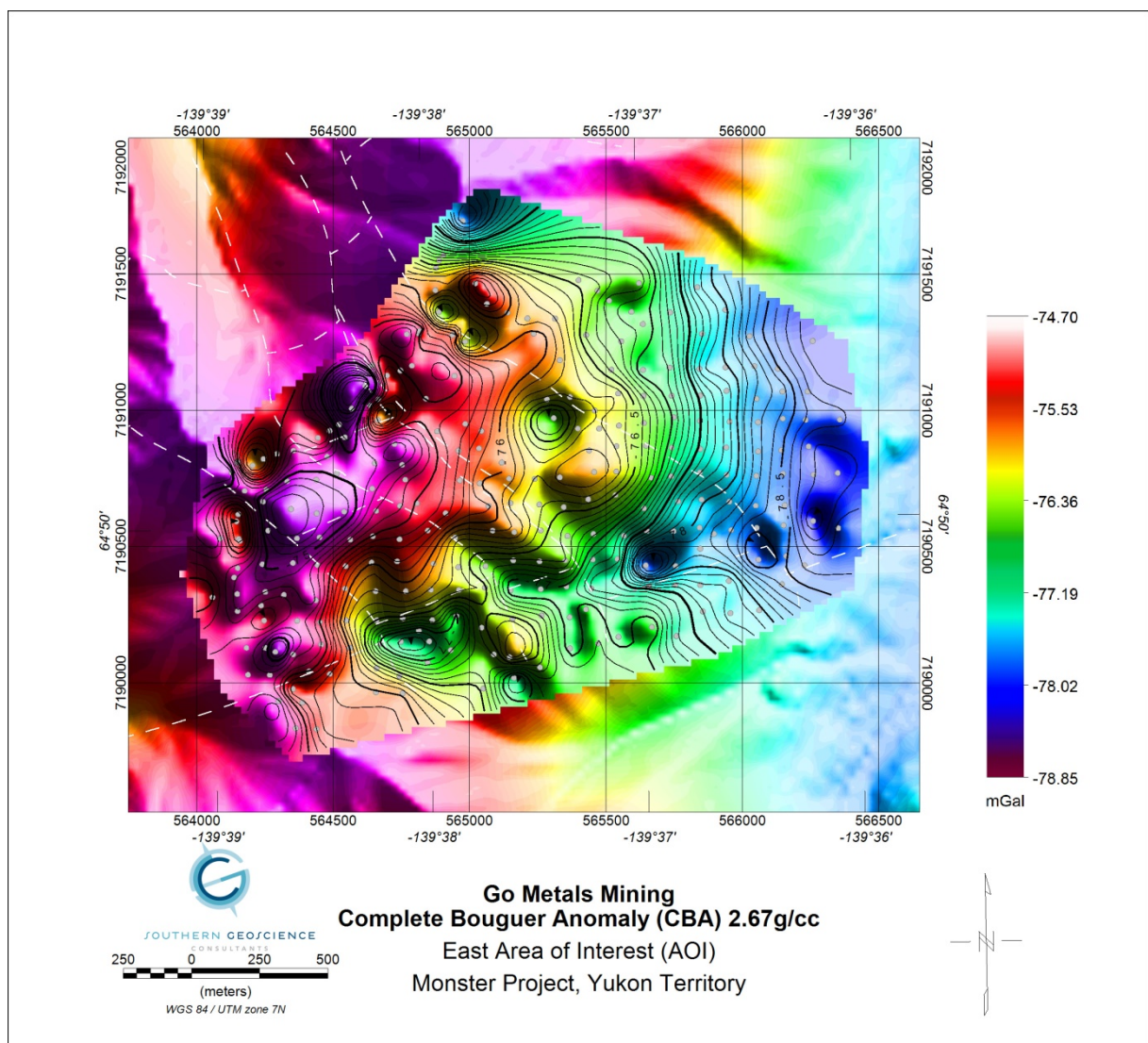


Figure 42: East AOI Complete Bouguer Gravity Anomaly (CBA) for Bouguer Density 2.67g/cm³. Gravity sites are indicated by grey dots. Contour interval is 0.1, 0.5 and 2.5 g/cm³. Mapped geologic faults (dashed white lines) are plotted. Background is drone DEM grid.

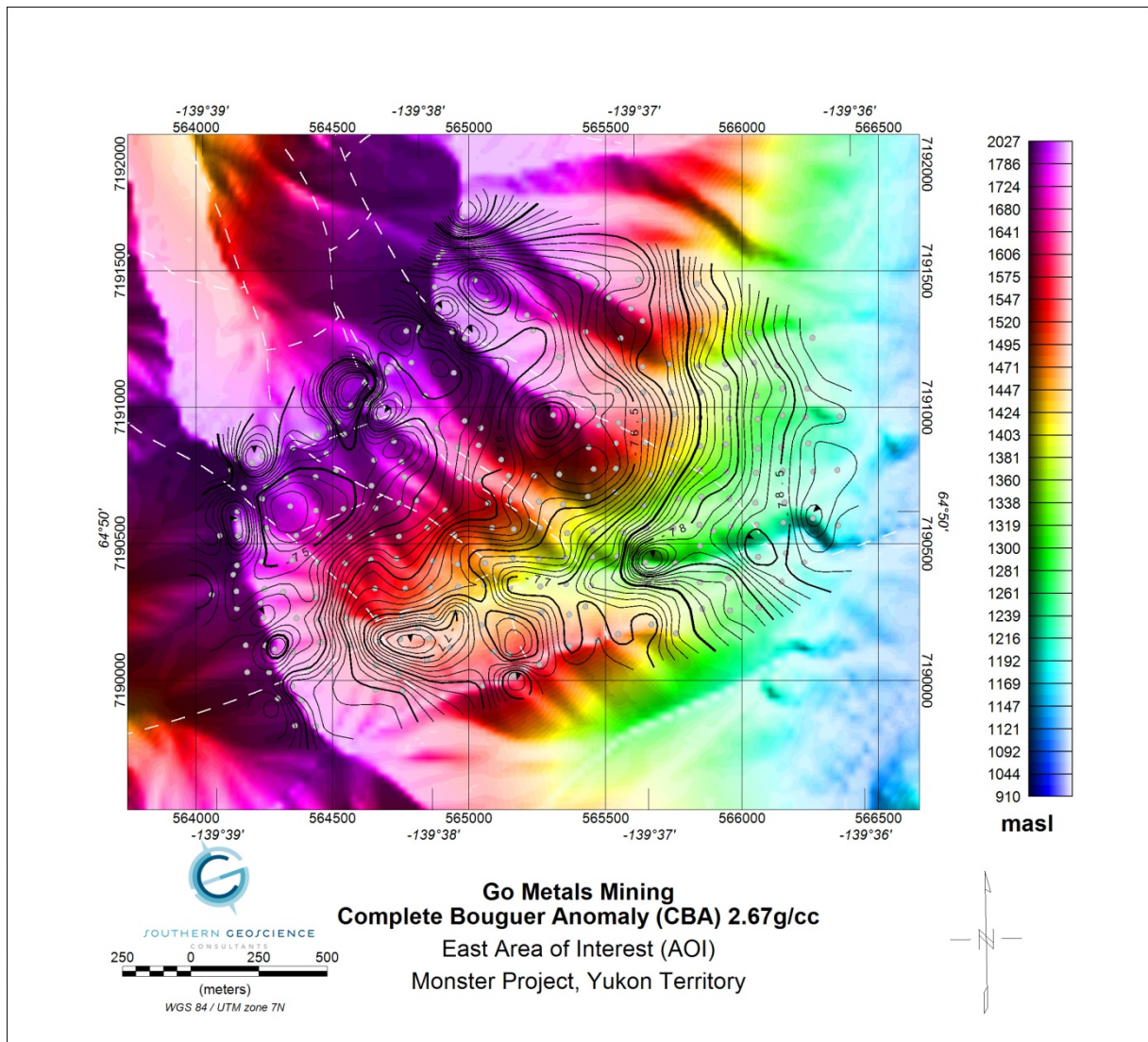


Figure 43: East AOI Complete Bouguer Gravity Anomaly (CBA) for Bouguer Density 2.67g/cm^3 . Gravity sites are indicated by grey dots. Contour interval is 0.1, 0.5 and 2.5g/cm^3 . Mapped geologic faults (dashed white lines) are plotted. Background is drone DEM grid.

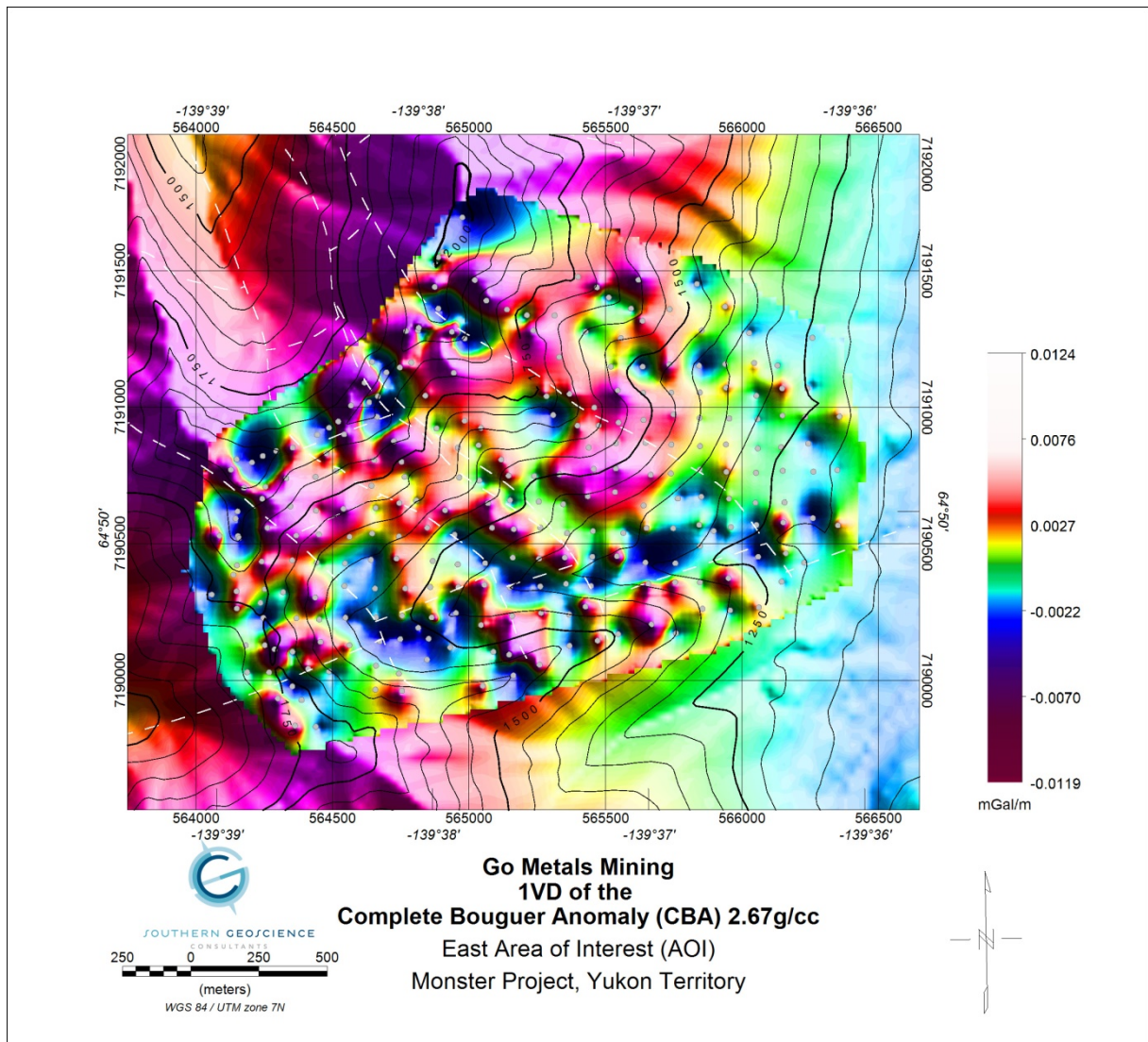


Figure 44: East AOI 1VD of the Complete Bouguer Gravity Anomaly (CBA) for Bouguer Density 2.67g/cm^3 . Gravity sites are indicated by grey dots. Mapped geologic faults (dashed white lines) are plotted. Background contours (50/250/1000 m) are elevations from the drone DEM grid in units of masl.

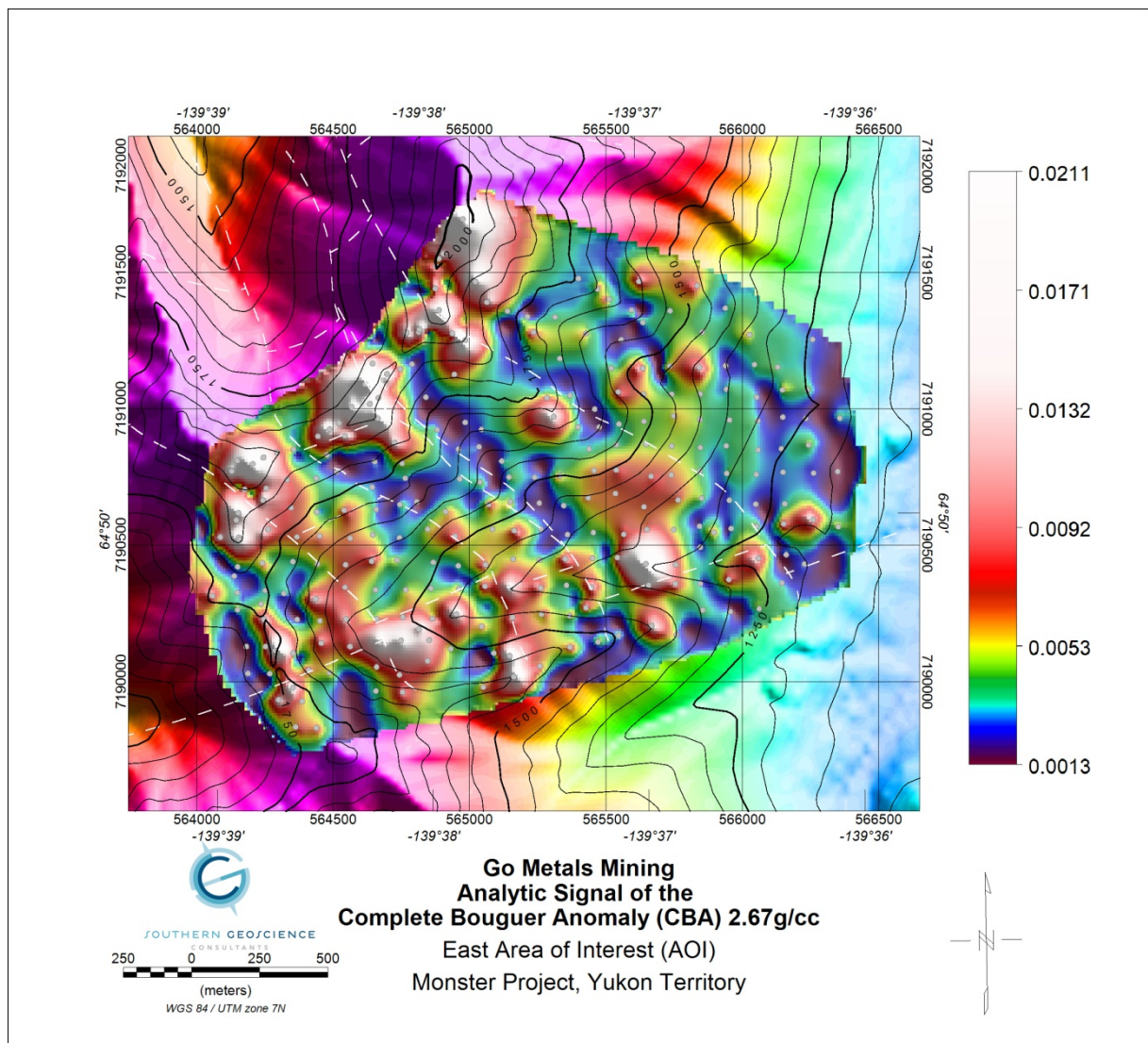


Figure 45: East AOI Analytic Signal of the Complete Bouguer Gravity Anomaly (CBA) for Bouguer Density 2.67g/cm³. Gravity sites are indicated by grey dots. Mapped geologic faults (dashed white lines) are plotted. Background contours and image (50/250/1000 m) are elevations from the drone DEM grid in units of masl.

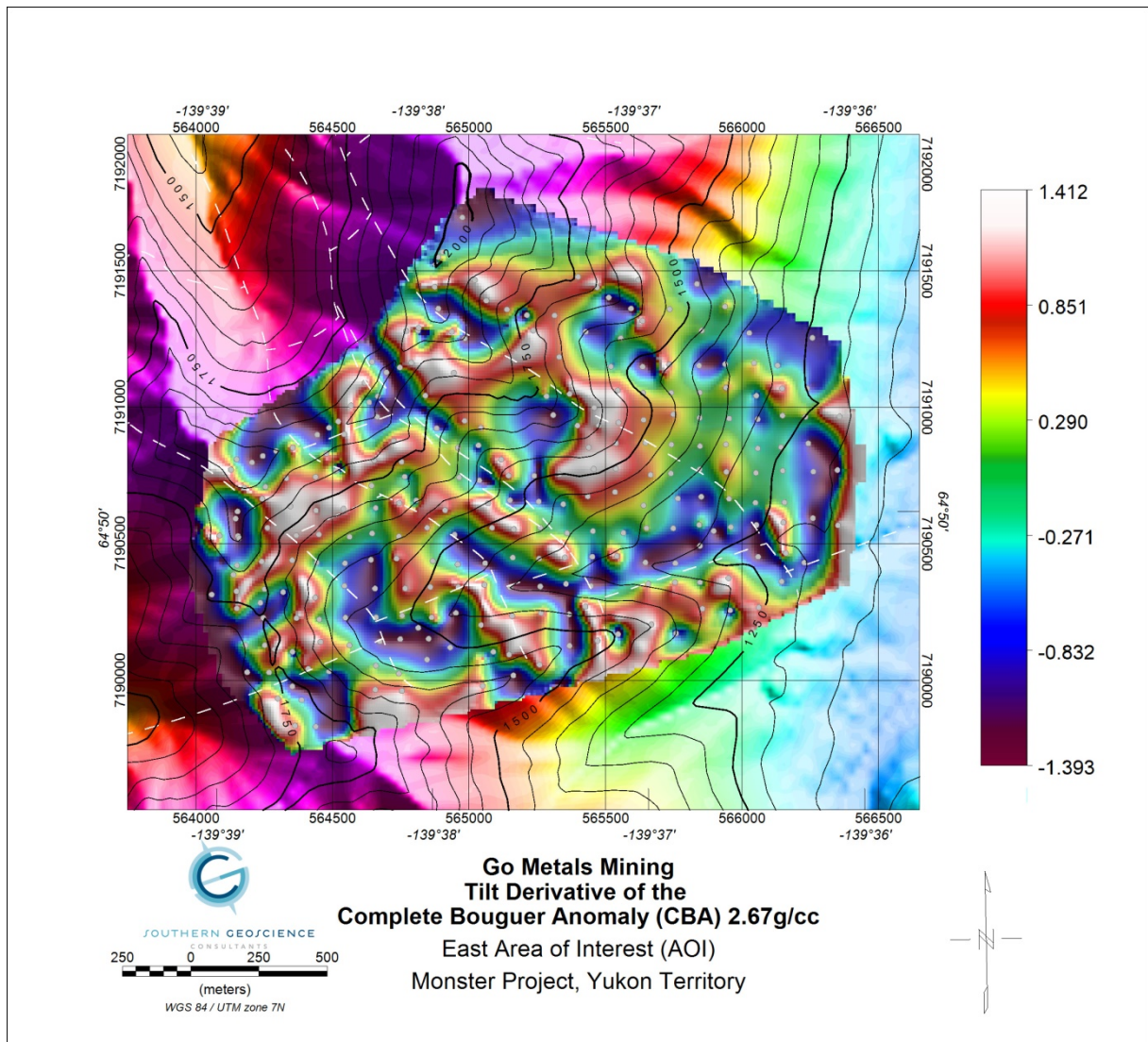


Figure 46: East AOI Tilt derivative of the Complete Bouguer Gravity Anomaly (CBA) for Bouguer Density 2.67g/cm^3 . Gravity sites are indicated by grey dots. Mapped geologic faults (dashed white lines) are plotted. Background colour/contours (50/250/1000 m) are elevations from the drone DEM grid in units of masl.

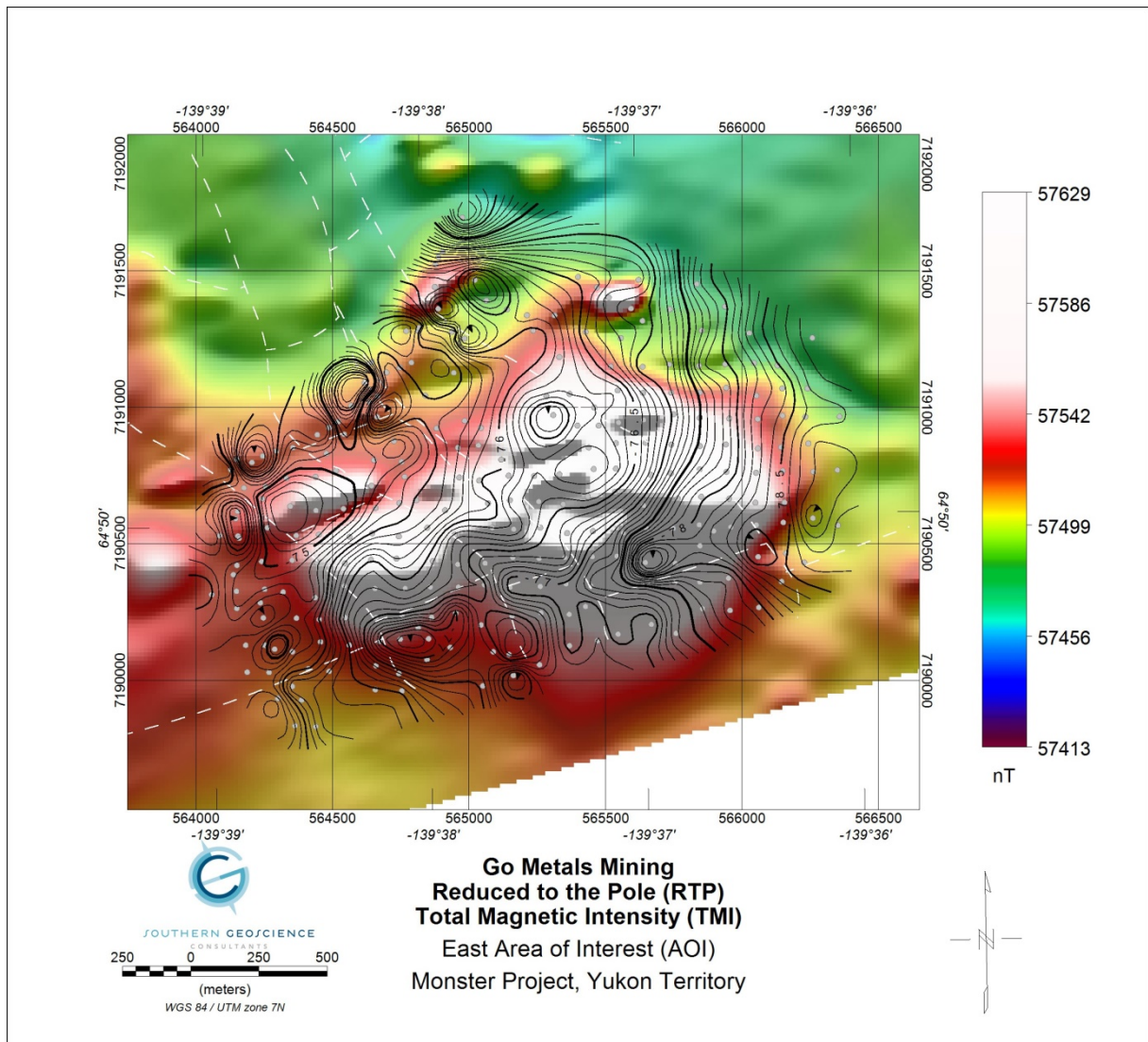


Figure 47: East AOI Reduced to the Pole (RTP) total magnetic intensity (TMI) from the airborne survey with contour overlay of the CBA 2.67g/cm³. Gravity sites are indicated by grey dots. Mapped geologic faults (dashed white lines) are plotted.

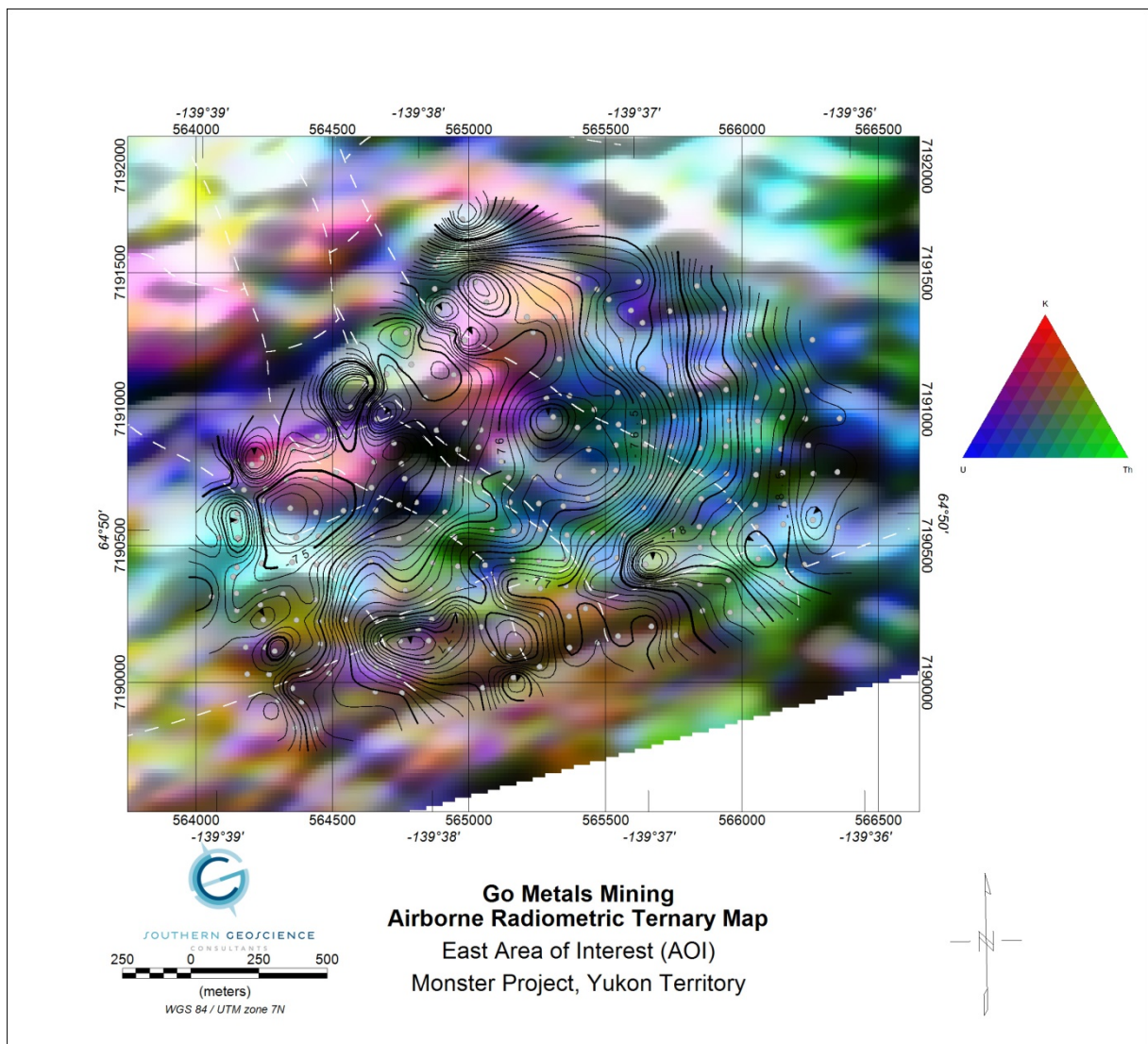


Figure 48: East AOI airborne radiometric Ternary plot with contour overlay of the CBA 2.67g/cm³.

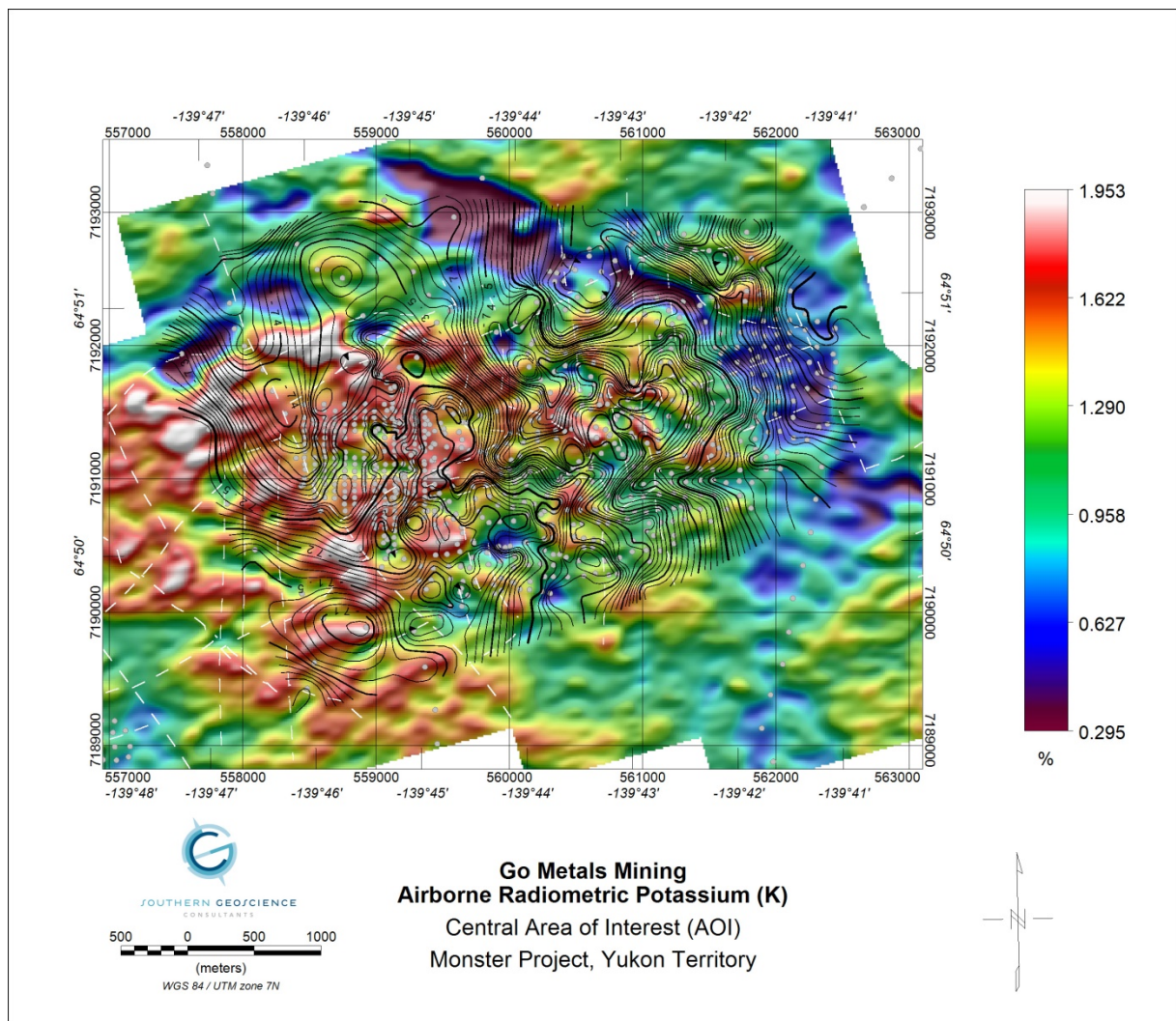


Figure 49: East AOI airborne radiometric Potassium (K) plot with contour overlay of the CBA 2.67g/cm³.

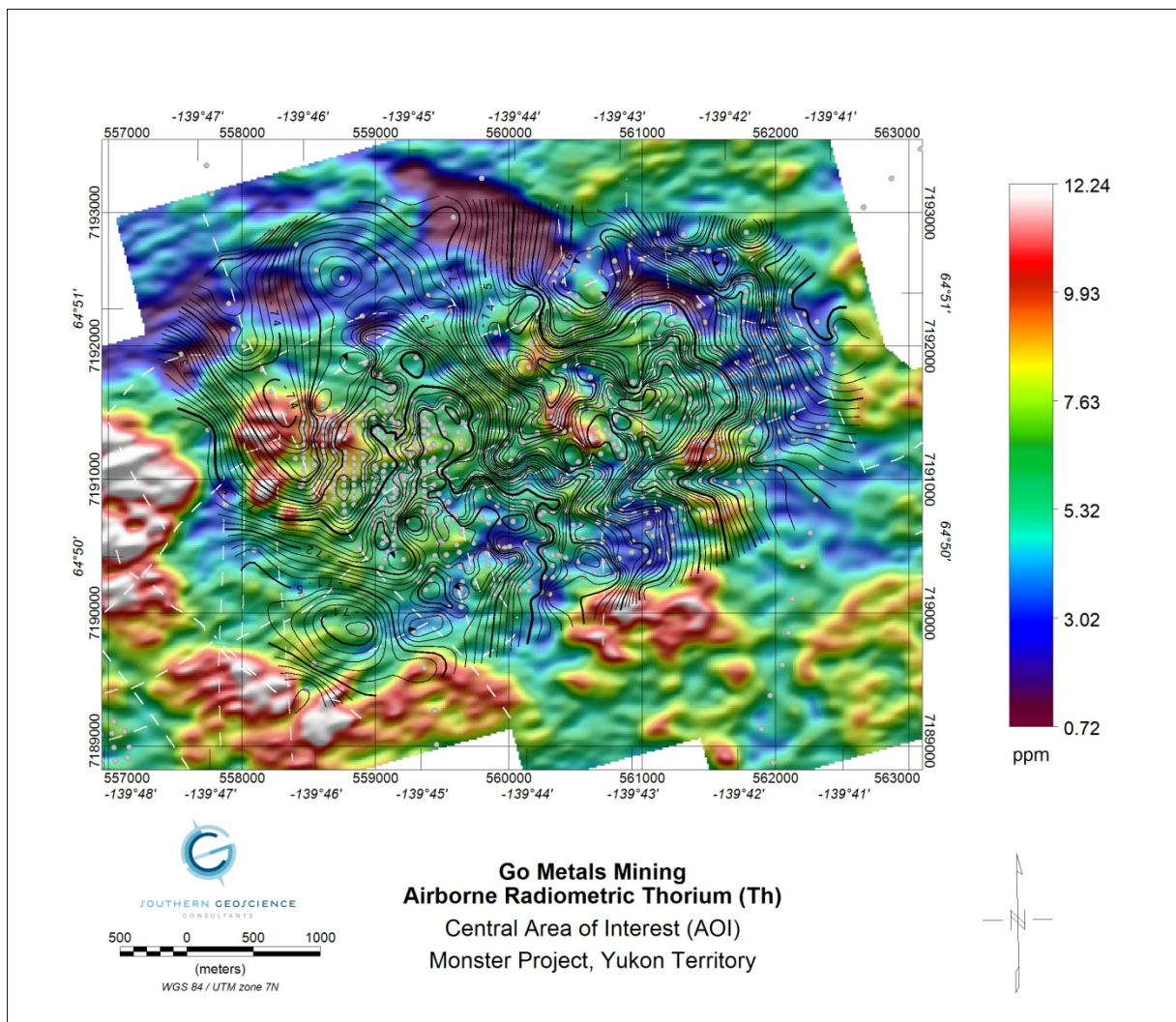


Figure 50: East AOI airborne radiometric Thorium (Th) plot with contour overlay of the CBA 2.67g/cm³.

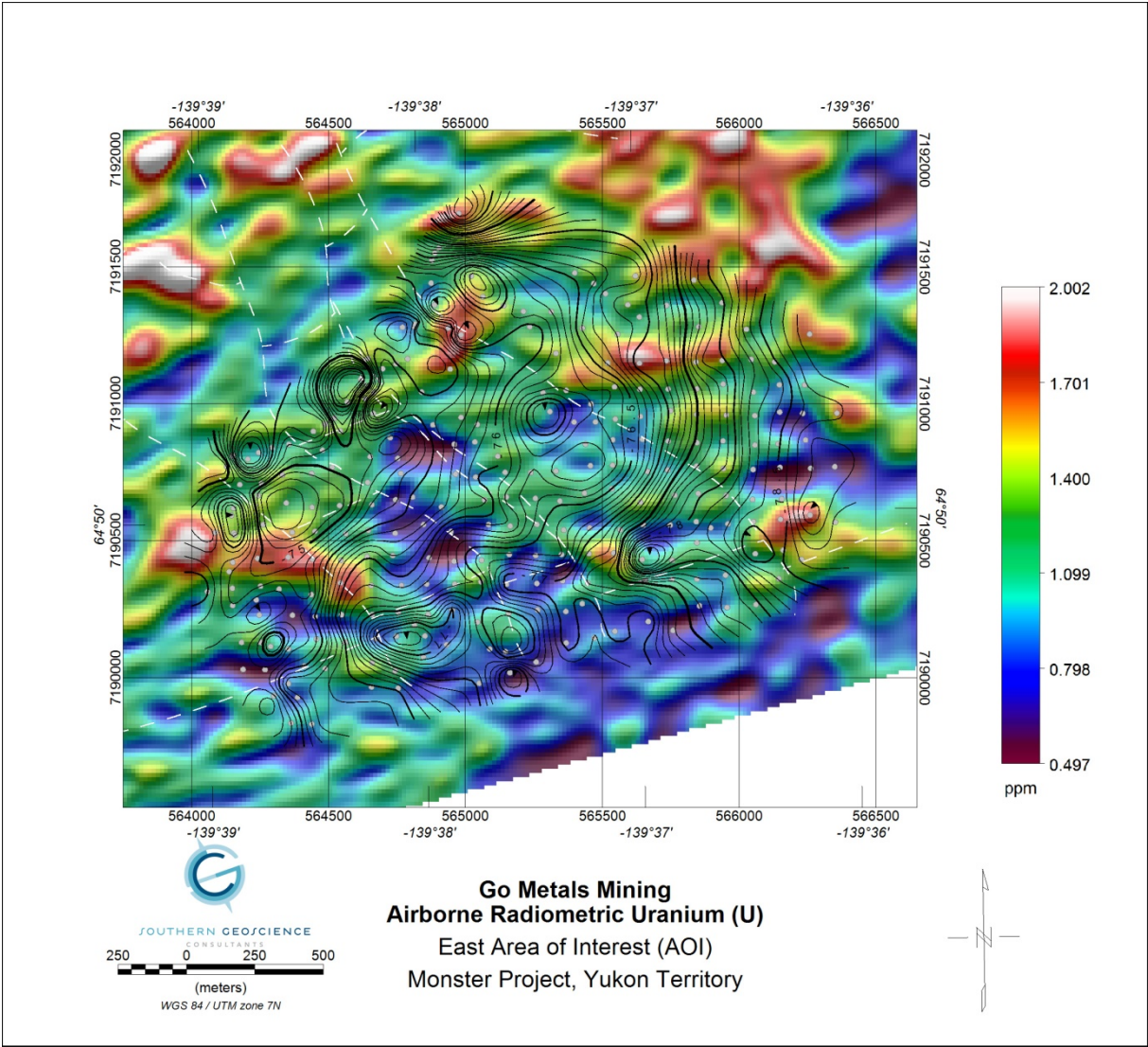


Figure 51: East AOI airborne radiometric Uranium (U) plot with contour overlay of the CBA 2.67g/cm³.

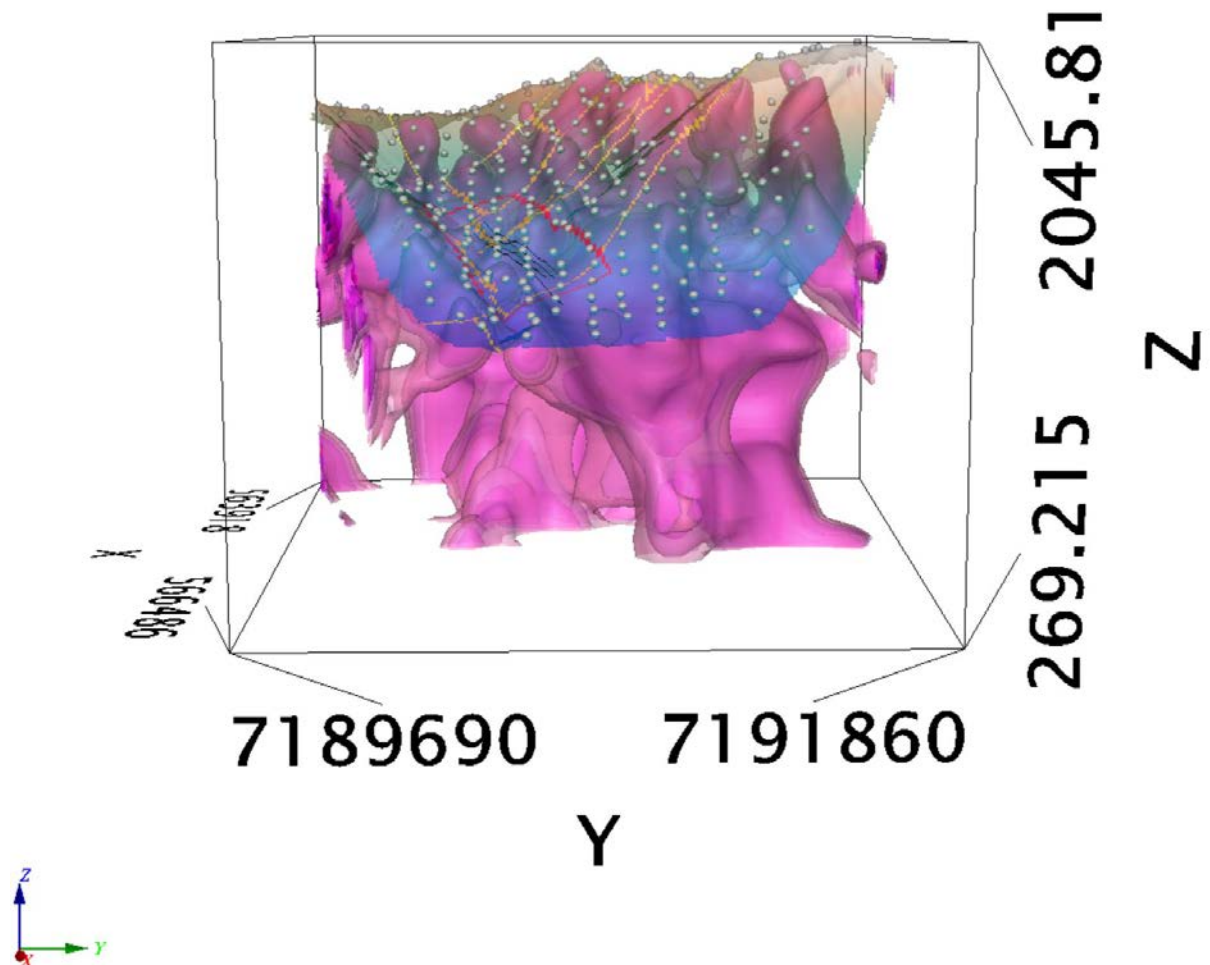


Figure 52: 3D Voxi inversion of the CBA 2.67g/cm³ data for the East AOI. View is looking west. The iso-surface/shell for a density contrast of 0.01 g/cm³ (corresponding to a density of 2.77 g/cm³) is shown. Topographic surface (drone DEM) is plotted in addition to surface mapped faults (yellow lines), gravity measurement sites (grey dots), DCIP Lines (black) and GMM defined AOI (red polygon).

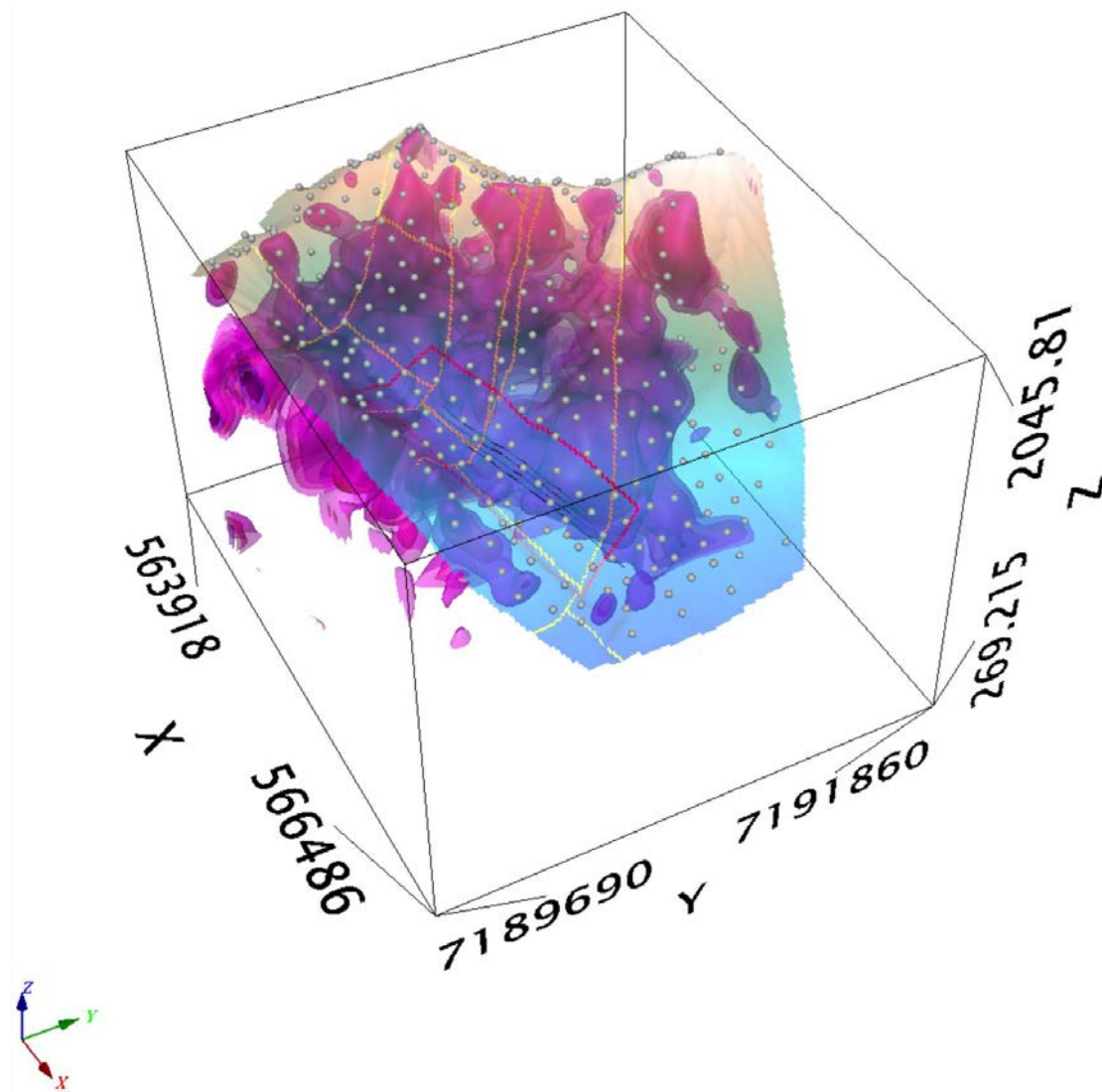


Figure 53: 3D Voxi inversion of the CBA 2.67g/cm^3 data for the East AOI. View is looking west. The iso-surface/shell for a density contrast of 0.015 g/cm^3 (corresponding to a density of 2.82 g/cm^3) is shown. Topographic surface (drone DEM) is plotted in addition to surface mapped faults (yellow lines), gravity measurement sites (grey dots), DCIP Lines (black) and GMM defined AOI (red polygon).

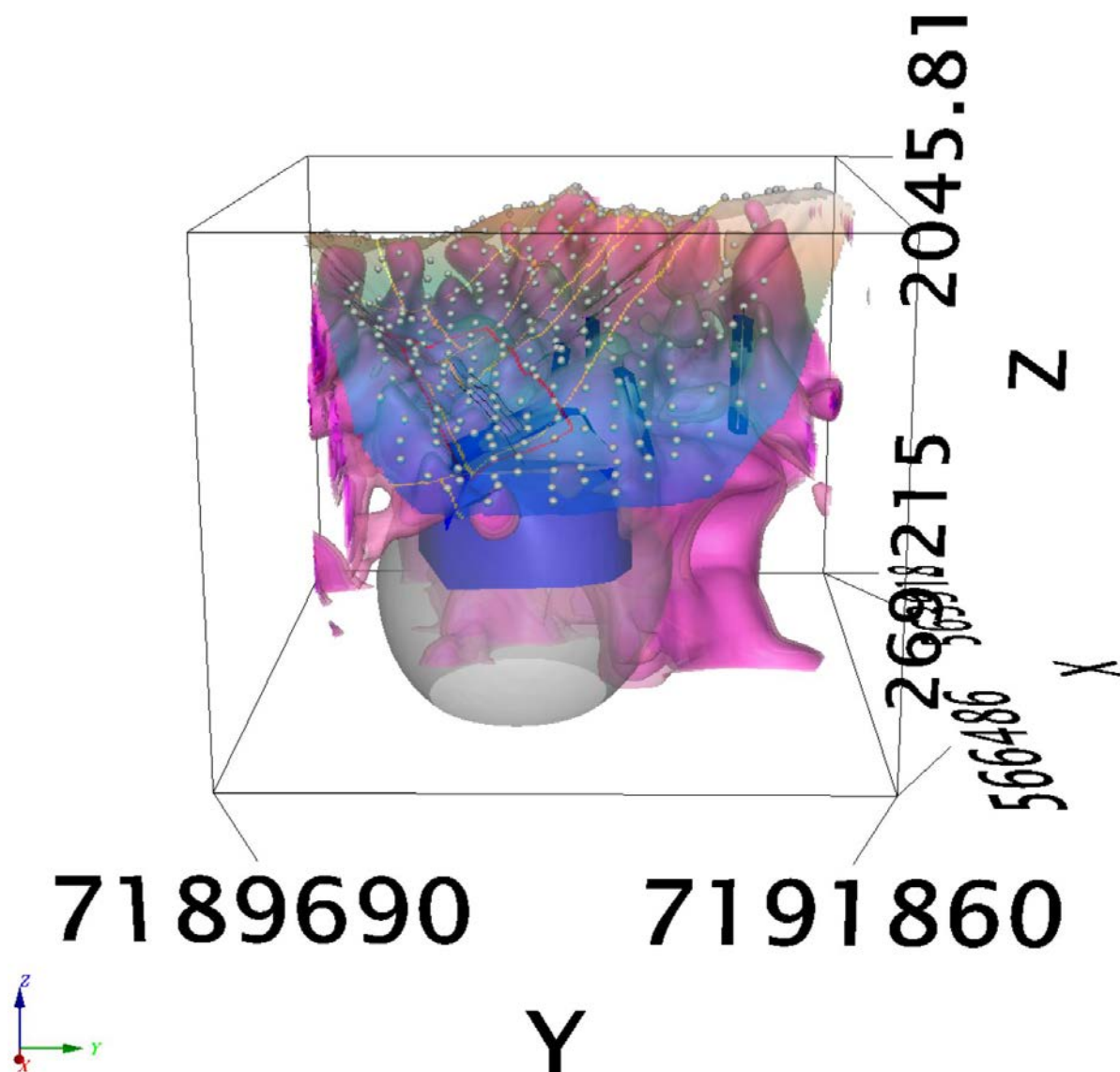


Figure 54: 3D Voxi inversion of the CBA 2.67g/cm³ data for the East AOI. View is looking west. The iso-surface/shell for a density contrast of 0.01 g/cm³ (corresponding to a density of 2.77 g/cm³) is shown. Magnetic susceptibility iso-surface (0.0024 SI; grey surfaces) are shown. The 2D magnetic modelling completed in the past is shown in dark blue. Topographic surface (drone DEM) is plotted in addition to surface mapped faults (yellow lines), gravity measurement sites (grey dots) and GMM defined AOI (red polygon).

6 CONCLUSIONS AND RECOMMENDATIONS

From the rock physical property data supplied it is apparent that the Wernecke Breccia covers a wide range of possibilities with respect to density and magnetisation. It is possible to have a light rock with very high magnetic susceptibility (Table 2, sample 179510, 2.58g/cm³, 58.76 SI, rock type not specified) to a very dense rock with low susceptibility (Table 1, 142.65m depth, 3.13 g/cm³, 0.20 SI, Wernecke Breccia). Unfortunately the physical property sampling has been somewhat limited due to the limited amount of outcrop and drilling completed on the property. Sampling is heavily biased towards the Wernecke Breccia, the average density of which from the most recent sampling is 2.58 g/cm³ and is based primarily on float/subcrop samples. All samples are assumed to be of Wernecke

Breccia and/or clasts contained in the Wernecke Breccia. All Wernecke samples are heavily dependent on the composition of the clasts and matrix materials. Shale values are almost exclusively from one drill hole and consist of five samples. A broader rock physical property study is required including other rocks of the Gillespie and Quartet Groups to be able to better determine if and how the Wernecke Breccia can be better identified. The assumption in this study was that the denser materials producing the gravity anomalies are Wernecke Breccia. Assuming that fresh breccia from the subsurface will reflect the higher densities encountered in the single drill hole, from the 3D gravity it is anticipated that the iso-surfaces of 0.015 and greater ($>2.77 \text{ g/cm}^3$) reflect the Wernecke Breccia.

Based on this assumption, it is apparent from the regional 3D inversion that there appears to be three main areas of high potential for Wernecke Breccia. These areas are similar to the three areas identified by GMM as areas of interest (AOI) but have been defined as significantly larger areas (Figure 2) in this study.

Given the complex and variable nature of the clasts comprising the Wernecke Breccia, the mottled texture of the processed products for the CBA in the regional as well as the East, Central and West AOIs could reflect the extent of the Wernecke Breccia.

There is a high degree of correlation between the gravity data and the mapped faults strongly suggesting that the Wernecke Breccia extent is indicated by fault controlled high density blocks and fault trends with an associated gravity anomaly.

The magnetic inversion data is arguably less effective, in part due to the lack of magnetic contrast in the rocks. A common relationship between the magnetic inversion and gravity inversion models is that the magnetic bodies are often shallower and flanked by high density bodies. Small features in the magnetic signal related to thin magnetic dikes are not imaged very well by the 3D modelling. The strikes and dips of the inverted data for both the magnetic and gravity data often differ as in the East and Central AOIs. When available, the introduction of a geologic model and/or drill hole data into the inversion process would be advantageous to improving the interpretability of the results.

A fairly high degree of correlation of between the gravity anomalies and the airborne radiometric data was noted in almost all AOIs. Arguably the most common correlation was with potassium being more dominant than thorium or uranium with dense bodies, particularly on slope sides as in the examples of the East and Central AOIs.

The greatest degree of correlation between the magnetic and gravity data appears to be the West AOI where the central anomaly is both a magnetic high and a gravity high anomaly (centred on 556000E, 7188250N) and at the intersection of NNW-SSE fault that offsets an ENE-WSW striking fault. The apparent ring structure around this anomaly is also of interest and worthy of further investigation. The inversion modelling suggests that both the magnetic and gravimetric sources are sub cropping, if not outcropping in this area.

In the Central AOI, two dominate trends have been identified. Trend one extends from 559800E, 7189600N to 558600, 713900N; trend two extends from 659500E, 7190150N to 561800E, 7192500N. These trends intersect at 659500E, 7190150N and range in width from 200m to 500m. There are weak associations with both the radiometrics and the magnetics suggesting that these may alteration zones related to faulting.

Also in the Central AOI, there is a partially overlapping gravity and magnetic model at 561000N, 7191750N that is bisected by a NNW striking fault. The modelling suggests subcropping/outcropping rocks in this area. The target is worthy of further work and follow-up.

The East AOI is interesting as the gravity modelling appears to flank the magnetic 3D inversion in almost all cases. This could indicate an intrusive centre (the magnetics) and alteration into the surrounding rock (density high). The magnetic core does not appear to shallow, but remains at depth below surface whereas the gravity inversion suggests that the dense rock outcrops/subcrops in the area.

A correlation between the magnetics and the gravity at 565500E, 7190700N that is fault controlled is worthy of follow-up and appears to be outcropping/sub-cropping.

A final target of interest is the apparent correlation between the radiometrics (potassium dominant over thorium and uranium) and coincident with a gravity high density anomaly along the slope of the cirque wall from 564300E, 7190750N to 565500E, 7191250N.

Unfortunately the DCIP resistivity test conducted during 2019 field season appears to have not looked deep enough to correlate with the magnetic anomaly at the centre of the East AOI.

7 REFERENCES

Doherty, R. Allen and Verbass, Jacob, 2018, Technical Report on the Geology of the Monster Property, Yukon Canada for Gorilla Minerals Corp.; 43-101 report filed on SEDAR.

Setterfield, T and Tykajlo, R., 2003, 2003 Geological Reconnaissance, Gravity Surveying and Diamond Drilling on the Monster Property; prepared for Monster Copper Resources Inc. and filed for assessment. Assessment report 094430.

APPENDIX A:

PRECISION SURVEYS AIRBORNE REPORT

PLANS